Guosong Zhang

Signal processing and field measurements for underwater acoustic communications

Thesis for the degree of Philosophiae Doctor

Trondheim, January 2013

Norwegian University of Science and Technology
Faculty of Information Technology,
Mathematics and Electrical Engineering
Department of Electronics and Telecommunications

NTNU – Trondheim
Norwegian University of
Science and Technology

NTNU
Norwegian University of Science and Technology

Thesis for the degree of Philosophiae Doctor

Faculty of Information Technology, Mathematics and Electrical Engineering
Department of Electronics and Telecommunications

ISBN 978-82-471-4173-1 (printed ver.)
ISBN 978-82-471-4174-8 (electronic ver.)
ISSN 1503-8181

Doctoral theses at NTNU, 2013:40

Printed by NTNU-trykk

Abstract

The present dissertation presents new developments in the signal processing of receiver structures for high-rate underwater acoustic communications, and describes the field measurements that test the structures in real oceanic environments. The signalling methods of spectrally efficient spread spectrum are also investigated to achieve long range underwater acoustic communications. The digital signal processing is of significance in recovering distorted information, and compensating waveform distortions introduced by the underwater acoustic propagation. Underwater acoustic channels, particularly horizontal underwater channels, are characterized by extended multipath reflections, which are difficult to be predicted precisely, especially for typical underwater telemetry at high frequencies. Thus field experiments are of importance for the research in this dissertation.

Time delayed multipath arrivals result in intersymbol interference (ISI) for coherent communications, which causes errors in recovering distorted information, and hence a channel equalizer is required to remove the ISI. In recent years, passive-phase conjugation (PPC) processing has been researched for underwater acoustic communications, since its focusing property mitigates ISI with an enhanced output signal-to-noise ratio. After the focusing achieved by PPC processing, a simplified channel equalizer removes residual ISI, as ISI cannot be eliminated by the focusing with side lobes.

Residual ISI can be mitigated by time reversal focusing, which exploits spatial diversity in the water column to suppress side lobes of the focusing. High-rate time reversal communications have been achieved, where only one channel adaptive equalizer is used after the focusing. Compared with an adaptive multichannel equalizer, the complexity of time reversal focusing with a single channel equalizer is low. However, spatial gain obtained by time reversal focusing is impacted by time-variant interchannel correlations, which exist in a real oceanic environment, as time reversal focusing is conducted prior to the adaptive channel equalizer. The means obtaining a large spatial gain of reduced complexity is of significance in real applications, especially with a small number of receiving hydrophones.

A receiver structure of joint PPC with adaptive multichannel combining is proposed. PPC processing in each individual channel reduces ISI by the temporal focusing (pulse compression), and a subsequent multichannel equalizer of reduced complexity is used to remove residual ISI. Spatial gain is obtained by the adaptive multichannel combining, which exploits spatial diversity as well as removing ISI. As the combining is dependent on the output of the channel equalizer, this scheme is advantageous to make full use of spatial diversity. In practice, it is preferred that a small number of receiving hydrophones is used to reduce the complexity of instrumentation. In particular, results of experimental data processing have shown that this structure achieves superior performance over the time reversal receiver structure.

PPC processing requires knowledge of the channel, e.g. the channel impulse response, which is often characterized as time-varying and sparse, especially at high

frequencies. In a time-varying channel, the temporal focusing degrades with time, and a block-based approach is applied to counter the channel variations. The channel is assumed constant within each block of short time duration, in which the channel response is estimated using detected symbols of the previous block. In a sparse channel, the matching pursuit (MP) algorithm can be used to exploit the channel sparsity for PPC processing. Compared with the conventional channel estimation method, e.g. the least squares (LS) method, the MP algorithm only obtains information of dominant arrivals. Without noise interference among dominant arrivals, the MP algorithm contributes improvement for communications using PPC processing.

In long range communications, a receiver structure has to counter acoustic attenuations together with waveform distortions. Hence spread spectrum techniques have advantages for communications at low input signal-to-noise ratios. During the work of this dissertation, two spread spectrum signalling schemes have been investigated with experimental demonstrations. Particularly, a spectrally efficient scheme using cyclic code shift keying has been proposed, and a time reversal receiver structure has been presented. This structure has obtained satisfactory performance in a field experiment over a range of 10 km. In this scenario, the time reversal structure takes advantage of spatial diversity to avoid deep fading occurring in each receiving channel, which usually happens in long range communications.

In the past 3 years of this dissertation, four major field measurements were carried out in Trondheim harbour. Those trials were designed to test underwater communications in different propagation conditions, e.g. in different months, as the environmental conditions changed over different seasons. In addition, the source locations were changed to test the communications in different experimental arrangements of source and receivers. For practical purposes of research, receiving waveforms were recorded for offline digital signal processing in the laboratory. Valuable experiences of instrumentation, data acquisition development, participation in instrument procurement, field experimental organization, etc., have been obtained during this dissertation. For the high-frequency (10-14 kHz) communications, it is infeasible to simulate the acoustic wave propagations in real ocean waveguide sufficiently accurately. Therefore, field experiments are of significant practical use for the research in underwater acoustic communications. As an important part in this dissertation, the major field experiments with instrumentation details are briefly introduced. Together with selected publications, selected results which have not previously been published are presented in this dissertation.

Preface

This thesis is submitted to the Norwegian University of Science and Technology (NTNU) for partial fulfilment of the requirements for the degree of *Philosophiae Doctor*.

This work has been performed at the Department of Electronics and Telecommunications at the Faculty of Information Technology, Mathematics and Electrical Engineering, NTNU in the period 2008-2011. My supervisors have been Professor Hefeng Dong and Professor Emeritus Jens M. Hovem at the Department of Electronics and Telecommunications, NTNU.

The work in this thesis has been supported by the Department of Electronics and Telecommunications, NTNU

Acknowledgements

I wish to specially thank my supervisors Hefeng Dong and Jens M. Hovem. They introduced me into this exciting and challenging subject of underwater acoustic communications, and have given help during the preparation of this thesis. They have acted as both researchers and friends in supporting my research and life.

I would like to thank Ph. D. candidate Bo Peng for creative discussions. It is grateful that my close friends NTNU Ph. D. students Qin Liu, Yan Jiang, Zhongxi Chao, Haohai Sun, Ganpan Ke, PostDoc Zhengliang Cao and PostDoc Duong Nguyen, and Professors Lanbo Liu and Ulf Kristiansen had ever helped me in carrying out the sea experiments in Trondheim harbour. Thanks to my colleagues Technical Engineer Øyvind Lervik and Tim Cato Netland, and the crews of R/V Gunnerus for preparing the instruments and deploying the equipment in sea trials. Thanks also give to the people that had ever joint the field measurements.

It is great grateful that the Professors Lanbo Liu from University of Connecticut had given valuable suggestions through discussions during his visit in the Acoustic Group, NTNU. I would also like to thank researcher of Norwegian Defence Research Establishment Paul A. van Walree for discussions.

I appreciate the help from my colleagues NTNU Ph. D. Anders Løvstad and Ph. D. candidate Erlend M. Viggen. I would like to thank the Professor Emeritus Tor Erik Vigran, Professor Peter Svensson and Professor Jan Tro in the Acoustic Group of the Department of Electronics and Telecommunications, NTNU, who never failed to provide a foreigner like me a pleasure life and unforgettable memory in Trondheim.

Finally, I wish to thank my family, particularly my wife Xiaonan Xu who has provided unconditional supports for my Ph. D. work.

Contents

Abbreviations

BER	Bit error rate
BPSK	Binary phase shift keying
dB	Decibel
CCSK	Cyclic code shift keying
CIR	Channel impulse response
CRA	Cross receiving array
DFE	Decision feedback equalizer
DPLL	Digital phase-locked loop
ISI	Intersymbol interference
LE	Linear equalizer
LFM	Linear frequency modulation
LS	Least squares
MP	Matching pursuit
McDFE	Multichannel decision feedback equalizer
MSE	Mean square error
PPC	Passive-phase conjugation
QPSK	Quadrature phase shift keying
RLS	Recursive least squares
SNR	Signal-to-noise ratio
SSP	Sound speed profile
TR	Time reversal
UWA	Underwater acoustic
8-PSK	8 Phase shift keying
8-QAM	8 Quadrature amplitude modulation

Chapter 1

Introduction

Underwater acoustic (UWA) communications are challenged by UWA channels, which are often characterized as bandwidth limited, highly dispersive, time-varying, etc. [1], especially for high-rate coherent communications [2]. Extended multipath arrivals result in intersymbol interference (ISI), which causes errors in recovering the distorted information. It is typical that multipath arrivals span several tens of symbol intervals for moderate to high-rate communications. High-frequency (10-14 kHz) signals are subject to rapid time variations that result in phase instabilities, which is a serious concern in long range UWA communications [1]. Coherent communication algorithms have to deconvolve the multipath arrivals in order to remove ISI, and track and compensate the channel variations during communications. Therefore, adaptive channel equalizers have been researched to achieve stable coherent communications.

As a single receiver is vulnerable to deep fading in a time-varying channel [3], multiple receivers that are spatially diverse can be used together to reduce the impact of deep fading. Thus array signal processing has succeeded in coherent UWA communications [4-8]. With multiple receivers, spatial diversity contributes to convergence of the adaptive multichannel decision feedback equalizer (DFE). Otherwise, a single channel DFE often loses its convergence in practice, as it is difficult to configure the adaptive channel equalizer for the current channel response, which could have peaks and nulls in the spectrum. In order to track rapid fluctuations of UWA channels, the recursive least squares (RLS) algorithm [9] is preferred for its fast rate of convergence, and its insensitiveness to the eigenvalue spread of the correlation matrix of the tap-input vector. However, such an adaptive multichannel DFE (McDFE) is computationally intensive, especially in high symbol rate communications in channels of long time spread, since more taps are required to deconvolve the channel effects. Even though advanced hardware development has increased the computational power, the computational load of McDFE still limits its implementations in UWA communications, particularly in applications with a large number of receivers.

A time reversal (TR) mirror achieves focusing in inhomogeneous media, as was demonstrated first by Fink [10] in an ultrasonic field. In a UWA channel, the focusing of the TR mirror was experimentally demonstrated by Kuperman et al [11]. The experimental research showed that ISI caused by the multipath arrivals was significantly suppressed for UWA communications [12], where two vertical arrays are involved in a two-way transmission to achieve the refocusing at the transmitter. With reduced complexity of one receiving array, passive TR communications [13-15] requires only one-way transmission, where passive-phase conjugation (PPC) processing is used. PPC

processing achieves pulse compression for time delayed arrivals [16, 17]. By sampling the sound field with multiple receivers, spatial diversity is obtained by passive TR to achieve spatial focusing. Flynn et al. [18, 19] have proposed a method of PPC communications. The channel estimations for PPC processing are updated in a decision-directed mode. However, this approach is computationally intensive in estimates, even though the LSQR algorithm is implemented [20]. In principle, this method does address the channel variations instead of attempting to suppress side lobes of the TR focusing.

The side lobes are determined by the channels' impulse response. As discussed by Yang [14], the propagation physics determines that ISI cannot be eliminated by the TR focusing. Even though the multipath is mitigated by the TR focusing, residual ISI caused by the side lobes of the TR focusing results in errors for high-rate UWA communications. Therefore, a subsequent adaptive channel equalizer with a reduced number of taps, e.g. a single channel adaptive DFE, is required to remove the residual ISI [15, 21-23]. In this thesis, the receiver structure that consists of TR focusing realized by PPC processing plus a single channel DFE is referred to as PPC-DFE.

Song has demonstrated PPC-DFE for high-rate [24], extreme long range [25], and multi-user [26, 27] communications. TR focusing obtains spatial diversity with the assumption that the receivers are independently distributed; the main lobes of multiple pulse compressions are added coherently while the side lobes are added non-coherently. In time-varying channels, the focusing degrades with time, and a block-based approach has been suggested by Song et al [28]. In principle, this block-based approach extends the idea of decision-directed PPC communications proposed by Flynn et al. [18, 19], in which the channel is updated within each symbol interval. It is assumed by the block-based approach that the channel is constant within each block of a short time interval. In the current block, the channel knowledge required by PPC processing is obtained based on detected symbols of the previous block.

The studies presented above show that TR communications are advantageous in an oceanic multipath propagation environment. However, spatial correlations exist in a real oceanic environment [29], and indeed there is no model that can precisely predict time-varying spatial coherence. The spatial correlations result in interchannel correlations among the multiple receivers. The correlations impact the spatial focusing which exploits the spatial diversity to suppress the residual ISI. For practical purposes, a small number of receivers are preferred to save cost, and instrumentations.

This thesis mainly focuses on the development of a receiver structure for high-rate communications. A receiver structure of joint PPC processing and McDFE (PPC-McDFE) has been proposed and analyzed. The structure reduces implementation complexity of McDFE and takes advantage of channel diversities. Details of the structure are shown in the attached papers. In addition, spread spectrum communications over long ranges are also investigated in this thesis. For instance, a spectrally efficient method using cyclic code shift keying is presented with experimental demonstration of the performance of three receivers, namely the correlation receiver, the PPC receiver, and the TR receiver. In terms of results, for bit error rate (BER), the TR receiver structure obtains superior performance. Since there is no model that adequately predicts the acoustic field in time-varying acoustic channels, especially for high frequencies, it is hardly to apply a channel model to evaluate receiver structures for

any practices. Field experiments are used to demonstrate the results. Without losing generality, received waveforms were collected in the experiment, and afterwards real data were processed and analyzed in the laboratory to demonstrate performance of receiver structures, algorithms, instrumentation, and etc.

Using real data, Zhang et al. [30] have reported superior performance of PPC-McDFE, while PPC-DFE achieved worst performance due to time variant spatial coherence in the channel. In other experiments conducted in Trondheim harbor, PPC-McDFE has also achieved better performance than PPC-DFE [31-33]. In comparison with the classical receiver structure of McDFE as a baseline, the performance of PPC-McDFE is approximately the same as that of McDFE, but with a reduced computational load by using a smaller number of taps. Both McDFE and PPC-McDFE employ the adaptive multichannel combining to exploit spatial diversity, and that is the reason that both structures achieve better performance than that of PPC-DFE. Moreover, PPC-McDFE has been investigated for application in a multicarrier system [34], where a data rate of 4 kilo bits per second (kbps) has been achieved over a range of 4 km.

In practice, temporal focusing obtained by PPC processing degrades with time evolution due to temporal variations. One idea to improve performance in such a channel is to update the channel estimate in order to counter the variations, e.g. the block-based approach [28]. The channel is treated as static within each block of short time duration. By applying the block-based approach, PPC-McDFE has been implemented in time-varying channels [35], in which it obtains better performance than PPC-DFE. Therefore, PPC-McDFE is advantageous in obtaining spatial gain. This property shows its potential in the scenarios in which a small number of hydrophones is preferred.

Underwater channels are often characterized as sparse, and this is especially true for the high-frequency regime [36], which is typical for high-rate acoustic telemetry. In sparse channels, the matching pursuit (MP) algorithm [37] is also investigated to improve the performance of communications using PPC processing. The information of the channel impulse response (CIR) is represented by dominant arrivals, which can be selected by the MP algorithm for PPC processing. Experimental assessments [32, 33] carried out in this thesis have demonstrated the MP algorithm for the communications using PPC processing.

In addition, spread spectrum communications are investigated for use in long range communications of low input signal-to-noise ratio (SNR). The signaling schemes of spectrally efficiency are significant in spread spectrum communications. Two spectrally efficient schemes are designed in research [38, 39], and respective receiver structures are given, for which experimental demonstrations have been conducted. The proposed modified cyclic code shift keying scheme, at a carrier frequency of 12 kHz, has been tested over a range of 10 km [38] in a sea trial in Trondheim harbor, where a TR receiver structure is designed. For this signaling scheme of modified cyclic code shift keying, experimental demonstration shows that the performance of the structure has been improved by exploiting spatial diversity.

As an important part of this thesis, field experimental work, including experiment designs and instrumentation, has been carried out. In the last two years, several sea trials have been conducted in Trondheim harbor. Various locations have been selected to test

different configurations, e.g. different ranges, for UWA communications. The trials involved the research vessel R/V Gunnerus, instruments, equipment, personnel, and costs. In order to maximize the output of each experiment, comprehensive tests at different communication data-rates were designed. In particular, periodic data packets were sent, and received waveforms were collected for offline analysis in the laboratory. Valuable experience, both in the laboratory and in the field, has been built up for field experiments of UWA research.

This thesis is organized as a collection of six papers, which are presented in Chapter 5. The rest of this thesis is organized as follows. Chapter 2 briefly introduces UWA communications and PPC processing, including the basic knowledge of digital communications, and shows block diagrams of receiver structures. Chapter 3 reviews major field experiments conducted in Trondheim harbor, and briefly introduces selected instruments and devices. Unpublished results and analysis of the experimental data are presented in Chapter 4. The summaries of six papers are presented in Chapter 5, in which a full publication list during the thesis work is included. Chapter 6 gives conclusions and future work.

Chapter 2

Underwater Acoustic Communications and Passive-phase Conjugation Processing

In this chapter, we introduce UWA communications and PPC processing for UWA communications. Section 2.1 describes UWA communications, and introduces major problems. Adaptive channel equalizers are briefly reviewed in Section 2.2. In Section 2.3, PPC processing is briefly introduced. Three types of receiver structures: (1) McDFE, (2) PPC-DFE and (3) PPC-McDFE are shown by block diagrams. Note that details about the receiver structures can be found in the published papers.

2.1 Underwater acoustic communications

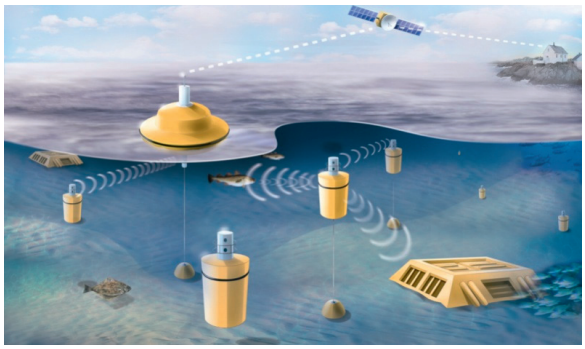

Figure 2.1. Illustration of an underwater sensor network. Illustration courtesy of Underwater Acoustic Network (http://www.ua-net.eu/).

UWA communications are used in underwater sensor networks [40] (illustrated in Figure 2.1) for long-term oceanic observation, surveillance, data transfer, etc. [41]. The underwater network is assumed to work in this way: there are several independent nodes that are deployed far from each other; data collected by the sensors at different nodes are transferred via UWA communications to a gateway node, which forwards the data to remote users by radio communications. In this network, robust acoustic communications between two nodes is a fundamental limitation, and the data rate between two nodes is the major factor which limits throughput of the network. In underwater channels, environmental conditions that affect acoustic propagation challenge the communications. Comparing with scenarios of vertical communications in which the vertical distance between two nodes is much larger than the horizontal distance, it is more difficult to achieve communications in horizontal channels. In this thesis, it is discussed to counter the horizontal channel effects to achieve UWA communications.

2.1.1 The underwater acoustic channel

In UWA channels, there is a high level of ambient noise, which is mainly caused by natural sound sources in the ocean and human activities, e.g. offshore oil industries. Comparing with electromagnetic counterparts, UWA channels are severely limited in bandwidth. This limitation originates from hardware, e.g. the acoustic transducer, and physical propagation conditions. It is typical that the CIR has a discrete structure which may span up to hundreds of symbol intervals, particularly in a multipath horizontal channel. Time delayed arrivals of energy result from acoustic energy propagation in paths of different lengths, which are caused by boundary reflections and refractions in the water. These multipath arrivals result in a large ISI for high-rate communications, and the presence of ISI introduces errors in making decisions of received symbols. Even in line-of-sight channels, there are shadow zones where little acoustic energy arrives due to refractions.

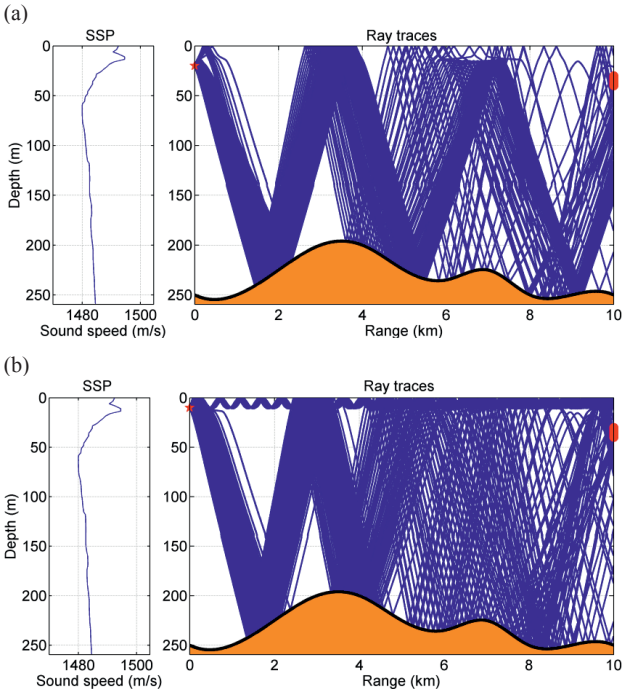

Figure 2.2. Illustrations of sound fields obtained by ray tracing with different source depths. (a) 20 m. (b) 10 m. The depth over a distance of 10 km is range dependent. SSP shown in the left panel was measured in Trondheim harbour on 7th September 2011. Ray traces are shown in the right panel. The acoustic source denoted as a red star in the right panel is deployed at two different depths. The vertical array of 10 elements shown as a red dot in the right panel is deployed from 30 to 40 m.

Physically, acoustic propagation in the water column is mainly governed by the sound speed profile (SSP) along the propagation track [42]. Assume that the SSP is constant along the horizontal direction, and we illustrate the acoustic propagation by ray tracing using a program developed by Hovem et al [43]. Figure 2.2 illustrates acoustic

energy propagation from a point source at different depths over a range of 10 km. For simplicity, transmission into the seabed is neglected for the illustration. As indicated in Figure 2.2(a), less acoustic energy is received if a receiving array is deployed close to the surface. If the source depth is changed from 20 m to 10 m, Figure 2.2(b) shows that more acoustic energy is received if the array is deployed close to the surface. At a distance of 2 km to the source, there are shadow zones in both cases. Besides the issue of geometry of the transmitter and receivers, UWA channels are time-variant.

It is known that the SSP changes with oceanographic parameters, such as water temperature and salinity. Over a large time scale, UWA channels change with time variant oceanography, e.g. on the scale of months. On the other hand, on a small time scale, UWA channels vary rapidly with time due to surface movement caused by wind, turbulence, under surface currents, etc., and this is especially true for high frequencies, which are typical for UWA telemetry [2]. In the scenario when a moving submerged vehicle is used in UWA communications, as indicated by the distribution of acoustic rays simulated in Figure 2.2, the channel response becomes even more time-variant due to the acoustic propagation. Besides, the Doppler effect due to relative movement between the source and the receiver is also a concern. Many acoustic communication signals have a high ratio of bandwidth to the carrier frequency. In this scenario, the Doppler effect cannot be assumed as a frequency shift of the carrier frequency [44], but dilation or compression of the transmitted waveform occurs. In this thesis, we only focus on UWA communications without moving platforms. However, small carrier frequency shifts due to a moving sea surface and underwater currents are apparent for high frequencies. Therefore, carrier phase synchronization at the receiver has to be implemented for high-rate coherent communications.

Over the same communication range, the channel response changes with depth due to the acoustic propagation. The effect of spatial diversity in the acoustic field can be observed in Figure 2.2, where the distribution of acoustic rays changes with depth at location of the receiving array. Spatial diversity can be exploited using multiple hydrophones distributed in space, e.g. a vertical receiving array. Comparing with the scenario of a single receiving hydrophone, the probability of deep fading caused by time variant channel responses [3] can be reduced by exploiting spatial diversity, as there is a low probability that all hydrophones of a receiving array are in deep fading at the same time. In the temporal domain, there are time delayed arrivals propagating along independent travel paths of different lengths. The arrivals spread within a time interval, and hence there is temporal diversity embedded in the multiple arrivals. Even though multipath arrivals result in ISI, the temporal diversity can be exploited by PPC processing.

The characteristics of a UWA channel are briefly introduced. Further details can be found in review articles [1, 2, 45]. In practice, it is quite frequent that properties of the bathymetry are unknown, and all the aforementioned features make underwater channels a complex and challenging medium for UWA communications. For underwater networks, increased data rates between two nodes are needed. Hence it is preferred that spectrally efficient UWA communications are used.

2.1.2 Coherent communications

Data rates are apparently increased by raising symbol rates, which requires larger bandwidths. This is particularly true for noncoherent communications, usually using multiple frequency shift keying [46]. With a constant transmission power, the received SNR is halved for one doubling of bandwidth because noise power is increased in the transmission band, and it results in reduced communication capability in terms of reliability. In addition, there is bandwidth limitation from the transducer and the channel. Thus spectrally efficient coherent schemes are often considered for high-rate UWA communications.

In coherent communications, phases of the signal waveforms are used in modulation. For example, a digital modulator maps a sequence of information symbols into a set of corresponding signal waveforms, which differs in phases or both phases and amplitudes. Coherent schemes can be: binary phase shift keying (BPSK), quadrature phase shift keying (QPSK), 8-phase shift keying (8-PSK), quadrature amplitude modulation (QAM), and so on. Figure 2.3 shows space diagrams of three modulated signals. At a constant symbol rate, data rate is increased by using higher order modulations (larger symbol constellations), as the number of bits per symbol is raised. For instance, within a symbol interval T, the data rate R is $1/T$ bits per second (bps) when BPSK is used, and R is $3/T$ bps when 8-QAM is used. This means that the spectral efficiency varies with the order of modulation.

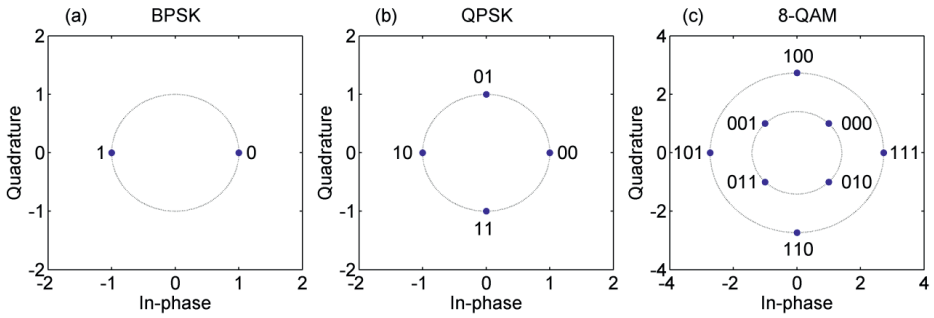

Figure 2.3. Signal space diagrams for different signals. (a) BPSK. (b) QPSK. (c) 8-QAM.

Using coherent modulations, the phase of the received waveforms contains transmitted information. There are several factors that may cause errors when recovering the phase information. The factors can be: (1) Consecutive symbols overlap due to ISI, and the phase information is distorted; (2) There is a carrier frequency shift due to the Doppler effect, and the frequency shift results in phase rotations; (3) At a low received SNR, the constellation of received symbols spreads in the signal space. In UWA channels, even though the received SNR is ideally satisfied, high-rate coherent communications are sensitive to the severe ISI and the frequency shift. A channel equalizer is required to invert the CIR as well as compensate the frequency shift.

2.2 Channel equalization

A multipath channel can be modelled as a finite impulse response filter of multiple taps. Assume that there are *K* receivers distributed in space, and the received baseband signal at the *k*th receiver is expressed as

$$v_k(t) = \sum_n I_n h_k(t - nT) + w_k(t),\ k=1,\ldots,K, \tag{1}$$

where $h_k(t)$ denotes the CIR which spans L symbol intervals of LT, I_n is the nth symbol of a sequence I that has N symbols, and $w_k(t)$ represents bandwidth limited noise. Channel equalization is mostly implemented in baseband digital signal processing. In a discrete form, Equation (1) is rewritten as

$$V_k^n = \sum_{l=0}^{L-1} H_k^l I_{n-l} + W_k^n, \tag{2}$$

where H_k^l denotes the lth tap of CIR vector H_k, which has a finite number of L taps. In multipath channels, when $L \neq 1$, errors occur due to ISI even if the channel is noiseless, and hence a channel equalizer is required to remove ISI. Three classical equalizers will be briefly introduced.

2.2.1 Maximum-likelihood sequence detector

Given the received vector V_k of the transmitted symbol sequence I, the maximum-likelihood sequence detector (MLSD) solves the optimization problem of maximizing the conditional probability as

$$\max P\{V_k | I\}. \tag{3}$$

This method does not intend to reconstruct the transmitted signal from the received signal that contains distorted data, but it generates the best estimated data with the least possible number of errors. When N becomes large in a long spread channel, it becomes computationally expensive to optimize the conditional probability [3]. The Viterbi algorithm solves the problem in an efficient manner.

The Viterbi algorithm treats the problem as estimating the state of a discrete-time finite-state machine, which is the discrete-time response H_k of L coefficients. In this case ISI spans L symbols, and there are $L-1$ interfering components. Given $L-1$ most recent symbols, the state at time n is written as

$$S_n = (I_{n-1}, I_{n-1}, \ldots, I_{n-L+1}) \tag{4}$$

where $I_n = 0$ for $n \leq 0$. If the symbols are generated by *M*-ary modulation, the channel as a filter has M^{L-1} states. Consequently, the channel can be treated as a trellis of M^{L-1} states, and the Viterbi algorithm determines the most probable path through the trellis. If the path is determined, the most likely data sequence is estimated. Details about the Viterbi algorithm can be found in [3].

As indicated, the number of states M^{L-1} grows exponentially with L, and the computational complexity of the Viterbi algorithm grows exponentially with the time spread of the channel. Hence it is typical that the Viterbi algorithm is used when L is small. In underwater channels, L often spans tens of symbols at high-rate

communications, and the Viterbi algorithm becomes infeasible due to the computational complexity. It is even expensive to implement the least order modulation—BPSK. Alternatively, a linear equalizer is of low complexity in removing ISI.

2.2.2 Linear equalizer

In this dissertation, the mean square error (MSE) criterion is applied for subsequent equalizers. Considering one receiving hydrophone denoted as the *k*th receiving channel, it is implied in Equation (2) that the estimate $\hat{I}_k^n$ of a linear equalizer (LE) can be given as

$$\hat{I}_k^n = \sum_{j=-\infty}^{\infty} c_k^j V_k^{n-j} \tag{5}$$

where $\{c_k^j\}$ is a set of tap coefficients of a linear filter. In order to obtain the estimate $\hat{I}_k^n$, the filter is supposed to invert the CIR H_k. If the response of the equalizer is equal to the inverse of H_k, it is called a zero-forcing filter. Figure 2.4 shows the block diagram of the LE using the minimum mean square error (MMSE) criterion. When $W_k(z)=0$, namely noiseless, ISI is eliminated by minimizing the MSE, and thus the equalizer $C(z)$ is equal to the inverse of CIR. Even though H_k has a finite length, the inverse of H_k has an infinite length. This means the number of taps of the LE $\{c_k^j\}$ needs to be infinite.

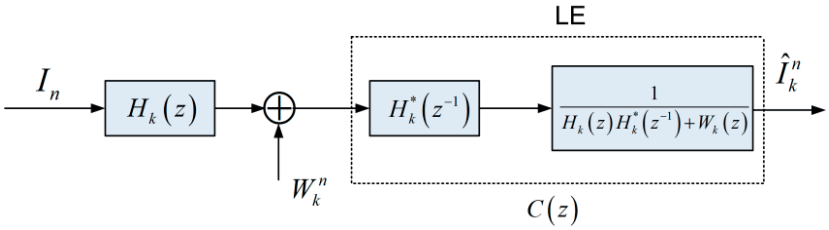

Figure 2.4. Block diagram of the LE using the MMSE criterion. $H_k(z)$ denotes the z transform of CIR H_k, $W_k(z)$ represents the z transform of noise W_k^n, and $z=e^{j\omega t}$. The equalizer $C(z)$ equals $1/H_k(z)$, when the channel is noiseless as $W_k(z)\neq 0$. Details of LE can be found in [3].

In practice, there are two limitations. First, there is no infinite filter, and the LE has a finite number of taps. Secondly, there is residual ISI and additive noise at the output, because in general there is noise in an oceanic environment as $W_k(z)\neq 0$. Due to multipath, UWA channels are frequency selective, and the spectrum of the received signal has components of small and large magnitude. When an LE attempts to invert the channel response, there is a noise exaggeration problem. In the process of inverting as shown in Figure 2.4, the noise $W_k(z)$ at the frequency components of small magnitude will be amplified greatly. Furthermore, $H_k(z)$ may have spectral nulls that cannot be

inverted at all. Consequently, errors are prone to occur in practice. A non-linear equalizer is an alternative.

2.2.3 Decision feedback equalizer

As a non-linear equalizer, a DFE generally has the form

$$\hat{I}_k^n = \sum_{j=-N_{ff}+1}^{0} a_k^j V_k^{n-j} + \sum_{j=1}^{N_{fb}} b_k^j \tilde{I}_k^{n-j} \tag{6}$$

where $\mathrm{a}_k = \left\{a_k^0, \ldots, a_k^{N_{ff}-1}\right\}^*$ and $\mathrm{b}_k = \left\{b_k^1, \ldots, b_k^{N_{fb}}\right\}^*$ are tap coefficient vectors for the feed-forward and feedback filters of respective lengths N_{ff} and N_{fb}, and $\tilde{I}_k^{n-j}$ represents a decided symbol which best matches the estimated symbol $\hat{I}_k^{n-j}$. Figure 2.5 shows the block diagram of a DFE. Comparing with the diagram of a LE shown in Figure 2.4, there is a feedback loop in which the filter $B_k(z)$ uses $\tilde{I}_k^n$ as input, and so the DFE is non-linear.

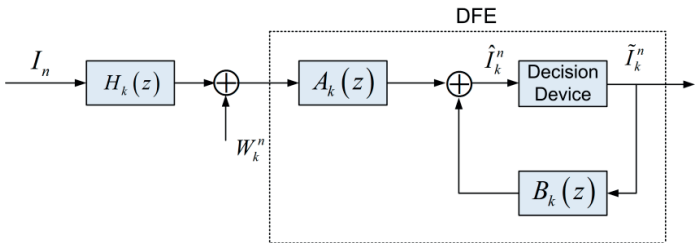

Figure 2.5. Block diagram of a DFE. W_k^n denotes additive noise, $A_k(z)$ and $B_k(z)$ represents the z transform of tap coefficients a_k and b_k for the feed-forward and feedback filters, respectively, where $z = e^{j\omega t}$.

Yang [15] has thoroughly discussed that a DFE is required by the channel physics—CIR. The values of b_k are uniquely determined by the CIR, and indeed N_{fb}=L-1 is required. Even though N_{ff} is independent of the CIR, a_k and b_k are interrelated. Assuming that previously detected symbols in the feedback filter are correct, the tap coefficients are obtained by minimizing output MSE

$$J_{mse}\left(\mathrm{a}_k, \mathrm{b}_k\right) = E\left(\left|I_n - \hat{I}_k^n\right|^2\right). \tag{7}$$

George et al. [47] have derived the fixed expression for a_k and b_k, where the DFE has obtained considerable better performance than the LE in numerical simulations. The computations for a_k and b_k assume that the CIR is known. However, CIR is always unknown in real communications, and moreover it is time variant. For instance, an UWA channel is not static due to environmental changes. In fact, the coefficients a_k and b_k are required to change with the channel variations. Therefore, an adaptive channel equalizer is considered for practical purposes.

The adaptive channel equalizer uses an adaptive algorithm to obtain the tap coefficients, which is required to invert the CIR. Take an adaptive DFE as example. In the beginning (training mode), training symbols are used by the adaptive algorithm to obtain the tap coefficients $\mathrm{a}_k[n]=\left\{a_k^n,\ldots,a_k^{n+N_{ff}-1}\right\}^*$ and $\mathrm{b}_k[n]=\left\{b_k^n,\ldots,b_k^{n+N_{fb}}\right\}^*$, where n indicates that the coefficients are time variant for each symbol. By minimizing the output MSE, the MMSE criterion, the adaptive algorithm converges to the tracking mode, when previous detected symbols are used to update $\mathrm{a}_k[n]$ and $\mathrm{b}_k[n]$ for the current estimate. In this manner, the adaptive equalizer recovers distorted information as well as tracks the channel variations. Two popular adaptive algorithms are introduced.

The least mean squares (LMS) algorithm is a widely used algorithm. See [9] for details. An important feature of LMS is simplicity. It neither requires measurements of pertinent correlation functions, nor requires matrix inversion. The rate of convergence is determined by the eigenvalue spread of the correlation matrix of input symbols. When the eigenvalue spread is large, the LMS algorithm slows down because it requires a large number of iterations for convergence, when the step-size is satisfied within the requirement. Although the step-size parameter is within the satisfied range, which is determined by the eigenvalue spread, its value also limits the rate of convergence. Usually, the eigenvalue spread is unknown beforehand in UWA communications, and a tentative small step-size is used to ensure convergence of the LMS algorithm. In this case, a slow rate of convergence is expected, and more training symbols are required. In practice, an adaptive algorithm that has a fast rate of convergence is preferred to track the channel variations.

The RLS algorithm has a fast rate of convergence, regardless of the eigenvalue spread of the correlation matrix [9]. This property makes the RLS algorithm attractive in UWA communications. In contrast to the LMS algorithm that aims to reduce the output MSE, the RLS algorithm recursively finds the tap coefficients that minimize a weighted linear least squares (LS) cost function relating to the input signals. The estimate of the DFE in Equation (6) can be rewritten in a vector form

$$\hat{I}_k^n=\left\{\mathrm{a}_k^*[n],\mathrm{b}_k^*[n]\right\}^H\begin{Bmatrix}V_k^n\\ \vdots\\ V_k^{n+N_{ff}-1}\\ \tilde{I}_k^{n-1}\\ \vdots\\ \tilde{I}_k^{n-N_{fb}}\end{Bmatrix}=\mathrm{w}_k^H[n]\mathrm{u}[n]. \tag{8}$$

For an adaptive DFE, the RLS algorithm jointly updates the tap coefficients for the feed-forward and feedback filters. Table 2.1 shows the iterations of the RLS algorithm for DFE, where λ is defined as the forgetting factor that is close to but less than 1. The smaller λ is, the smaller contribution of previous input samples, and this makes the RLS algorithm sensitive to recent input samples. The RLS algorithm has an order of magnitude faster rate of convergence than the LMS algorithm only when the input SNR is high. The superior properties of the RLS algorithm can be found in [9]. Thus the RLS algorithm is used in this thesis.

Since the CIR is usually unknown, N_{ff} and N_{fb} are often selected in an *ad hoc* manner. It is infeasible to optimize the number of taps without the information of the CIR. In practice, an adaptive DFE often does not converge due to an impropriate selection of N_{ff} and N_{fb}, despite whether the RLS algorithm is used or not. This problem is prominent in the scenario of a single hydrophone. One of the main reasons is that noise is exaggerated by the DFE when there are spectral nulls.

Table 2.1. Iterations of the RLS algorithm for a single channel DFE.

Initialize the RLS algorithm by setting

$\mathrm{P}[n] = \delta^{-1}\mathrm{I}$, δ = a small constant

$\mathrm{w}_k[n] = 0$,

For each instant of time, $n = 1, 2, \ldots$, compute

$$\mathrm{q}[n] = \frac{\lambda^{-1}\mathrm{P}[n-1]\mathrm{u}[n]}{1+\lambda^{-1}\mathrm{u}^H[n]\mathrm{P}[n-1]\mathrm{u}[n]}$$

$$\alpha[n] = I_n - \mathrm{w}_k^H[n-1]\mathrm{u}[n]$$

$$\mathrm{w}_k[n] = \mathrm{w}_k[n-1] + \mathrm{q}[n]\alpha^*[n]$$

$$\mathrm{P}[n] = \lambda^{-1}\mathrm{P}[n-1] - \lambda^{-1}\mathrm{q}[n]\mathrm{u}^H[n]\mathrm{P}[n-1]$$

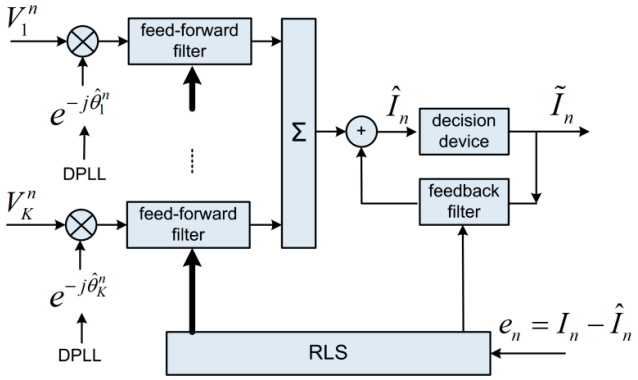

Figure 2.6. Block diagram of the adaptive McDFE. The RLS algorithm is used. $\hat{\theta}_k^n$ denotes the *n*th phase estimate from the DPLL at the *k*th receiving hydropone.

Stojanovic et al. [4, 5, 7] have proposed a multichannel DFE (McDFE), where multiple hydrophones are used by the receiver. The diagram of the McDFE is shown in Figure 2.6. In addition, the technique of a second order digital phase-locked loop (DPLL) for carrier-phase tracking has been proposed. The DPLL operates on a symbol-by-symbol basis. The purpose of the DPLL is to correct the phase rotations of input samples, which are caused by a carrier frequency shift. The frequency shift can be caused in two ways. One is the instrumentation, e.g. the small sampling frequency

difference between the transmitter and the receiver. The other is a frequency shift due to the Doppler effect. Without corrections, the McDFE is prone to fail to converge, as it fails to correct the phase variations as well as recover the distorted information. It is necessary to remove phase rotations caused by the frequency shift, and then the RLS algorithm updates the tap coefficients of the K-channel feed-forward filters and the feedback filter to remove ISI.

As introduced in Section 2.1, multiple hydrophones are preferred for use in UWA communications. There are few reports that analytically discuss the superior properties of a McDFE over a single channel adaptive DFE, but it is easily understood that spatial diversity is exploited in the process of multichannel combining. The obtained spatial diversity decreases the probability of noise exaggeration in reconstructing a distorted signal, since the number of spectral nulls is significantly reduced. Hence spatial diversity contributes robustness of the McDFE.

Comparing with the LMS algorithm, the disadvantage of the RLS algorithm is computational complexity. In Figure 2.6, the computational load becomes a drawback of the McDFE, as arithmetic operations for a McDFE are required on the order of $\{N_{ff}K+N_{fb}\}^2$ in each iteration. The number of taps of a McDFE is determined by the time spread of the CIR, and actually increases with the time spread. Under the same channel condition, the number of taps increases by one fold in doubling the symbol rate, as the density of taps needs to increase with an increased symbol rate. The computational load becomes intractable when the number of receivers is large, and it hinders the implementation of the McDFE.

2.3 Communications using PPC processing

With the purpose of reducing the computational complexity of channel equalizations, PPC processing has been implemented in UWA communications [48, 49] in which one receiving hydrophone is used. PPC processing can be treated as matched filtering the CIR [3], as it coherently recombines multipath arrivals. With multiple receiving hydrophones, TR communications are realized using PPC processing [13, 18, 22]. In this subsection, we introduce two receiver structures that use PPC processing.

2.3.1 TR communications

TR focusing is based on back-propagation in an acoustic waveguide that is rich in reflections and refractions. It refocuses time delayed arrivals, so the time spread is significantly reduced. TR communications take advantage of the focusing to mitigate ISI, and afterwards a channel equalizer of reduced complexity removes residual ISI to recover the transmitted information. The focusing can be understood in two aspects: (1) temporal focusing, and (2) spatial focusing. Temporal focusing is determined by independent time delayed arrivals, and thus the rate of channel variation (i.e. temporal coherence) determines the time duration of temporal focusing. Spatial focusing originates from spatial diversity [50], and hence physical conditions of the medium, e.g. reflections and refractions, determines the tightness of spatial focusing.

TR focusing can alternatively be interpreted as matched-field processing, when the sound field (the channel information) in a water column is sampled by multiple independent hydrophones. It is assumed that the channel information is flawlessly

obtained by a large number of hydrophones, the focusing function noted as the *Q*-function behaves like a *sinc* function [15], whose main lobe width is determined by the signal's bandwidth. This physical limitation explains that ISI cannot be eliminated by TR focusing. Since UWA channels are time variant, the focusing degrades with time. Following the focusing, an adaptive channel equalizer is required to remove residual ISI as well as track channel variations.

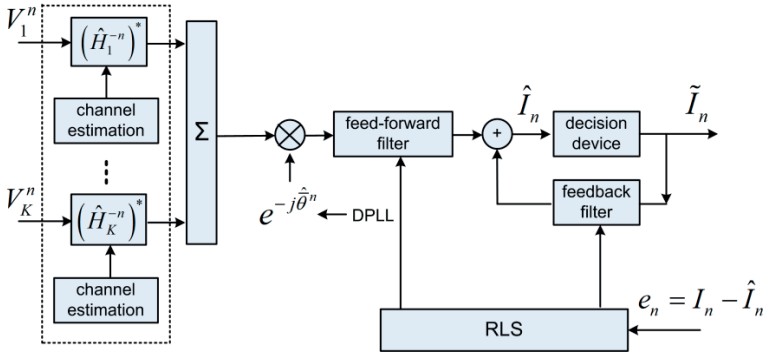

Figure 2.7. Block diagram of TR receiver structure PPC-DFE. The RLS algorithm is used. $\left(\hat{H}_k^{-n}\right)^*$ denotes the conjugation of time reversed CIR estimate at the *k*th receiving hydrophone.

Figure 2.7 shows the block diagram of the TR receiver structure—PPC-DFE. The focusing is obtained by multichannel combining of the output of PPC processing in *K* independent receiving channels, and subsequently one channel adaptive DFE is implemented to remove residual ISI, when one DPLL is used for carrier-phase synchronization. The DPLL compensates an averaged frequency shift of the *K* channels. The configuration of the DPLL is thoroughly introduced in [51]. In the process of TR focusing, temporal focusing is realized by PPC processing, and spatial focusing is simply obtained by equal-weighted multichannel combining. The TR focusing mitigates ISI significantly, and the complexity of the subsequent DFE is reduced [23]. For instance, Zhang et al. [52] have demonstrated successful communications using PPC-DFE with N_{ff}=2 and N_{fb}=1, where the feed-forward and feedback filters span only one symbol interval, respectively. Comparing the structure of the McDFE shown in Figure 2.6, PPC-DFE achieves UWA communications with reduced complexity. In Figure 2.7, it is shown that spatial diversity is exploited in the process of multichannel combining.

There are sidelobes in each individual pulse compression that is obtained by PPC processing. The peak-to-sidelobe ratio is determined by the CIR. The ratio can be increased by spatial focusing, when spatial diversity is exploited. The CIRs are independent at the *K* hydrophones, so sidelobes of the *K* pulse compressions are uncorrelated. In the process of multichannel combining, main lobes of the pulse compressions are coherently summed, and the uncorrelated sidelobes are averaged. Consequently, the peak-to-sidelobe ratio is enhanced to suppress ISI [14, 22, 30], when spatial diversity contributes the tightness of the TR focusing.

In a real oceanic environment, there are unpredictable interchannel correlations that impact the spatial focusing. The spatial gain obtained by PPC-DFE is reduced due to the

loss of spatial diversity. Stojanovic [53] has developed a model that predicts the upper bound of the performance of TR communications. In practice, the model is inadequate to evaluate real performance of the PPC-DFE, as it neglects the spatial coherence. At present, there is no model which adequately predicts the spatial coherence in a real oceanic environment [29]. Zhang et al. [30, 52] have shown measurements of time variant spatial coherence in field experiments, where the coherence was measured every two minutes. In Section 4.1, snapshots of spatial coherence measured every 2 s show that fast variations of spatial coherence occurred in the trial.

With a small number of receivers, up to 11, Yang [15] has shown that the McDFE outperforms the PPC-DFE in both numerical simulations and real data processing. Zhang et al. [30] have also demonstrate that the McDFE achieves superior performance, in which 18 data packets in total were transmitted within 50 min. The adaptive multichannel combining is advantageous in exploiting spatial diversity. Thus the TR receiver structure PPC-DFE is modified.

2.3.2 Joint PPC with a McDFE

With the purpose to obtain spatial gain by adaptive multichannel combining, an alternative receiver structure which also takes advantage of PPC processing is presented. Figure 2.8 shows the block diagram of joint PPC with a McDFE which is referred to as PPC-McDFE. Following PPC processing in K individual channels, a subsequent McDFE is implemented to remove residual ISI. The aim of PPC processing is to reduce the complexity of a subsequent McDFE, as the number of taps is decreased because of pulse compression. Note that the major difference between PPC-DFE and PPC-McDFE is the scheme of multichannel combining. Performance difference has been observed in the trials [30-33, 52], where PPC-DFE achieves the poorest performance. In [52], with the same condition of one DPLL, N_{ff}=2 and N_{fb}=1, PPC-McDFE outperforms PPC-DFE. The performance differences originate from spatial diversity gains obtained by the two different multichannel combining methods. The experimental results show that the adaptive multichannel combining is advantageous to make use of spatial diversity.

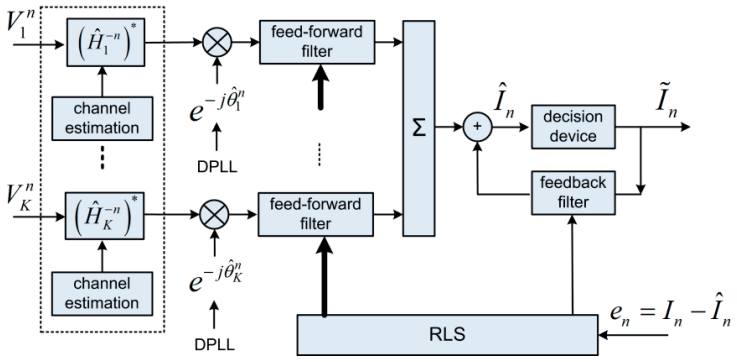

Figure 2.8. Block diagram of PPC-McDFE. The RLS algorithm is used. There are K DPLLs that track carrier-phase.

PPC processing requires knowledge of the channel, namely the CIR, which can be obtained by either a channel probe signal or training symbols. Using the channel probe

signal, the received probe signal is immediately used for PPC processing, and this method has been used in our trials [30, 52, 54-56] for its simplicity. For the latter method, a short sequence of known symbols is sent prior to the sequence of communication symbols, when the CIR is estimated at the receiver using the known preamble symbols. There is an obvious advantage of flexibility in choosing an estimation method. Regardless of which method is used to obtain the channel characteristics, pulse compression namely temporal focusing degrades with time in time-variant UWA channels, as the CIR is only estimated in the beginning of a communication packet.

The idea proposed by Flynn et al. in [18, 19] is to update the channel information every symbol interval when PPC processing is performed. The frequent updating increases the computational load, even though an LSQR algorithm is suggested. Song et al. [28] has proposed a block-based approach for PPC-DFE implemented in time-varying channels. The channel is assumed constant within each block of a short time interval. In the current block, the channel estimation used for PPC processing is obtained using detected symbols of the previous block. As understood, the block-based approach avoids the degradation of temporal focusing by updating the CIR every block. Obviously, it can also be implemented for PPC-McDFE. See [33, 35] for details.

Regarding the estimation methods when training symbols are used for PPC processing, the classical method of LS is popular for its simplicity, and the matching pursuit (MP) algorithm [37, 57] is promising in sparse channels. At high frequencies, UWA channels are often sparse, when there are only several dominant multipath arrivals spanning within time spread. The LS method estimates the CIR within a preset time interval. In sparse channels, it introduces noise-like estimations between dominant arrivals, while the MP algorithm only estimates the dominant arrivals and treats the others as zeros. The MP algorithm has been demonstrated for high-frequency TR communications in a sparse channel [36]. In this thesis, it has been thoroughly assessed for PPC-McDFE in both the conventional one-block approach [32] and a multi-block approach [33], and unpublished results are shown in Section 4.3.

At the high-frequency regime (10-14 kHz), several field experiments have been carried out in Trondheim harbor, when the received waveforms were recorded for offline data processing in the laboratory. Experimental configuration details and results can be found in published papers [30-35, 38-39, 52, 54-56].

Chapter 3

Field Experiments

In this chapter, major field experiments conducted in the last two years are briefly reviewed, and general experimental setups and selected instruments are introduced. We start reviewing the experiments in Section 3.1. NTNU's research vessel R/V Gunnerus is introduced in Section 3.2, as the vessel played a significant role in the experiments. Section 3.3 shows selected instruments and devices, including an acoustic projector and receiving arrays.

3.1 Experimental setups

Figure 3.1 shows an overview of the experimental locations in Trondheim harbour. In this area, the sea depth indicated by the blue colour changes from tens of meters to about 400 m. In these experiments, a cross receiving array (CRA) denoted by the black dot was near-shore deployed in shallow water less than 10 m, and an omni-directional transducer denoted by other coloured dots was suspended at various depths by NTNU's research vessel R/V Gunnerus. Table 3.1 gives a list of general setups at each experimental location, including trial dates, source depths and Tx-Rx ranges are shown. However, details of the trials, e.g. the communication method, are presented in published papers.

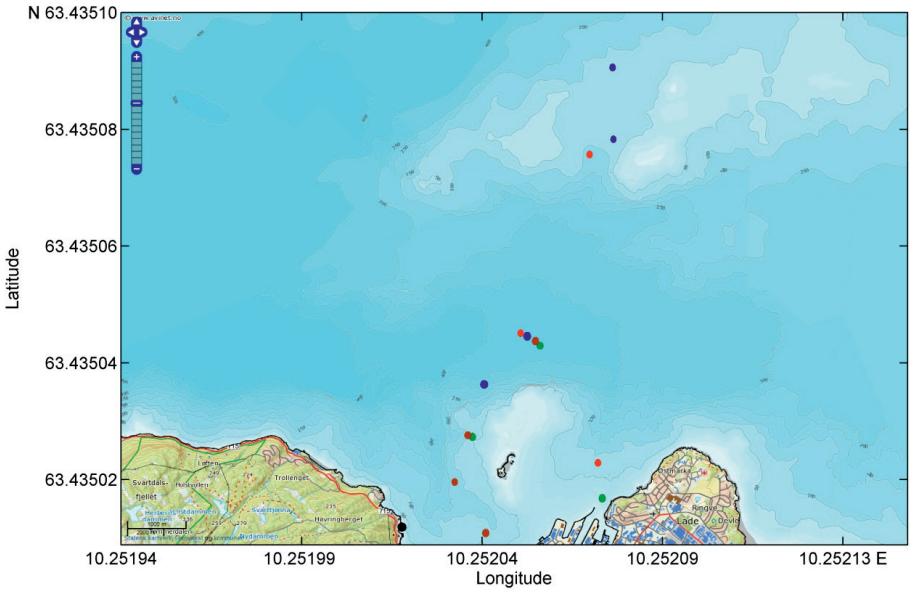

Figure 3.1. Overview of the experimental locations in Trondheim harbor. The locations are denoted by the colored dots. The black dot denotes the receiving array deployed at Trondheim Biological Station, and the others denote the acoustical source locations. The dates of experiments are shown by colors as: 30th June 2010 (●), 9th September 2010 (●), 16th June 2011 (●), and 7th September 2011 (●). Map of courtesy of Fylkesatlas Sogn og Fjordane (http://www.fylkesatlas.no).

Table 3.1. List of major field experiments conducted between 2010 and 2011. Tx denotes transmitter and Rx denotes receiver.

No.	Date	No. of Rx Channels	Tx-Rx Range (km)	Tx Depth (m)	Symbol Rate (kilosymbols/s)
A	30th Jun. 2010	10	1.0	20	1.0
B	30th Jun. 2010	10	2.0	20	1.0
C	30th Jun. 2010	10	4.0	20	1.0
D	30th Jun. 2010	10	1.5	20	1.0
E	9th Sep. 2010	10	2.0	20	0.5, 1.0, 2.0
F	9th Sep. 2010	10	3.7	20	0.5, 1.0, 2.0
G	9th Sep. 2010	10	4.0	20	0.5, 1.0, 2.0
H	16th Jun. 2011	10	3.0	40	1.0, 2.0
I	16th Jun. 2011	10	4.0	10, 20, 40	1.0, 2.0
J	16th Jun. 2011	10	8.0	45	0.5, 1.0, 2.0
K	16th Jun. 2011	10	10.0	20	0.25, 1.0, 2.0
L	7th Sep. 2011	12	3.4	40	2.0, 2.0
M	7th Sep. 2011	12	3.7	40	1.0, 2.0
N	7th Sep. 2011	12	7.4	20, 40	1.0, 2.0

A block diagram of experimental configurations is shown in Figure 3.2. The diagram illustrates how the experiments listed in Table 3.1 were carried out. First, random binary information generated by MATLAB was used as the source information. Digital modulations and file conversions were conducted using MATLAB. Finally, the communication signals were saved as audio files of Microsoft WAVE format. The audio files were transferred to the instrument Sound Devices 722 [58], which played the audio files through the line out connection. The electrical signals provided by line out were power amplified, and then the amplified signals entered into an omni-directional broadband projector, which converted the electrical signals into acoustic signals. Usually each packet of the communication signals was repeatedly transmitted for several times in one trial. In order to avoid random delays that occurred during the playback, all the periodic signals were saved as a single audio file that was transferred into the internal memory of Sound Devices 722. In order to maximize the output of each trial, the audio file covered different modulations, e.g. BPSK, QPSK, and others, and different symbol rates. Communication signals of different data rates were sent through real oceanic channels, and received waveforms were recorded for offline analysis in the laboratory.

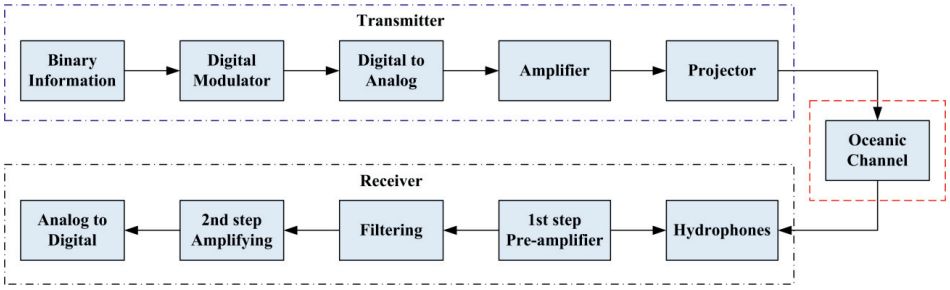

Figure 3.2. Block diagram of experimental configurations.

On the receiving side, the instrumentation method of two-step amplifying was designed for data acquisitions. The output signals from hydrophones were pre-amplified for subsequent filtering, as the electrical signals from hydrophones were weak. During the 1st step amplifying, there is low-frequency noise and the amplifying ratio has to be set with care. For example, a small ratio is suitable for a large range of input analog signals. Otherwise, overloading might appear during amplifying. The filtering process removed ambient noise, e.g. the noise generated by sea surface waves. Since most ambient noise was low-frequency noise, high-pass or band-pass filters worked well to exclude the noise interference for quantizing. In order to well satisfy the range of quantizing during recording of the electrical signals, e.g. from -5 volts to +5 volts, the filtered signals were amplified again (the 2nd step amplifying) as shown in Figure 3.2. With multiple receivers in the experiments, multichannel amplifiers and filters were used. The received waveforms were recorded by the digitizing devices. Afterwards, the collected data were offline processed and analyzed in the laboratory.

3.2 R/V Gunnerus

NTNU's research vessel, R/V Gunnerus [59] shown in Figure 3.3, was put into operation in spring 2006. The ship is fitted with a dynamic positioning system, and

equipped with the latest technology for a variety of research activities within biology, geology, archeology, oceanography and fisheries research. For example, conductivity-temperature-depth (CTD) profiles can be measured. In addition, the ship is also used for educational purposes and is an important platform for marine courses at all levels and disciplines.

Figure 3.3. NTNU's R/V Gunnerus.

Table 3.2. Main dimensions of R/V Gunnerus.

Length over All (m)	31.25
Length between Perpendiculars (m)	28.9
Length in Waterline (m)	29.9
Breadth Middle (m)	9.6
Breadth Extreme (m)	9.9
Depth mld. Main deck (m)	4.2
Draught, mld. (m)	2.7
Mast Height / Antenna (m)	19.7
Dead Weight (ton)	17

The diesel electric system of R/V Gunnerus has been specially designed for low UWA noise levels to accommodate testing and development of UWA equipment. The vessel is arranged with a wet lab, a dry lab and a computer lab in addition to a large aft deck. The main dimensions are given in Table 3.2, and other specifications can be accessed on the website [59]. For practical purposes in the experiments, the omni-directional acoustic projector was suspended from R/V Gunnerus. In order to avoid drifting, the dynamic positioning system was always activated to during the trials of UWA communications.

3.3 Instruments and Devices

Selected instruments and devices used in the trials are briefly introduced in this subsection.

3.3.1 The omni-directional projector

It is practical that operationally convenient to use an omni-directional acoustic source in field experiments. Otherwise it becomes inconvenient to use a rigid rack for mounting a directional acoustic projector, especially deploying a projector at depths of tens of meters. In the first half of 2009, two horizontal omni-directional projectors were purchased from the manufacturer Chelsea Technologies Group (CTG) [60]. The technical specifications are given in Table 3.3, and those filled our requirements in the research. The transmit response is shown in Figure 3.4; a carrier frequency of 12 kHz was used in all the experiments. The acoustic projector is approximately omni-directional as indicated by the vertical beam pattern shown in Figure 3.5.

Table 3.3. Technical specifications of projector CTG1330.

Nominal Resonant Frequency	8 & 12 kHz
Transmit Sensitivity	139 dB re 1 µPa/V @ 1 m @ 12 kHz
Pressure Output for 1Vrms	8.9×106 µPa/V @ 1 m
Receive Sensitivity	-170 dB re 1V/ µPa @ 10 kHz
Useable Frequency Range	6-20 kHz
Horizontal Beam Pattern	Omni-directional (± 1 dB)
Vertical Beam Pattern	Hemispherical (± 1 dB)
Dimensions (length/diameter)	74/108 mm
Operating Depth	Full Ocean Depth

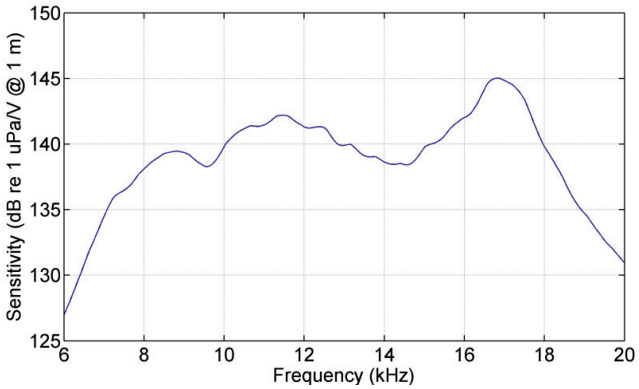

Figure 3.4. Tuned transmit response measured by CTG.

An omni-directional source is suitable for the concept of sensor networks, where the sensor nodes are supposed to be easily deployed in an area. In the aforementioned experiments, the projector from CTG was suspended by R/V Gunnerus using a nylon rope as shown in Figure 3.6. A 10 kg weight was attached to the projector in order to reduce drifting caused by waves and currents. However, it was hardly to keep the projector at the intended depths due to the drifting.

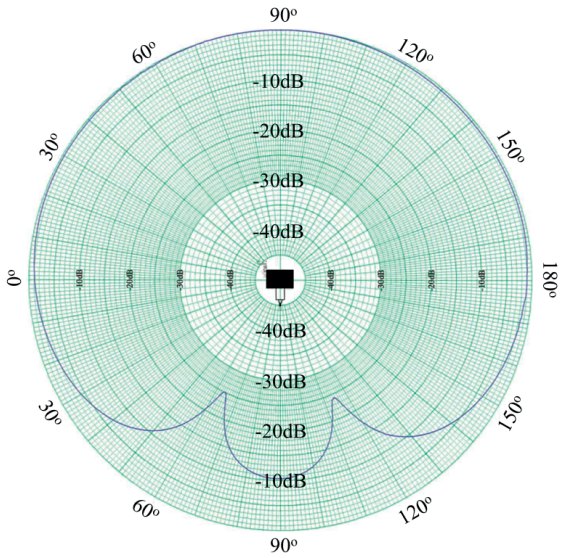

Figure 3.5. Vertical beam pattern given by CTG (at a frequency of 10 kHz).

Figure 3.6. High-frequency broadband projector used in experiments.

3.3.2 The receiving arrays

Figure 3.7 shows one vertical receiving array (VRA) of 6 elements, which was acquired from CTG in June 2010. Technical specifications of the array are in Table 3.4. Figure 3.8 shows one hydrophone receive sensitivity, which satisfies our requirements for high-frequency communications. This array was manufactured without built-in charge amplifiers, and it requires external charge amplifiers prior to the 1st step filtering shown in Figure 3.2.

Figure 3.7. The vertical array of 6 elements (2255-004-PD).

Table 3.4. Technical specifications of the VRA (2255-004-PD).

Array Length (m)	5
No. of Elements	6
Element Spacing (m)	1
Operating Depth (m)	0-100
Orientation	Vertical
Hydrophone Tx Sensitivity	151 dB re 1 µPa/V@1 m@ 105 kHz
Hydrophone Rx Sensitivity	-203 dB re 1 V/µPa @ 135 kHz
Voltage Output	$0.56 \times 10^{-10} V_{rms}$ for 1 µPa
Useable Frequency Range	1-150 kHz
Maximum Input Voltage	300 V_{rms} (cable limit)
Maximum Input Power	14 W
Maximum Acoustic Input Level	182 dB re 1 µPa @ 1m

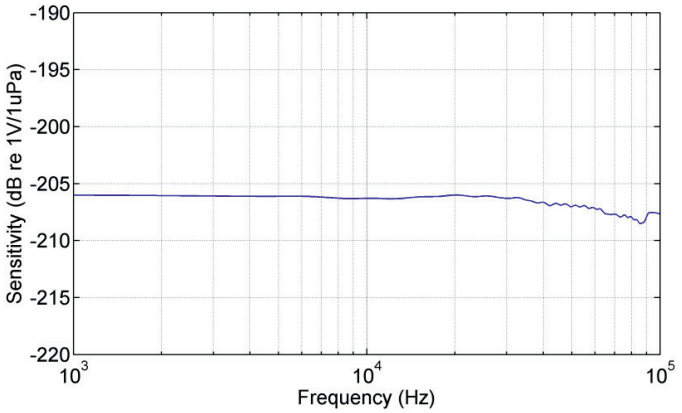

Figure 3.8. Hydrophone receive sensitivity given by CTG (from 1 kHz to 100 kHz).

Usually, careful calibrations are required to achieve good matching between the VRA (2255-004-PD) and available charge pre-amplifiers. This array was used in the trials conducted in 2010 and June 2011. In experience, it is quite difficult to optimize the matching without facilities for the calibrations, as there were no factory calibrations due to the small purchasing budget. In September 2011, three arrays with built-in charge pre-amplifiers were acquired by the laboratory.

The three arrays were manufactured by CTG to fulfil our requirements for UWA research in the scenarios of both shallow and deep waters. Each array of different cable lengths consists of 8 hydrophones with element spacing of 1 m. Table 3.5 shows the technical specifications. One representative hydrophone's receive sensitivity is shown in Figure 3.9, which was calibrated by Wraysbury Open-Water Facility run by the National Physics Laboratory, UK. The flat frequency range (from 10 kHz to 20 kHz) fills our requirements of testing UWA communications. The built-in pre-amplifiers perform the 1st step amplifying, and they reduce the complexity of instrumentation. One array of 50 m cable length was used in the trial conducted in September 2011. An RME OctaMic II [61] multichannel pre-amplifier was used for the 2nd step amplifying.

Table 3.5. Technical specifications of the VRA (2255-013-HB).

Array Length (m)	7
No. of Elements	8
Element Spacing (m)	1
Operating Depth (m)	0-150
Orientation	Vertical
Hydrophone Differential Rx Sensitivity	-160 dB re 1 V/μPa @ 10 kHz norminal
Preamplifier Gain	46dB nominal
Nominal Resonant Frequency	110 KHz
Useable Frequency Range	0.01 - 150 kHz
Linear Frequency Range	0.1 - 20 kHz
Power Supply	± 12 V
Maximum Output Signal	3 V_{rms}(differential into 100 Ohms)
Maximum Acoustic Input Level	170 dB re 1 μPa @ 1 m @ 10 kHz

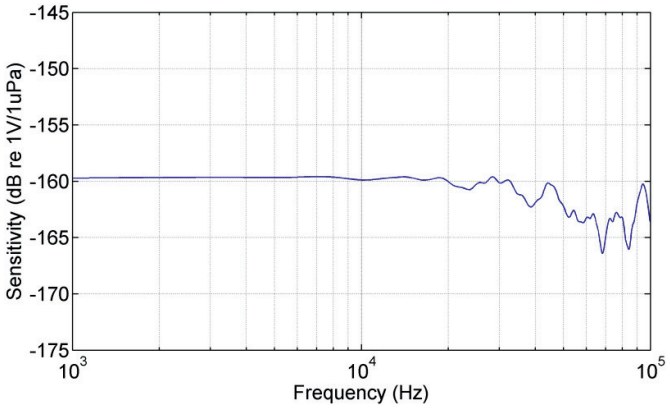

Figure 3.9. Hydrophone receive measured by Wraysbury Open-Water Facility.

In the experiments a vertical receiving array and one horizontal receiving array (HRA) of 4 hydrophones were deployed at a depth of 4.5 m. The two arrays formed a cross receiving array. The HRA shown in Figure 3.10 was assembled in the laboratory. It consisted of 4 hydrophones with 1.5 m element spacing, with the hydrophones mounted on a rigid steel rod. In Figure 3.1, the bathymetry shows that there are 3-D effects in this area. Hence, the CRA was used to exploit spatial diversity, which will be discussed in Chapter 4.

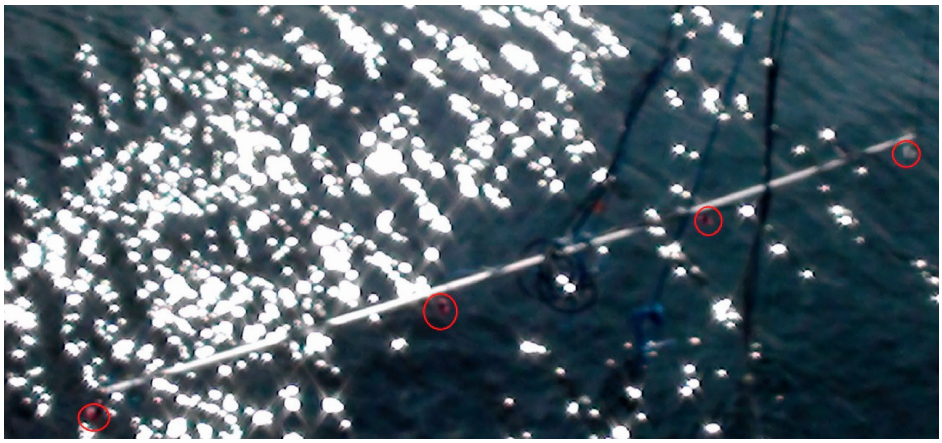

Figure 3.10. HRA of 4 hydrophones. Positions of hydrophones are shown in the red cycles.

3.3.3 Data acquisition devices

Data acquisition is the process of sampling electrical signals from sensors and converting the samples to digital values. In this thesis, data acquisition devices were used to record received waveforms from hydrophones, and the field measurement data were saved on a hard disc. Considering the cost of ship time, the digital data were offline processed in the laboratory. An RMEs Fireface 400 [62] was used as an external sound card for data recording in the experiments. The Fireface 400 is controlled by software executed on a PC, e.g. *Adobe Audition* 3.0 (see Figure 3.11). In the trials, collected data were saved as the format of Microsoft WAVE in the internal disc of the PC or an external hard disc using *Adobe Audition* 3.0. There are other different user-friendly and free software that can be selected. However, the sampling rate is limited by the data transmission rate limitation between the devices and the PC, and Fireface 400 offers only 10 analog input channels in maximum.

Figure 3.12 shows a 32-channel data acquisition system. This system was designed and completed by the UWA laboratory of NTNU for UWA research. The system includes 32-channel filters, 32-channel pre-amplifiers, and a multichannel data logger. The data logger is built on National Instruments Corporation's PXI platform, which provides possibilities of 32-channel data logging at a high sampling rate. A graphic user interface (GUI) was developed using LabView, which is provided by National Instruments Corporation. In Figure 3.13, a 12-channel data logging GUI is shown. The application was developed by the author, and it was successfully used in the experiments conducted in 7th September 2011. In addition, a 32-channel application

was also developed. With the GUIs, there is flexibility to select parameters in data acquisition, such as, quantizing range, sampling frequency, and so on. There are sub-windows which provide real time observations of waveforms of 100 ms and display of the magnitude of spectrum. These observations help users to adjust the parameters for data logging, e.g. the 2nd step pre-amplifying ratio.

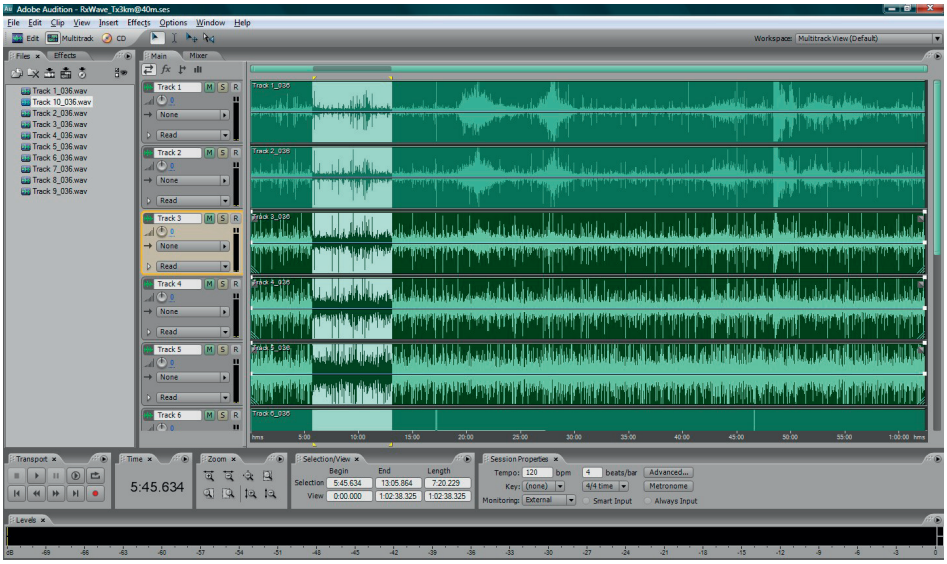

Figure 3.11. Data acquisition using *Adobe Audition* 3.0.

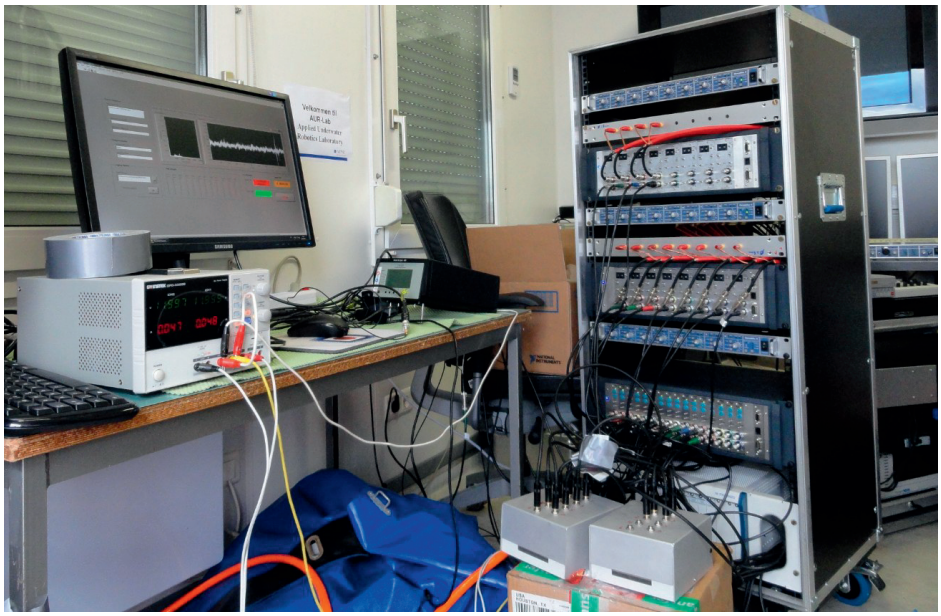

Figure 3.12. 32-channel data acquisition system completed by the UWA laboratory.

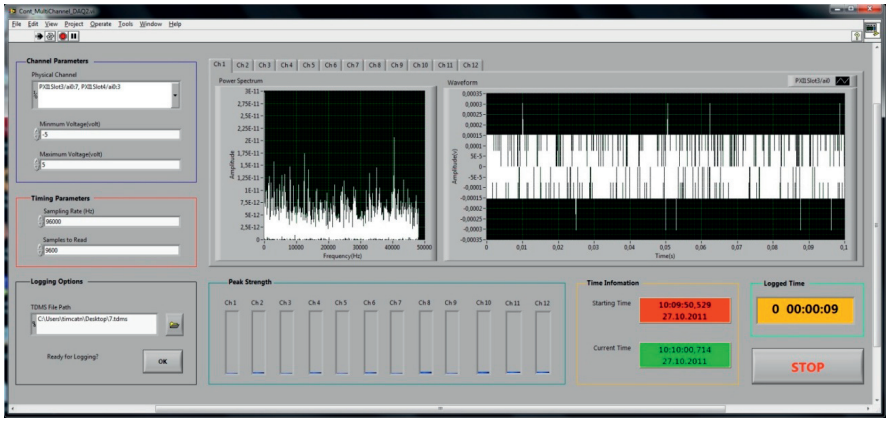

Figure 3.13. GUI of 12-channel data logging.

Field experiments help develop in depth understanding UWA communications, and also provide invaluable experiences for how to carry out a research project. In the field trials, crews of R/V Gunnerus and well-organized participants were required to provide technical support and valuable help. Figure 3.14 shows the participants in the trial conducted on 30th June 2010. Unfortunately, in this thesis, there is not enough space to show all of them who had participated, but it does not mean that their help is not appreciated.

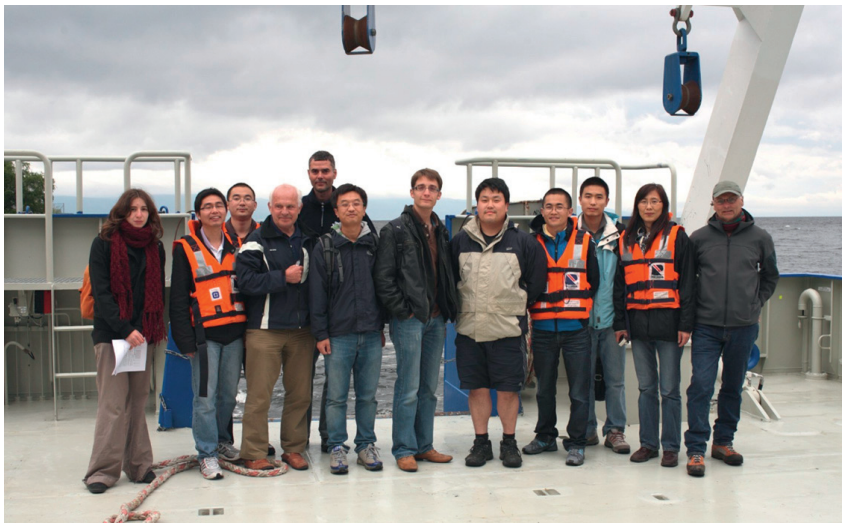

Figure 3.14. Participants of the trial conducted on 30th June 2010. They are (from the left): [a] Mailys Pache, [b] Ganpan Ke, [b] Zhongxi Chao, [c] Jens M. Hovem, [d] P. A. van Walree, [b] Yan Jiang, [a] Charlie Galle, [e] Tim Cato Netland, [b] Guosong Zhang, [b] Qin Liu, [c] Hefeng Dong, and [c] Ulf Kristiansen. [a] Visting master student. [b] NTNU Ph. D. candidate. [c] NTNU Professor. [d] Norwegian Defence Research Establishment researcher. [e] NTNU technical engineer.

Chapter 4

Results and Analysis

This chapter presents results and analysis in three aspects. In Section 4.1, exploitation of spatial diversity with a CRA is discussed. Section 4.2 discusses temporal diversity to demonstrate the advantage of PPC processing. Section 4.3 investigates the MP algorithm that exploits channel sparsity for PPC processing. Unless otherwise specified, note that parameters required by the receiver structures are fixed in processing all the data collected at each location, and the over sampling rate is 2, namely 2 samples per symbol.

4.1 Spatial diversity

Spatial diversity in the water column can be exploited by multichannel signal processing [3]. The trial introduced in [30] was conducted over a range of 4 km on 30th June 2010, where the transmission period was 202.734 s. The collected data of BPSK modulation are first processed by the McDFE. In terms of output SNR calculated by (1-MSE)/MSE [3], Figure 4.1 shows receiver performance for different numbers of vertical receiving hydrophones. Best performance is obtained by the McDFE in all the 18-period data packets, when 6 receiving hydrophones are used. The McDFE frequently fails with 3 receiving channels, e.g. in the first 6 periods, while it achieves stable performance with 6 receiving channels. Obviously, the output SNR increases with the number of vertical receiving channels, because more spatial gain is obtained when more receiving hydrophones are used to exploit spatial diversity.

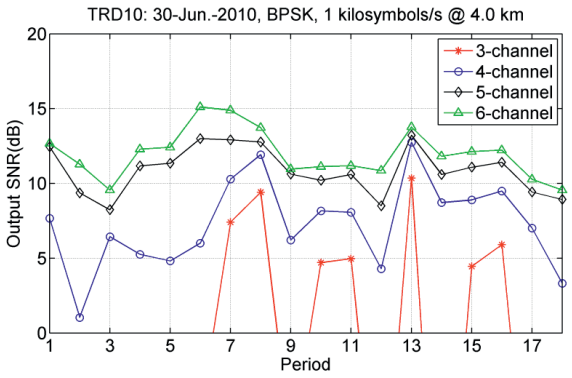

Figure 4.1. Receiver performance in terms of output SNR using different numbers of vertical receiving channels.

In the trials, there was also an HRA that consisted of 4 hydrophones. The basic reason for using the HRA was to exploit spatial diversity at the same depth, as the sound

field is 3-dimensional in the experimental area (see Figure 3.1). Figure 4.2 shows an example for which the performance of the McDFE is improved by using 4 additional receiving channels. In terms of output SNR, there is improvement of 5.1 dB, when the HRA is used together with the VRA. The number of bit errors is reduced from 24 to zero in a total of 15565 bits. In order to observe the improvement during the 50-min trial, the BPSK data of 18 periods are processed by the McDFE.

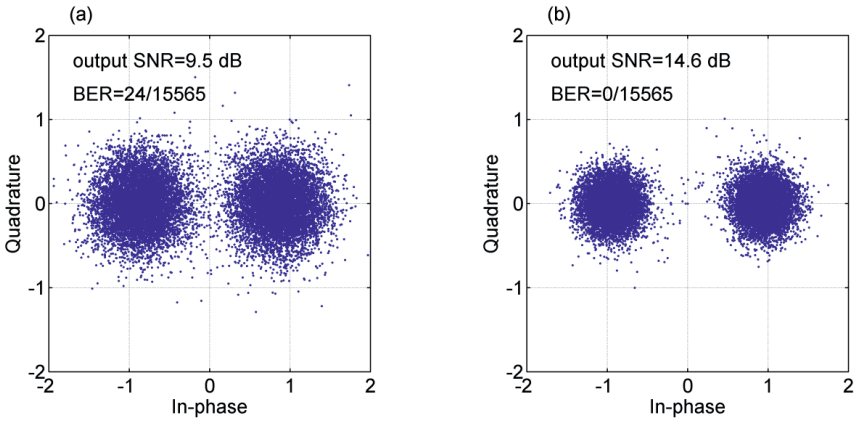

Figure 4.2. Scatter plot of the soft output of McDFE. (a) Only VRA is used (1-6 receiving channels). (b) Both VRA and HRA are used (1-10 receiving channels).

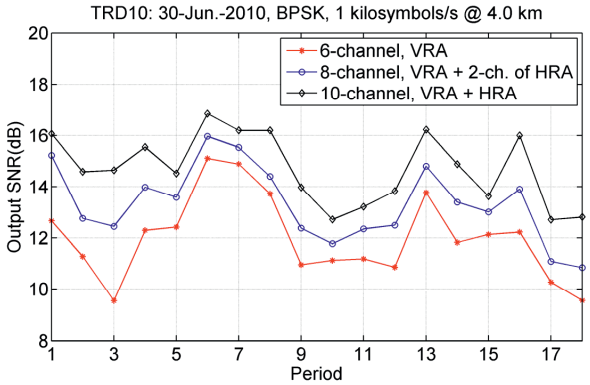

Figure 4.3. Receiver performance in terms of output SNR using different numbers of receiving channels.

Figure 4.3 shows performance using different numbers of receiving channels. Time-variant performance is observed in 18 periods (about 60 min), as the output SNR changes with transmission period. During this experiment, all the instrumental parameters were kept constant in recording the received waveforms. Hence the performance variations are caused by UWA channel variations. The output SNR increases with the number of receiving channels, and the best performance is obtained when both HRA and VRA are used. In detail, the performance improvement from an increased number of receiving channels changes with transmission period. Let us compare two scenarios as follows: only the VRA of 6 hydrophones is used; both the

VRA and HRA are used for a total of 10 hydrophones. In terms of output SNR, the highest improvement is 5.1 dB (the 3rd period), the lowest improvement is 1.5 dB (the 15th period), and the mean improvement is 2.7 dB. It is found that there was spatial diversity among the vertical hydrophones as well as the horizontal hydrophones at the receiving location; spatial diversity could be exploited by the McDFE.

The TR receiver structure is used to process the data collected in the trials conducted on 7th September 2011 [33]. Note that CIRs of 40 ms are estimated by the LS method for PPC processing. Figure 4.4 shows the performance improvement from using horizontal receiving channels, where all the vertical receiving channels were used. In Figure 4.4(a), the input SNR of the 10th period is quite low, when the PPC-DFE fails even though all the receiving channels are used. At the 3 locations, time-variant improvement is obtained by using different numbers of horizontal channels. For instance, in Figure 4.4(b), the maximal improvement is 3.0 dB (the 13rd period), and the minimal improvement is -0.3 dB (the 7th period). Apparently, the improvement increases with the number of horizontal receiving channels. Thus there was spatial diversity at the same depth, and the gain could also be obtained by the PPC-DFE.

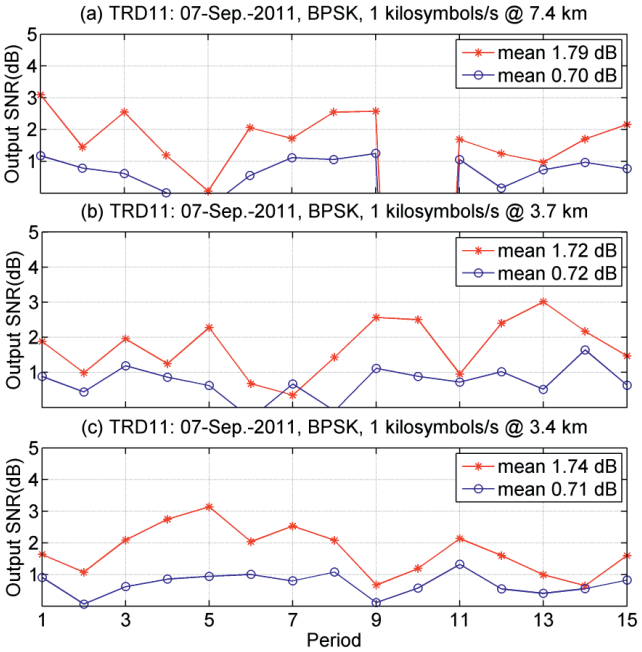

Figure 4.4. Performance improvement by using horizontal receiving channels obtained by the PPC-DFE at different distances. (a) 7.4 km. (b) 3.7 km. (c) 3.4 km. Two horizontal receiving channels are used (○), and four horizontal receiving channels are used (*).

The data used in Figure 4.4 are re-processed by the PPC-McDFE for comparison of its performance with that for the PPC-DFE. Figure 4.5 shows the improvement obtained by the PPC-McDFE increases with the number of horizontal receiving channels, as found for the PPC-DFE. In terms of mean improvement, when 4 horizontal channels are

used, the PPC-McDFE obtains greater improvement than the PPC-DFE. Zhang et al. [30, 33] have discussed the advantage of adaptive multichannel combining to make use of spatial diversity. Comparing the improvement obtained by the PPC-McDFE and PPC-DFE, there is consistency in each transmission. For instance, using 4 horizontal receiving channels in the 9th period, Figure 4.5(c) shows that the improvement is 1.7 dB for the PPC-McDFE, while correspondingly the improvement shown in Figure 4.4(c) for the PPC-DFE is 0.7 dB. As mentioned in Section 2.3, the differences originate from the two multichannel combining schemes.

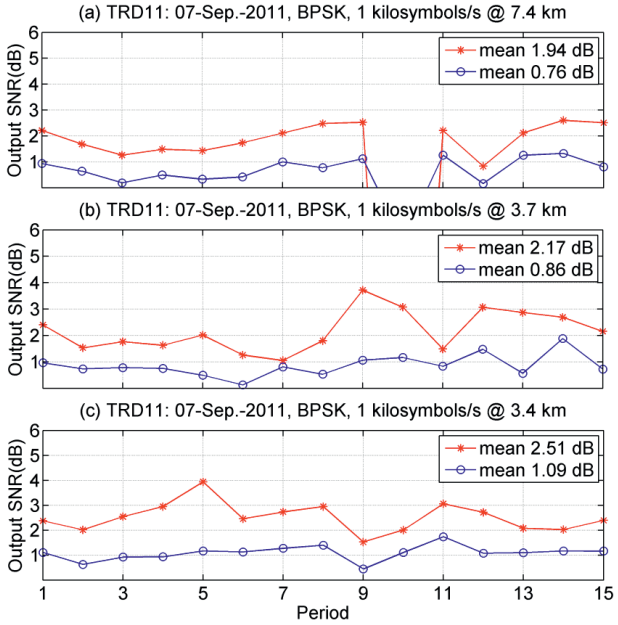

Figure 4.5. Performance improvement obtained by PPC-McDFE at different distances to the receiving array. (a) 7.4 km. (b) 3.7 km. (c) 3.4 km. Two horizontal receiving channels are used (○), and four horizontal receiving channels are used (*).

The results presented here show that the performance of the three receiver structures is improved by using the HRA. Therefore there was spatial diversity at the same depth. In the analysis as below, all receiving channels of the CRA are used.

The data used in Figures 4.4-4.5 were processed by the receiver structures, namely, the McDFE, PPC-McDFE and PPC-DFE. Figure 4.6 shows the performance comparison among the structures, and Table 4.1 gives statistics of the output SNRs shown in Figure 4.6. At the 3 locations, the McDFE displays the best performance in general, the performance of PPC-McDFE approximates that of McDFE, and PPC-DFE, the receiver structure of lowest complexity, displays the poorest performance. Again, the results demonstrate that it is advantageous to exploit spatial diversity using the adaptive multichannel combining scheme [31]. The performance difference between PPC-McDFE and PPC-DFE changes with transmission period. The differences are caused by time variant spatial diversity, which is influenced by interchannel correlations among the multiple receiving channels.

Table 4.1. Statistics of receiver performance in terms of output SNR.

Receiver Structure	7.4 km			3.7 km			3.4 km		
	Min	Max	Mean	Min	Max	Mean	Min	Max	Mean
	(dB)			(dB)			(dB)		
McDFE	2.2	19.6	11.4	7.8	13.4	10.2	8.2	17.3	12.0
PPC-McDFE	4.1	17.3	11.6	5.3	11.7	8.9	6.4	13.8	10.5
PPC-DFE	1.9	12.5	7.9	1.3	8.9	5.6	2.8	9.1	6.5

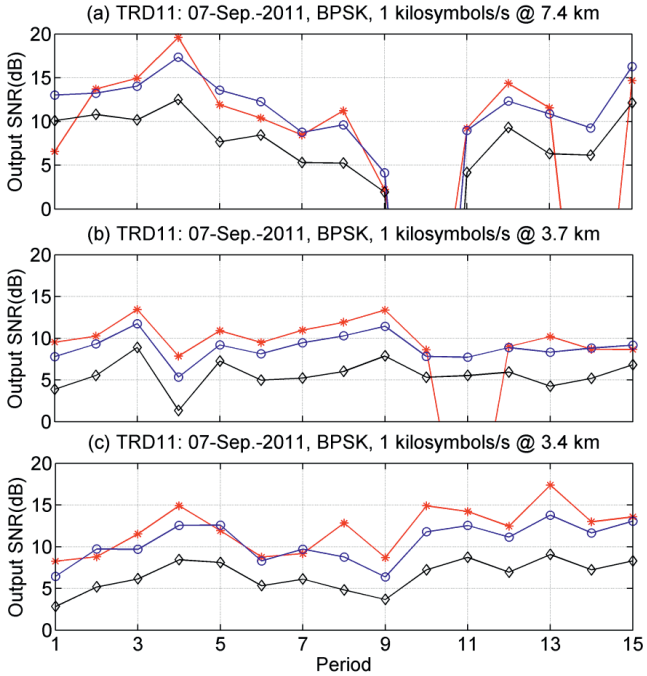

Figure 4.6. Receiver performance in terms of output SNR at different distances to the receiving array. (a) 7.4 km. (b) 3.7 km. (c) 3.4 km. The three receiver structures are McDFE (*), PPC-McDFE (○) and PPC-DFE (◊). For the McDFE, N_{ff}=40 and N_{fb}=5, correspondingly, the feed-forward filters span 20 symbol intervals. N_{ff}=8 and N_{fb}=2 are configured for both the PPC-McDFE and PPC-DFE, and the feed-forward filters span 4 symbol intervals.

Interchannel correlation is measured by spatial coherence, which is calculated by

$$\psi(k,m)=\frac{\left|r_k(-t)\otimes r_m(t)\right|_{\max}}{\sqrt{\left|r_k(-t)\otimes r_k(t)\right|_{\max}\left|r_m(-t)\otimes r_m(t)\right|_{\max}}}, \tag{9}$$

where $|r_k(-t)\otimes r_m(t)|_{\max}$ denotes the maximum absolute value of the correlation between $r_k(t)$ and $r_m(t)$, and $r_m(t)$ is the received signal at the mth hydrophone. In order to observe

the variations, spatial coherence is calculated at every second using Equation (9). Figure 4.7 shows 6 snapshots of the spatial coherence measurements. Even though the element spacing of 1m for the VRA is much larger than half wave length of the frequency 11 kHz, namely the lowest frequency of the broadband communication signals, there are high correlations among 8 vertical receiving channels. For instance, the correlation coefficient between the 6th and 7th hydrophones is 0.79 in Figure 4.7(a). There are also correlations among the four horizontal receiving channels, while there are weak correlations between the 12nd receiving channel and the other 11 receiving channels. The correlation strength among the 12 receiving channels changes with time. However, there is no determined pattern. As the array was deployed near the shore in water less than 10 m, which was different from the source depth of 20 m, time variant reverberation probably occurred due to complex reflections in this shallow water region.

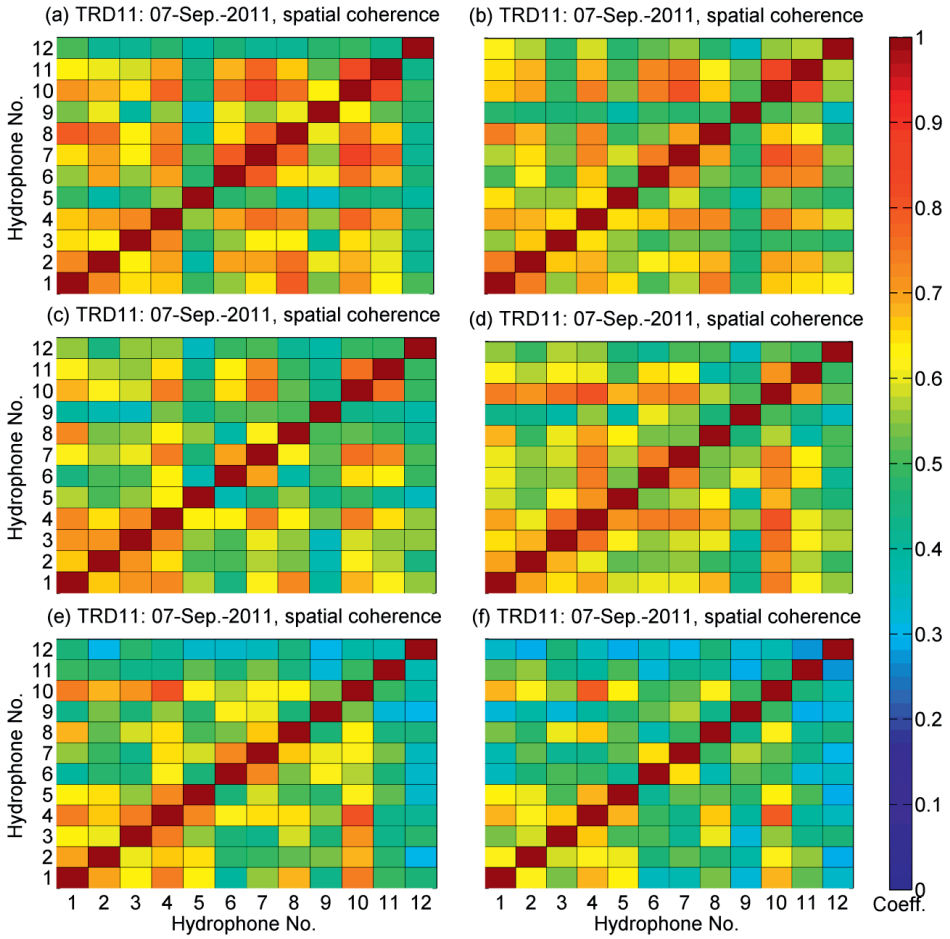

Figure 4.7. Spatial coherence measured at different time. (a) The 1st second. (b) The 3rd second. (c) The 5th second. (d) The 7th second. (e) The 9th second. (f) The 11th second. Hydrophones of No. 1-8 are the elements of the VRA, where No.1 denotes the deepest hydrophone. Hydrophones of No. 9-12 are the elements of the HRA.

Spatial coherence is calculated for a time interval of 15.565 s. Figure 4.8 shows 15 calculations at three distances to the receiving array, where $k = 8$ and m changes from 1 to 12. In this large time scale, time variant interchannel correlations are also observed. In Figure 4.8(a) and 4.8(c), high correlations are observed between the deepest and the shallowest receiving channels, namely the 1st and 8th hydrophones. It is surprising that there are high correlations between two receiving channels at a depth distance of 7 m. The array was deployed in the shallow water that extends about 200 m to the harbour (see Figure 1). The incoming acoustic energy attenuated in the shallow region, when there were severe reflections that resulted in complex interchannel correlations. There are no models that adequately predict time-variant spatial coherence in a real oceanic environment [29], and the measurements are consistent with this statement.

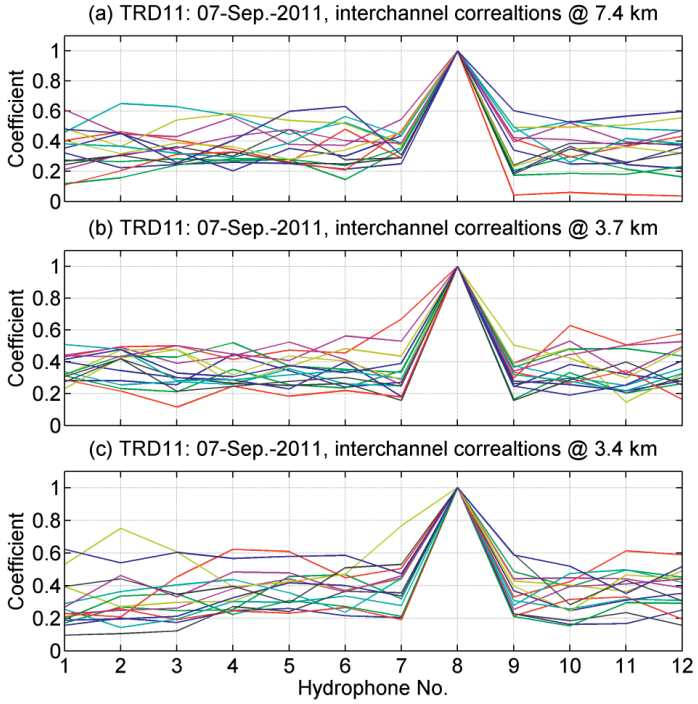

Figure 4.8. Interchannel coherence as a function of the receiver index measured at different distances to the receiving array. (a) 7.4 km. (b) 3.7 km. (c) 3.4 km.

For practical purposes, e.g. reduced instrumentation, it is preferred to make full use of spatial diversity with a small number of hydrophones. In long time spread UWA channels, the computational load of the McDFE grows with an increased number of taps, which is determined by the CIRs. Usually the number of taps is selected in an *ad hoc* manner, because it is impossible to specify the number of taps without knowledge about the channel. In the 14th period in Figure 4.6(a) and the 11th period in Figure 4.6(b), the McDFE failed in obtaining comparable performance. PPC-McDFE provides an alternative. Based on pulse compression in each individual channel, complexity of the subsequent McDFE is much decreased with a reduced number of taps. For instance, stable performance is obtained for all the periods with fixed configuration of N_{ff}=8 and

N_{fb}=2. The temporal diversity, embedded in the multipath arrivals, is exploited by the pulse compression.

4.2 Temporal diversity

Temporal diversity originates from time delayed arrivals which propagate along independent paths of different travel lengths. In UWA channels with multipath arrivals, there are possibilities to make use of temporal diversity. Obviously, the diversity could be obtained using rake receivers for spread spectrum communications [3, 63], where both the magnitudes and phases of the multipath components are required in order to achieve coherent combining. However, it is difficult to implement rake receivers for non-spread spectrum communications. Conventionally, temporal diversity is obtained in the process of removing ISI using adaptive channel equalizers.

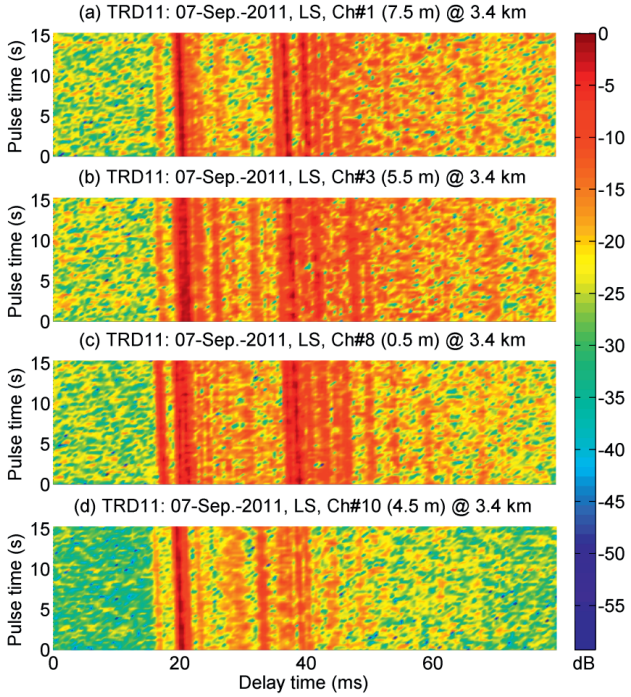

Figure 4.9. CIR as a function of time at four receiving channels. (a) The 1st channel at a depth of 7.5 m. (b) The 3rd channel at a depth of 5.5 m. (c) The 8th channel at a depth of 0.5 m. (d) The 10th channel at a depth of 4.5 m. The data were collected over a range of 3.4 km on 7th September 2011.

Figure 4.9 shows CIRs as a function of time in four selected receiving channels at 3.4 km range, where there are multiple time delayed arrivals in each receiving channel. Apparently, time spread of the multipath arrivals is about 25 ms in the 1st, 3rd and 8th channels, while it is about 20 ms in the 10th channel. The McDFE is used to process this transmission period, and Figure 4.10 shows the output MSE as a function of time. When N_{ff} is changed from 30 to 50, it means the feed-forward filters span from 15 ms to

25 ms, where there are two samples per symbol in base band signal processing. As seen in Figure 4.9, a group of dominant arrivals arrive within a time interval of 20 ms, for which the output MSE is reduced by 0.50 dB when the time span of the feed-forward filters is increased from 15 ms to 20 ms, namely N_{ff} is increased from 30 to 40, and less gain is obtained when N_{ff} is increased from 40 to 50. The output MSE is reduced with an increased time span of the feed-forward filters of the McDFE, as it exploits the temporal diversity during the equalizing process.

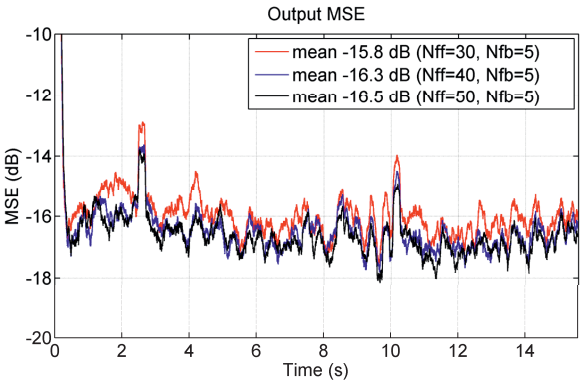

Figure 4.10. Output MSE obtained by McDFE with different numbers of taps for the feed-forward filters.

Figure 4.11 shows the performance in terms of output SNR. In 15 transmission periods, the output SNR is increased when N_{ff} is changed from 30 to 40, and trivial improvement is obtained when N_{ff} is further increased from 40 to 50. Without considering contributed arrivals, it is impractical to improve the performance by increasing the number of taps, at a cost of increasing the computational load; on the contrary, the level of numerical noise is increased thus degrading the performance [47].

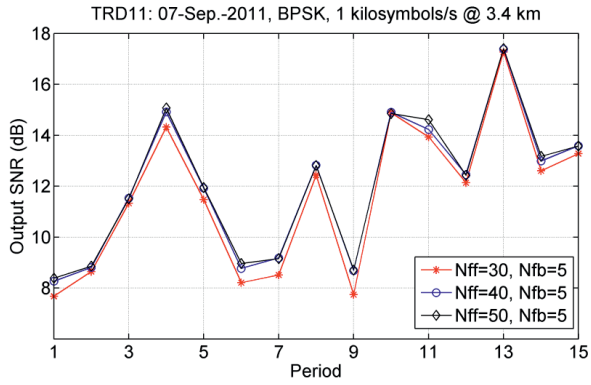

Figure 4.11. Performance of McDFE in terms of output SNR.

Figure 4.12 shows CIRs measured at a distance of 7.4 km to the source. Apparently, dominant arrivals are limited within 5 ms. In Figure 4.12(a, d), there are arrivals at a delay time of 50 ms, but there are no obvious strong arrivals of large magnitude. Figure 4.13 shows the performance of the McDFE for BPSK, where N_{ff} is changed from 30 to

80. The feed-forward filters span 20 ms in maximum, as the symbol rate is 2 kilosymbols/s. Coarse time synchronization is achieved by using the first arrivals of largest magnitude, and there are no contributed arrivals between 7.5 ms and 20 ms after the first arrivals. Consequently, the output SNR is decreased when N_{ff} is increased from 30 to 80. Since the level of numerical noise is raised due to increase N_{ff}, the performance of the McDFE is degraded.

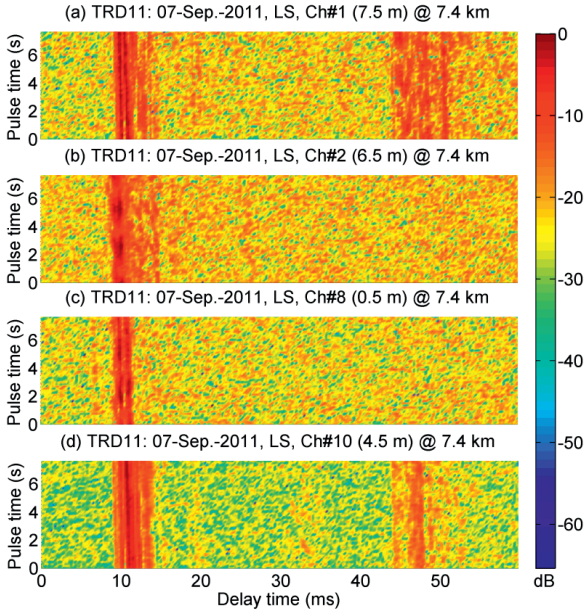

Figure 4.12. CIR as a function of time at four receiving channels. (a) The 1st channel at a depth of 7.5 m. (b) The 2nd channel at a depth of 6.5 m. (c) The 8th channel at a depth of 0.5 m. (d) The 10th channel at a depth of 4.5 m. The data were collected over a range of 7.4 km on 7th September 2011.

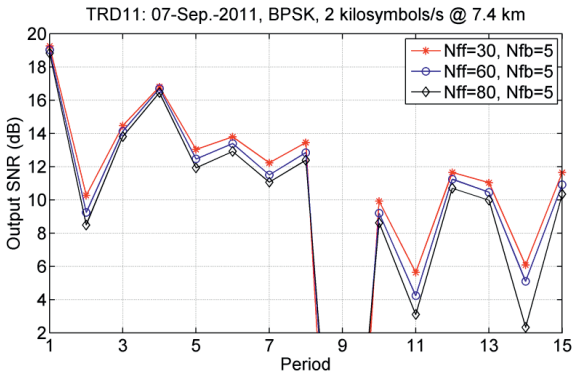

Figure 4.13. Performance of the McDFE in terms of output SNR at a symbol rate of 2 kilosymbols/s.

As shown by the above results, the McDFE exploits temporal diversity by increasing the number of taps. It is indicated that the computational load of the McDFE is increased to obtain the diversity in long time spread channels. Moreover, the computational load grows with the symbol rate due to the increase of taps. For instance, if N_{ff}=30 is configured at a symbol rate of 1 kilosymbols/s, N_{ff}=60 is required at a symbol rate of 2 kilosymbols/s, and thus the arithmetic operations are much increased at each iteration. Alternatively, the diversity can be obtained by PPC processing, which recombines time delayed arrivals.

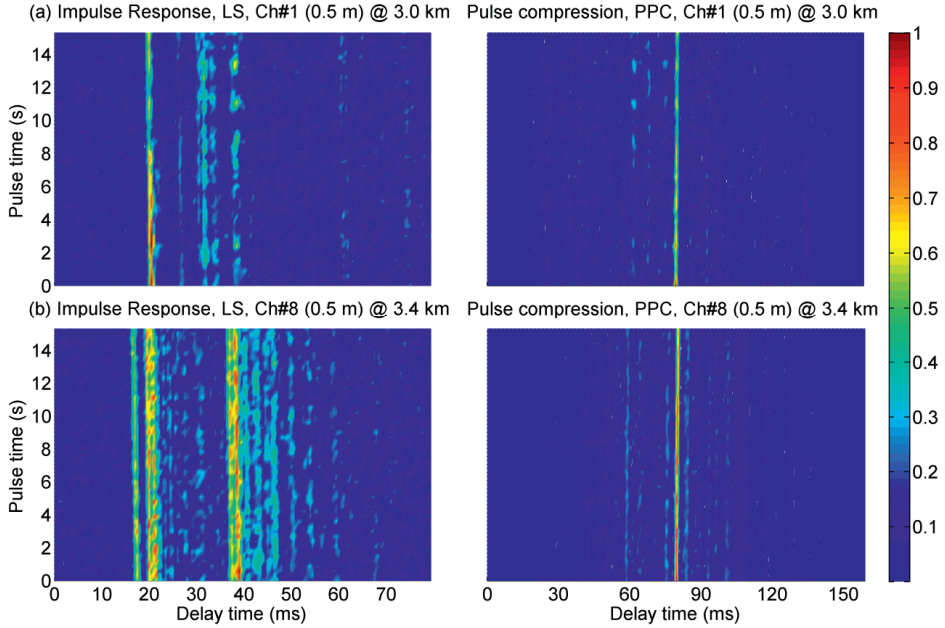

Figure 4.14. CIR as a function of time estimated by the LS method (left panel). Pulse compression by PPC processing (right panel). The receiving channel is deployed at a depth of 0.5 m. (a) Data were collected over a range of 3.0 km on 16th June 2011 (upper panel). (b) Data were collected over a range of 3.4 km on 7th September 2011 (bottom panel).

As illustrated in Figure 4.14, two examples of pulse compression (temporal focusing) are obtained by PPC processing, where CIR is estimated using the LS method. The left panel shows estimated CIR, and the right panel shows the respective pulse compression within 15.565 s. In Figure 4.14(a), the response that has a time spread of 20 ms is time variant over very short time scales, and hence pulse compression degrades rapidly with time evolution. In Figure 4.14(b), stable pulse compression has been achieved within 15.565 s, where the impulse response has a time spread of 25 ms. In observation of the right panels, peak-to-sidelobe ratios of the pulse compressions are different, and actually are determined by the CIR shown in the left panels. PPC processing converts time delayed multipath arrivals into a response of temporal focusing in which most of the energy of the arrivals is concentrated within the main

lobe after focusing. The focusing has sidelobes that can cause ISI, which is referred to as residual ISI.

TR focusing can be used to suppress residual ISI in UWA communications; for this case, the main lobes of multiple independent pulse compressions are coherently summed but the independent sidelobes in each channel are averaged. Figure 4.15 shows an example of TR focusing with different numbers of receiving channels. Obviously, the sidelobe level decreases with an increased number of receiving channels. However, the sidelobes cannot be eliminated due to the physics, as the communication is bandwidth limited. Hence a subsequent channel equalizer, e.g. DFE, is required to remove residual ISI as well as track slow channel variations.

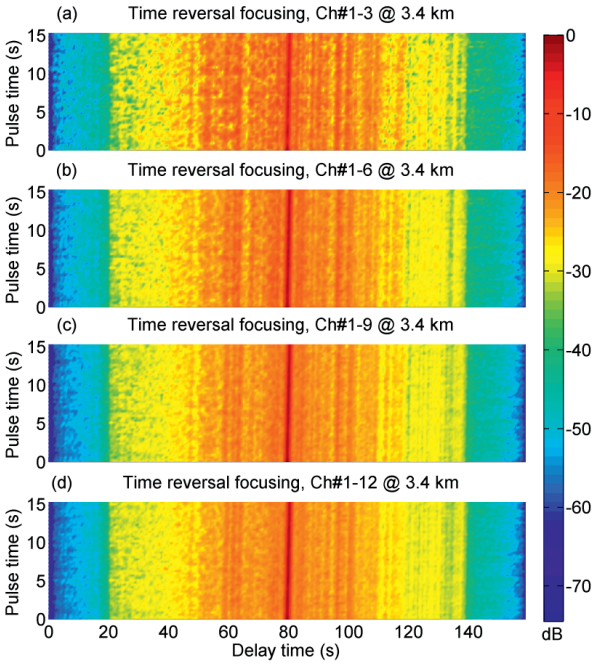

Figure 4.15. TR focusing using different numbers of receiving channels. (a) 3 channels. (b) 6 channels. (c) 9 channels. (d) 12 channels.

Let time duration T_{LS} denote the time interval used by the LS method for estimating the channel response. Figure 4.16 shows the performance of the PPC-DFE, when T_{LS} is changed from 10 ms to 55 ms. Generally, the output SNR increases when T_{LS} is increased from 10 ms to 25 ms, and it decreases when T_{LS} is further increased from 25 ms to 55 ms. As shown in Figure 4.9, the dominant arrivals span 25 ms. The PPC-DFE achieves the best performance when T_{LS}=25 ms. Temporal diversity contributes to improve the performance when T_{LS} is increased from 10 ms to 25 ms. However, the performance degrades when T_{LS} is further increased greater than the true time spread, e.g. from 25 ms to 55 ms, because extra noise is introduced to the PPC processing. The diversity gain is obvious if we compare the results in two scenarios, namely T_{LS}=10 ms and T_{LS}=40 ms, and better performance is obtained in most periods when T_{LS}=40 ms.

Temporal diversity from the multipath arrivals contributes the performance improvement.

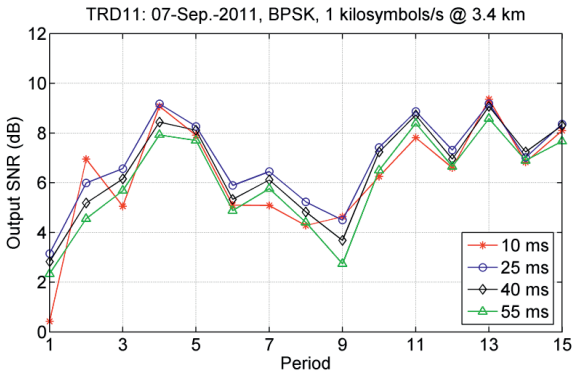

Figure 4.16. Performance of the PPC-DFE in terms of output SNR. T_{LS} is changed from 10 ms to 55 ms. BPSK data were collected over a range of 3.4 km on 7th September 2011.

Figure 4.17 shows the performance of the PPC-McDFE for BPSK communications at two symbol rates. The output SNR decreases when T_{LS} is increased from 25 ms to 40 ms. For instance, the output SNR is reduced by 0.96 dB (the 2nd transmission period in Figure 4.17(a)) and 1.48 dB (the 15th period in Figure 4.17(b)) at the two symbol rates, respectively. The diversity gain determined by the CIR can be obtained by PPC processing. Therefore, both the PPC-DFE and PPC-McDFE achieve best performance if T_{LS} equals the time spread of the most dominant arrivals. Comparing the structures' performance (Figures 4.16 and 4.17(a)), the PPC-McDFE achieves the best performance. With the same condition T_{LS}=25 ms, the superior performance of PPC-McDFE attributes to the spatial gain.

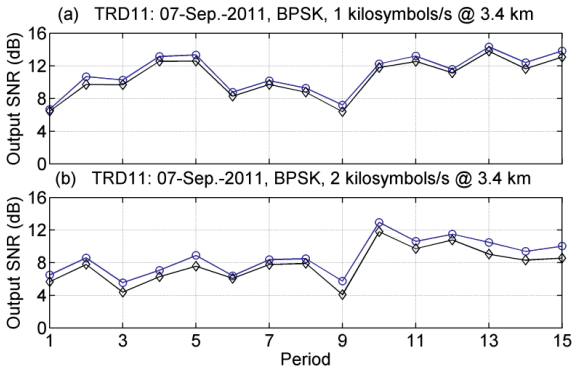

Figure 4.17. Performance of the PPC-McDFE for BPSK communications at two symbol rates. (a) BPSK, 1 kilosymbols/s. (b) BPSK, 2 kilosymbols/s. T_{LS}=25 ms (○), and T_{LS}=40 ms (◊). The data were collected over a range of 3.4 km on 7th September 2011.

As discussed in Section 4.1, time-varying interchannel correlations impact the spatial focusing, and this resulted in degraded performance of the PPC-DFE [30]. In further experimental research, Figure 4.18 shows the performance comparison of communications at four data rates over a range of 3.4 km. It is found that the PPC-DFE demonstrates the poorest performance. On 7th September 2011, there were two other trials over two ranges of 3.7 km and 7.4 km, in which the PPC-DFE also achieved the poorest performance as shown in Figure 4.6 and [33, 35]. The results have demonstrated the advantage of the adaptive multichannel combining. For instance, the McDFE achieves superior performance at a rate of 2 kilosymbols/s, and PPC-McDFE obtains satisfactory performance.

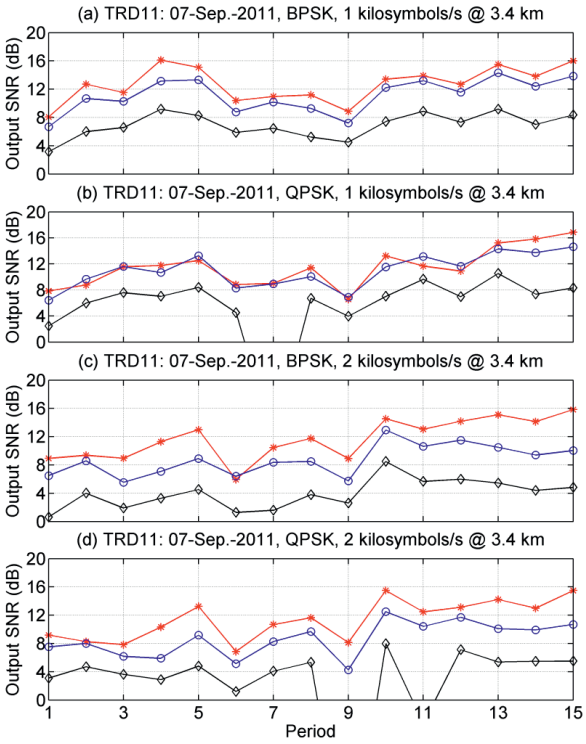

Figure 4.18. Performance comparison at four data rates. (a) BPSK, 1 kilosymbols/s. (b) QPSK, 1 kilosymbols /s. (c) BPSK, 2 kilosymbols/s. (d) QPSK, 2 kilosymbols/s. McDFE (*), PPC-McDFE (○) and PPC-DFE (◊). For the McDFE, the number of taps is configured as: (1) N_{ff}=25 and N_{fb}=1 at 1 kilosymbols/s, and (2) N_{ff}=50 and N_{fb}=5 at 2 kilosymbols/s. For the PPC-McDFE and PPC-DFE, T_{LS}=25 ms, N_{ff}=8 and N_{fb}=2 are configured at the two symbol rates. The data were collected over a range of 3.4 km on 7th September 2011.

In each iteration for the RLS algorithm to update the tap coefficients, arithmetic operations are performed on the order of $\{(N_{ff}K+N_{fb})\}^2$ [9]. In terms of computational load, a decreasing order of the three receiver structures is: (1) McDFE, (2) PPC-McDFE, and (3) PPC-DFE. We illustrate an example using the parameters which are used in Figure 4.18(c-d). In each iteration, the arithmetic operations of the three

respective receiver structures are on the order of (1) 435600, (2) 14400, and (3) 100. The computational load of the McDFE limits its application when a large number of taps is required, e.g. in a UWA channel of long time spread, especially in the case of many receiving hydrophones. As an example, about 2 hours were needed using the desktop PC to obtain one result in Figure 4.18(c-d). The PPC-DFE of the least complexity neglects spatial coherence among the receiving channels, and it achieves the poorest performance. As an alternative, the PPC-McDFE obtains satisfactory performance by taking advantage of PPC processing and adaptive multichannel combining. PPC processing is indeed an environmentally adaptive method for exploiting temporal diversity.

4.3 Channel sparsity

UWA channels are often characterized as sparse, especially at high frequencies. As an example, Figure 4.9 shows that there are multipath arrivals of time resolution, and hence the UWA channel is sparse. Figure 4.19 shows CIR measured at four receiving channels. Over a range of 3.7 km, the multipath arrivals are well resolved in time among the receiving channels, e.g. a time resolution of 25 ms is shown in Figure 4.19(c). As discussed in Section 4.2, temporal diversity is determined by the independent arrivals. The dominant arrivals represent the information of UWA channels.

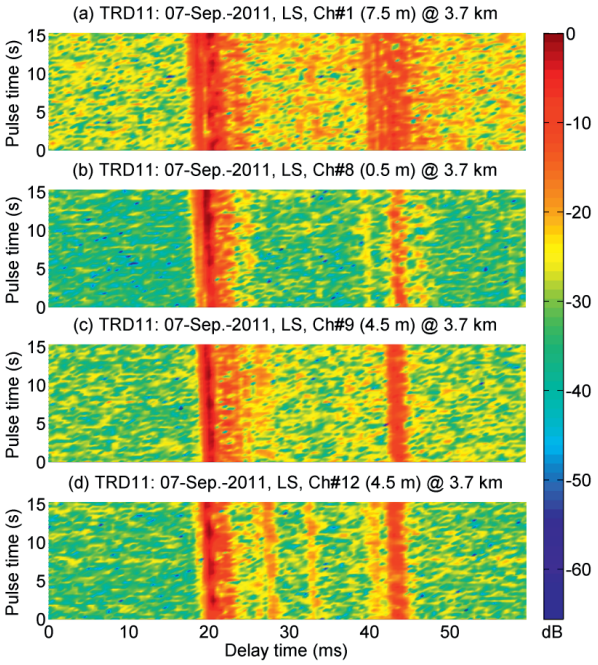

Figure 4.19. CIR as a function of time estimated by the LS method at four receiving channels. (a) The 1st channel at a depth of 7.5 m. (b) The 8th channel at a depth of 0.5 m. (c) The 9th channel at a depth of 4.5 m. (d) The 12th channel at a depth of 4.5 m. The data were collected over a range of 3.7 km on 7th September 2011.

The LS method estimates channel response within a time interval, and it generates noise between the sparse arrivals. As shown in Figure 4.16 and 4.17, performance of the PPC-DFE and PPC-McDFE degrades with improper T_{LS}, when the LS method is used to estimate the response. In further discussion of temporal diversity, we would like to select dominant arrivals for PPC processing, and then the problem of impropriate selection of T_{LS} can be avoided. Figure 4.20 shows examples that dominant arrivals can be estimated by the MP algorithm [37] and the others are nulled to zeros. Afterwards, the diversity preserved by the dominant arrivals can be obtained by PPC processing.

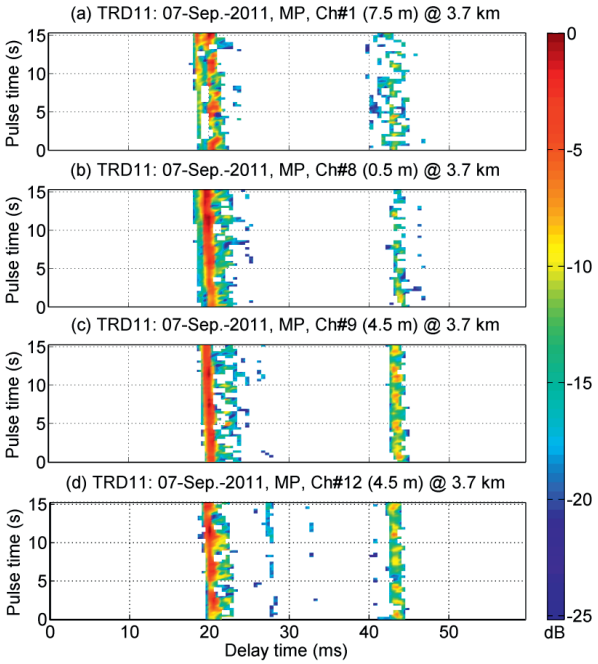

Figure 4.20. Dominant arrivals estimated by the MP algorithm at four different receiving channels. (a) The 1st channel at a depth of 7.5 m. (b) The 8nd channel at a depth of 0.5 m. (c) The 9th channel at a depth of 4.5 m. (d) The 12th channel at a depth of 4.5 m. The data were collected over a range of 3.7 km on 7th September 2011.

In order to observe the performance difference from the channel estimation, T_{LS} is changed from 25 ms to 45 ms for the LS method, and within the same time interval dominant arrivals are selected by the MP algorithm. With different values of T_{LS}, Figure 4.21 shows the performance comparison. By using the MP algorithm, both the PPC-DFE and PPC-McDFE become insensitive to T_{LS}, namely the time interval of channel estimations, and moreover there is obvious performance improvement comparing with the performance using the LS method. For instance, when T_{LS}=25 ms, the performance of the PPC-DFE is improved by 1.2 dB at the 7th transmission period, and by 1.8 dB at the 5th period. The channel information represented by the dominant arrivals can be used by PPC processing, when the diversity from the dominant arrivals is exploited but less noise is introduced in PPC processing. In addition to the results published in [33],

the MP algorithm is further assessed to demonstrate performance improvement in exploiting channel sparsity.

Figure 4.22 shows performance of the McDFE, PPC-McDFE and PPC-DFE for communications at two symbol rates. The performance of McDFE is selected as a benchmark. In Figure 4.22(a), McDFE failed in the 4th, 5th, and 14th transmission periods while the PPC-McDFE succeeds in these periods. This is probably because inappropriate parameters were selected for the McDFE. N_{ff} for McDFE was adjusted several times, such as N_{ff}=20, N_{ff}=35 and N_{ff}=50, but there was no obvious improvement. Another example is shown in Figure 4.22(b). For instance, using the MP algorithm, the output SNR of the PPC-DFE is increased by 3.3 dB (the 11th period); the output SNR of the PPC-McDFE approximates that of the McDFE. Even though the performance of the PPC-DFE is improved, it still lags behind that of the PPC-McDFE. It is concluded that the performance improvement originates from exploiting the channel sparsity. The analysis also shows that PPC processing obtains the diversity embedded in the time delayed arrivals.

The data have been analysed in the three aspects—spatial diversity, temporal diversity and channel sparsity. The results above have demonstrated satisfactory performance of the PPC-McDFE, the instrumentation of a cross receiving array, and the applicability of the MP algorithm.

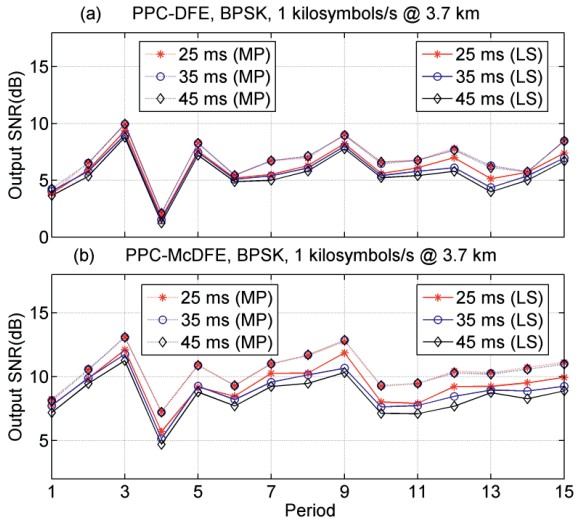

Figure 4.21. Performance of two receiver structures. (a) PPC-DFE. (b) PPC-McDFE. Dominant arrivals are selected by the MP algorithm. N_{ff}=8 and N_{fb}=2 are configured for both structures. The data were collected over a range of 3.7 km on 7th September 2011.

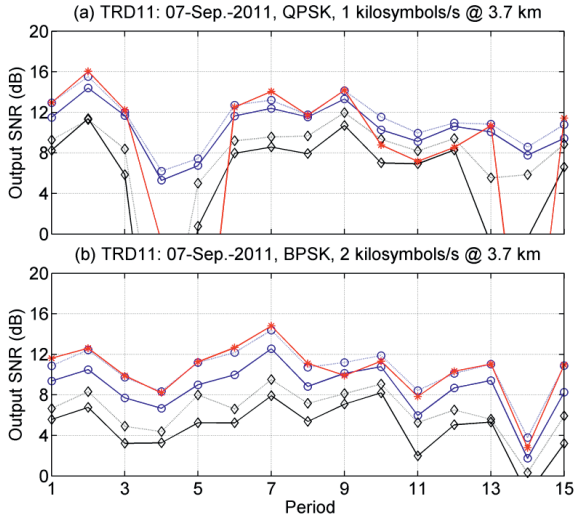

Figure 4.22. Performance of the McDFE, PPC-McDFE and PPC-DFE for communications at two symbol rates. (a) QPSK, 1 kilosymbols/s. (b) BPSK, 2 kilosymbols/s. McDFE (*), PPC-McDFE (○), and PPC-DFE (◊). The MP algorithm is used (dot line), and the LS algorithm is used (solid line). N_{ff}=25 and N_{ff}=50 are configured for the McDFE at 1 and 2 kilosymbols/s, respectively, where N_{ff} =5.N_{ff}=8 and N_{fb}=2 are configured for the PPC-McDFE and PPC-DFE with the condition T_{LS}=25 ms. The data were collected over a range of 3.7 km on 7th September 2011.

Chapter 5

Summary of Papers

Six papers are included in this thesis, and summaries of them are presented in this chapter. A full publication list during the Ph. D. work is attached in the end of this chapter.

Paper 1: Spatial diversity in multichannel processing for underwater acoustic communications (*Ocean Engineering*, vol. 38, pp. 1611-1623, 2011**)**

This paper discusses spatial diversity for underwater communications and presents a passive-phase conjugation (PPC) based multichannel equalizer. Multichannel processing involves taking advantage of multiple receivers distributed in space to take advantage of spatial diversity. The multichannel decision feedback equalizer (DFE) uses multiple nonlinear adaptive filters to remove intersymbol interference (ISI), and its complexity increases with time spread plus the number of receiving channels. Passive time reversal realized by the passive-phase conjugation (PPC) approach refocuses time delayed arrivals at the receiving array, where spatial diversity is obtained by the multichannel combining. The property of refocusing can be used to mitigate ISI for underwater communications, and only one single channel equalizer is required to remove residual ISI. PPC achieves pulse compression for time delayed arrivals, where the number of taps is significantly reduced for a PPC based equalizer. Based on temporal diversity obtained by pulse compression, the proposed structure improves the performance of time reversal communications by adaptive diversity combining. Three receiver structures are evaluated by processing real data collected in an experiment, which was conducted in a range-dependent acoustic channel over a range of 4 km. Results have demonstrated superior performance of the proposed receiver structure.

Paper 2: Experimental assessment of a multicarrier underwater acoustic communication system (*Applied Acoustics*, vol. 72, pp. 953-961, 2011**)**

This paper presents a multicarrier communication system which transmits information on independent subcarriers to achieve an increased data rate. For this system, a passive-phase conjugation (PPC) based receiver structure is assessed by processing data collected in sea trials. Based on temporal diversity (pulse compression) exploited by PPC processing, an adaptive multichannel decision feedback equalizer is used to remove intersymbol interference, where spatial diversity is exploited by adaptive multichannel combination. The digital phase-locked loop (DPLL) technique is implemented for carrier-phase tracking. In the scenario of low input signal-to-noise ratios (SNRs), the receiver structure achieved superior performance using a common DPLL. In a depth-fluctuated environment, two sea experiments were conducted over

ranges of 2 km and 4 km, respectively, and this communication system was assessed with a data rate of 4 kbps. In terms of mean square error, output SNR and bit error rate, this receiver structure has demonstrated its performance for the multicarrier communication system.

Paper 3: Joint passive-phase conjugation with adaptive multichannel combining for coherent underwater acoustic communications (*Applied Acoustics*, vol. 73, pp. 433-439, 2012**)**

This paper presents a receiver structure which exploits spatial diversity by adaptive multichannel combining, which improves the performance of passive time reversal communications realized by passive-phase conjugation (PPC). PPC processing achieves pulse compression for the time delayed arrivals at the receiver, and this property is used for coherent communications to reduce the computational load. The presented structure takes advantage of pulse compression and performs adaptive multichannel combining, where the number of taps for adaptive multichannel processing is significantly reduced in order to decrease the computational load. With a previous output mean square error (MSE), the adaptive combining minimizes current output MSE, where spatial diversity is exploited by the adaptive combining. This structure improves performance of the passive time reversal approach, even though the taps for combining span one symbol interval. The performance improvement is demonstrated by a set of real data collected in a recent sea experiment, which was conducted in a range dependent acoustic channel over a range of 4 km.

Paper 4: Experimental demonstration of spread spectrum communication over long range multipath channels (*Applied Acoustics*, vol. 73, pp. 872-876, 2012**)**

This paper presents a spread spectrum scheme, which is designed for long range underwater acoustic communications of low signal-to-noise ratios. This scheme uses two maximum length sequences, which are overlapped in time. One is used as a time reference, and the other applies code cyclic shift keying (CCSK) to carry information. Compared with conventional spread spectrum techniques, CCSK achieves a higher spectral efficiency, and this property is of significance in spread spectrum communications. With the help of a time reference, performance impairment from timing errors for CCSK is reduced, as each CCSK symbol has its own time reference. For this scheme, three receiver structures are presented, and they are: (1) correlation receiver, (2) passive-phase conjugation receiver, and (3) time reversal receiver structures. A recent sea experiment was carried out in a range dependent channel over a distance of 10 km. By real data processing, performance of the three receiver structures are compared and discussed. The presented results demonstrate the feasibility of this spread spectrum scheme.

Paper 5: Underwater communications in time-varying sparse channels using passive-phase conjugation (*Applied Acoustics*, vol. 74, pp. 421-424, 2013**)**

Passive-phase conjugation (PPC) achieves the pulse compression for the time delayed arrivals. This property has been used in underwater acoustic communications. In a time-varying channel, the temporal focusing degrades with time evolution. The block-based approach is implemented to avoid the impact of channel variations. The basic idea is that the channel is assumed constant within each block of a short time interval, and the channel is updated using detected symbols in the previous block. Using real data collected in a recent sea trial, this paper investigates: (1) the communications using PPC processing, where the block-based approach is used, (2) the matching pursuit (MP) algorithm exploiting the channel sparseness. It is found that the MP algorithm improves performance of the communications using PPC processing.

Paper 6: Experimental Assessment of Different Receiver Structures for Underwater Acoustic Communications over Multipath Channels (*Sensors*, vol. 12, pp. 2118-2135, 2012**)**

Underwater communication channels are often complicated, and in particular multipath propagation may cause intersymbol interference (ISI). This paper addresses how to remove ISI, and evaluates the performance of three different receiver structures and their implementations. Using real data collected in a high-frequency (10–14 kHz) field experiment, the receiver structures are evaluated by off-line data processing. The three structures are multichannel decision feedback equalizer (DFE), passive time reversal receiver (passive-phase conjugation (PPC) with a single channel DFE), and the joint PPC with multichannel DFE. In sparse channels, dominant arrivals represent the channel information, and the matching pursuit (MP) algorithm which exploits the channel sparseness has been investigated for PPC processing. In the assessment, it is found that: (1) it is advantageous to obtain spatial gain using the adaptive multichannel combining scheme; and (2) the MP algorithm improves the performance of communications using PPC processing.

Publications during Ph. D. Study

Journal papers

- G. Zhang and H. Dong, "Joint passive-phase conjugation with adaptive multichannel combining for coherent underwater acoustic communications," *Applied Acoustics*, vol. 73, pp. 433-439, 2012.
- G. Zhang and H. Dong, "Experimental demonstration of spread spectrum communication over long range multipath channels," *Applied Acoustics*, vol. 73, pp. 872-876, 2012.
- G. Zhang, J. M. Hovem, and H. Dong, "Experimental assessment of different receiver structures for underwater acoustic communications over multipath channels," *Sensors,* vol. 12, pp. 2118-2135, 2012.
- G. Zhang and H. Dong, "Underwater communications in time-varying sparse channels using passive-phase conjugation," *Applied Acoustics*, vol. 74, pp. 421-424, 2013.
- G. Zhang and H. Dong, "Spatial diversity in multichannel processing for underwater acoustic communications," *Ocean Engineering*, vol. 38, pp. 1611-1623, 2011.
- G. Zhang and H. Dong, "Experimental assessment of a multicarrier underwater acoustic communication system," *Applied Acoustics*, vol. 72, pp. 953-961, 2011.
- G. Zhang, J. M. Hovem, H. Dong, and L. Liu, "Coherent underwater communication using passive time reversal over multipath channels," *Applied Acoustics*, vol. 72, pp. 412-419, 2010.
- G. Zhang, J. M. Hovem, H. Dong, S. Zhou, and S. Du, "An efficient spread spectrum pulse position modulation scheme for point-to-point underwater acoustic communication," *Applied Acoustics*, vol. 71, pp. 11-16, 2010.
- G. Zhang, J. M. Hovem, H. Dong, and T. A. Reinen, "A design for timing pulse acquisition in underwater multipath environments," *Electronic Journal "Technical Acoustics" <http://www.ejta.org>*2009, 11.

Conferences with full-paper review

- G. Zhang, B. Peng, and H. Dong, "Experimental assessment of sparse channel estimations for passive-phase conjugation communications," in *Proc. 2012 IEEE International Conference on Acoustics, Speech and Signal Processing (ICASSP)*, pp. 2701-2704, Kyoto, Japan, Mar. 2012.
- G. Zhang, J. M. Hovem, H. Dong, and P. A. van Walree, "A novel probe processing method for underwater communication by passive-phase conjugation," in *Proc. 2011 IEEE International Conference on Acoustics, Speech and Signal Processing (ICASSP)*, pp. 2700-2703, Prague, Czech Republic, May 2011.
- G. Zhang and H. Dong, "Experimental research on adaptive multichannel equalization for underwater communications," in *Proc. 2011 IEEE Instrumentation*

and Measurement Technology Conference (I2MTC), pp. 1-5, Hangzhou, China, May. 2011.

- G. Zhang, J. M. Hovem, and H. Dong, "Experimental assessment of adaptive spatial combining for underwater acoustic communications," in *Proc. The Fifth International Conference on Sensor Technologies and Applications (SENSORCOMM)*, pp. 178-183, Nice/Saint Laurent du Var, France, Aug. 2011.
- G. Zhang, J. M. Hovem, H. Dong, and L. Liu, "Experimental studies of underwater acoustic communications over multipath channels," in *Proc. The Fourth International Conference on Sensor Technologies and Applications (SENSORCOMM)*, pp. 458-461, Venice/Mestre, Italy, Jul. 2010.
- G. Zhang, J. M. Hovem, H. Dong, and T. A. Reinen, "A simple time synchronization method for underwater communication receivers," in *Proc. The Third International Conference on Sensor Technologies and Applications (SENSORCOMM)*, pp. 289-293, Athens/Glyfada, Greece, Jun. 2009.

Other conferences

- G. Zhang, S. Zhou, J. M. Hovem, H. Dong, and J. Jiao, " Experimental Research of Chirp Spread Spectrum for High-rate Underwater Acoustic Communication," in *Proc. The 10th Western Pacific Acoustics Conference (WESPAC X)*, Paper 0048, Beijing, China, Jun. 2009.
- G. Zhang, J. M. Hovem, and H. Dong, "Experimental studies of underwater acoustic communication in Trondheim fjord," in *Proc. Joint 159th Meeting of the Acoustical Society of America (ASA) and NOISE-CON 2010*, Baltimore, MD, U.S.A, Apr. 2009.

Chapter 6

Conclusions and Future Work

This thesis presents research on UWA communications and field experiments. The main focuses are on the development of a channel equalizer for high-rate coherent communications over short distances, and the methods of spread spectrum communications over long ranges. These two scenarios are representative of practical applications.

Firstly, a PPC-McDFE receiver structure for high-rate communications was developed. This structure has been assessed in four major field experiments and it has demonstrated satisfactory performance:

- In the experiments, time-varying channels were observed as the channel response changed in different experiments due to different environmental conditions, e.g. SSP in the water. As an environmentally adaptive matched-filter, PPC processing reduces the complexity for subsequent channel equalization. Despite the condition that the receiving hydrophones were deployed with an element spacing that was larger than the half wave length of the lowest frequency used in communications, time-varying spatial coherence was also observed. The offline data processing and analysis showed that it is advantageous to exploit spatial diversity using the scheme of adaptive multichannel combining.
- For practical purposes, a small number of receivers are preferred to reduce hardware complexity, cost, etc. It is significant that the receiver performance is maximized by taking advantage of spatial diversity. In channels of long time spread, the PPC-McDFE is recommended for high-rate communications. Moreover, in Paper 2, the PPC-McDFE has also been used in a multicarrier system.
- Implementing the block-based approach (Papers 5-6), PPC-McDFE has been extended to time-varying channels. Compared with the TR receiver structure, PPC-McDFE is insensitive to the channel variations. In addition, the MP algorithm has been investigated to exploit channel sparsity for PPC processing. In sparse channels, the MP algorithm has demonstrated its improvement for communications using PPC processing, particularly for the block-based approach.
- In the environment with a complex bathymetry, it is found that there is spatial diversity at the same depth. The diversity has been observed in the analysis of communication results, where the transmissions were received by a horizontal

array with an aperture of 4.5 m. In the experimental area, the diversity at the same depth probably originates from 3-dimensional propagation effects.

Secondly, spread spectrum schemes have also been investigated for UWA communications over long range multipath channels. It is preferred that the schemes are spectrally efficient. The technique presented in Paper 4 has demonstrated feasibility of communication over a range of 10 km at a high-frequency regime (11-13 kHz), with a TR receiver structure. It is found that:

- It is a spectrally efficient technique. As desired, it has potential for long range UWA communications.
- Due to difficulties in phase synchronization at low input SNRs, there are cross-correlations between two orthogonal carriers. Recombining multipath arrivals, PPC processing is used to suppress the cross-correlations and interference from multipath arrivals.
- In time variant UWA channels, spatial diversity is obtained by TR focusing to avoid deep fading for robust communications.

As a key part of this thesis, field experiments were carried out that provided insights into UWA research. Experiences from operating the instruments and on-site organizations led to better experimental designs with higher quality data. All the results in this thesis are obtained by real data analysis. From the output of DPLL, time variant frequency shifts have been observed in each packet of communications. Due to available facilities and instrumentations, the difference of sampling frequencies between the transmitter and the receivers cannot be eliminated in field experiments. Here, a further proposal of instrumentation is given. Both the transmitter and the data logging devices can be synchronized with the GPS clock, and then frequency shifts caused by Doppler could be more precisely monitored in field experiments.

Considering what have been done during the thesis, future work also includes,

- implementing a PPC-McDFE to multiuser communications, where successive interference cancellation can be used [64-67];
- developing the spread spectrum scheme (presented in Paper 4) in fast varying channels, e.g. communications in moving scenarios, and over longer ranges;
- hardware-based real-time demonstrations of UWA communications using a PPC-McDFE or a PPC-DFE;
- investigating Turbo equalization in the scenarios of a single user [68-70] and multiuser [71] for high-rate UWA communications;
- experimental testing for high-rate communications, if possible, on moving platforms, e.g. a remotely operated underwater vehicle.

References

[1] J. A. Catipovic, "Performance limitations in underwater acoustic telemetry," *IEEE J. Ocean. Eng.*, vol. 15, pp. 205-216, 1990.

[2] D. B. Kilfoyle and A. B. Baggeroer, "The state of the art in underwater acoustic telemetry," *IEEE J. Ocean. Eng.*, vol. 25, pp. 4-27, 2000.

[3] J. G. Proakis, *Digital Communications*. New York: McGraw-Hill, 2001.

[4] M. Stojanovic, J. Catipovic, and J. G. Proakis, "An algorithm for multichannel coherent digital communications over long range underwater acoustic telemetry channels," in *Proc. MTS/IEEE OCEANS '92*, pp. 577-582, Rhode Island, 1992.

[5] M. Stojanovic, J. Catipovic, and J. G. Proakis, "Adaptive multichannel combining and equalization for underwater acoustic communications," *J. Acoust. Soc. Am.*, vol. 94, pp. 1621-1631, 1993.

[6] M. Stojanovic, "Coherent digital communications for rapidly fading channels with applications to underwater acoustics," *J. Acoust. Soc. Am.*, vol. 96, pp. 2596, 1994.

[7] M. Stojanovic, J. A. Catipovic, and J. G. Proakis, "Phase-coherent digital communications for underwater acoustic channels," *IEEE J. Ocean. Eng.*, vol. 19, pp. 100-111, 1994.

[8] M. Stojanovic, J. A. Catipovic, and J. G. Proakis, "Reduced-complexity spatial and temporal processing of underwater acoustic communication signals," *J. Acoust. Soc. Am.*, vol. 98, pp. 961-972, 1995.

[9] S. Haykin, *Adaptive Filter Theory*. Upper Saddle River, New Jersey: Prentice Hall, 2001.

[10] M. Fink, "Time reversal of ultrasonic fields. I. Basic principles," *IEEE Trans. Ultrason., Ferroelectr. and Freq. Control,* vol. 39, pp. 555-566, 1992.

[11] W. A. Kuperman, W. S. Hodgkiss, H. C. Song, T. Akal, C. Ferla, and D. R. Jackson, "Phase conjugation in the ocean: Experimental demonstration of an acoustic time-reversal mirror," *J. Acoust. Soc. Am.*, vol. 103, pp. 25-40, 1998.

[12] G. F. Edelmann, T. Akal, W. S. Hodgkiss, K. Seongil, W. A. Kuperman, and S. Hee Chun, "An initial demonstration of underwater acoustic communication using time reversal," *IEEE J. Ocean. Eng.*, vol. 27, pp. 602-609, 2002.

[13] D. Rouseff, D. R. Jackson, W. L. J. Fox, C. D. Jones, J. A. Ritcey, and D. R. Dowling, "Underwater acoustic communication by passive-phase conjugation: theory and experimental results," *IEEE J. Ocean. Eng.*, vol. 26, pp. 821-831, 2001.

[14] T. C. Yang, "Temporal resolutions of time-reversal and passive-phase conjugation for underwater acoustic communications," *IEEE J. Ocean. Eng.*, vol. 28, pp. 229-245, 2003.

[15] T. C. Yang, "Differences between passive-phase conjugation and decision-feedback equalizer for underwater acoustic communications," *IEEE J. Ocean. Eng.*, vol. 29, pp. 472-487, 2004.

[16] D. R. Jackson and D. R. Dowling, "Phase conjugation in underwater acoustics," *J. Acoust. Soc. Am.*, vol. 89, pp. 171-181, 1991.

[17] D. R. Dowling, "Acoustic pulse compression using passive phase-conjugate processing," *J. Acoust. Soc. Am.*, vol. 95, pp. 1450-1458, 1994.

[18] J. A. Flynn, J. A. Ritcey, W. L. J. Fox, D. R. Jackson, and D. Rouseff, "Decision-directed passive phase conjugation: equalisation performance in shallow water," *Electr. Letters*, vol. 37, pp. 1551-1553, 2001.

[19] J. A. Flynn, J. A. Ritcey, D. Rouseff, and W. L. J. Fox, "Multichannel equalization by decision-directed passive phase conjugation: experimental results," *IEEE J. Ocean. Eng.*, vol. 29, pp. 824-836, 2004.

[20] C. P. Christopher and A. S. Michael, "LSQR: An algorithm for sparse linear equations and sparse least squares," *ACM Trans. Math. Softw.*, vol. 8, pp. 43-71, 1982.

[21] T. C. Yang, "Correlation-based decision-feedback equalizer for underwater acoustic communications," *IEEE J. Ocean. Eng.*, vol. 30, pp. 865-880, 2005.

[22] H. C. Song, W. S. Hodgkiss, W. A. Kuperman, W. J. Higley, K. Raghukumar, T. Akal, and M. Stevenson, "Spatial diversity in passive time reversal communications," *J. Acoust. Soc. Am.*, vol. 120, pp. 2067-2076, 2006.

[23] H. C. Song, W. S. Hodgkiss, W. A. Kuperman, M. Stevenson, and T. Akal, "Improvement of time-reversal communications using adaptive channel equalizers," *IEEE J. Ocean. Eng.*, vol. 31, pp. 487-496, 2006.

[24] H. C. Song, W. S. Hodgkiss, W. A. Kuperman, T. Akal, and M. Stevenson, "High-frequency acoustic communications achieving high bandwidth efficiency," *J. Acoust. Soc. Am.*, vol. 126, pp. 561-563, 2009.

[25] H. C. Song, W. A. Kuperman, and W. S. Hodgkiss, "Basin-scale time reversal communications," *J. Acoust. Soc. Am.*, vol. 125, pp. 212-217, 2009.

[26] H. C. Song, J. S. Kim, W. S. Hodgkiss, W. A. Kuperman, and M. Stevenson, "High-rate multiuser communications in shallow water," *J. Acoust. Soc. Am.*, vol. 128, pp. 2920-2925, 2010.

[27] H. C. Song, W. S. Hodgkiss, W. A. Kuperman, T. Akal, and M. Stevenson, "Multiuser communications using passive time reversal," *IEEE J. Ocean. Eng.*, vol. 32, pp. 915-926, 2007.

[28] A. Song, M. Badiey, H. C. Song, W. S. Hodgkiss, M. Porter, B, and G. the KauaiEx, "Impact of ocean variability on coherent underwater acoustic communications during the Kauai experiment (KauaiEx)," *J. Acoust. Soc. Am.*, vol. 123, pp. 856-865, 2008.

[29] T. C. Yang, "A study of spatial processing gain in underwater acoustic communications," *IEEE J. Ocean. Eng.*, vol. 32, pp. 689-709, 2007.

[30] G. Zhang and H. Dong, "Spatial diversity in multichannel processing for underwater acoustic communications," *Ocean Eng.*, vol. 38, pp. 1611-1623, 2011.

[31] G. Zhang, B. Peng, and H. Dong, "Adaptive diversity combining for underwater communications using passive-phase conjugation," submitted to *2012 IEEE International Conference on Acoustics, Speech and Signal Processing (ICASSP)*, Kyoto, 2012.

[32] G. Zhang, B. Peng, and H. Dong, "Experimental assessment of sparse channel estimations for passive-phase conjugation communications," in *Proc. 2012 IEEE International Conference on Acoustics, Speech and Signal Processing (ICASSP)*, pp. 2701-2704, Kyoto, Japan, Mar. 2012.

[33] G. Zhang, J. M. Hovem, and H. Dong, "Experimental assessment of different receiver structures for underwater acoustic communications over multipath channels," *Sensors,* vol. 12, pp. 2118-2135, 2012.
[34] G. Zhang and H. Dong, "Experimental assessment of a multicarrier underwater acoustic communication system," *Applied Acoustics*, vol. 72, pp. 953-961, 2011.
[35] G. Zhang and H. Dong, "Underwater communications in time-varying sparse channels using passive-phase conjugation," *Applied Acoustics*, vol. 74, pp. 421-424, 2013.
[36] H. C. Song, "Time reversal communication in a time-varying sparse channel," *J. Acoust. Soc. Am.*, vol. 130, pp. EL161-EL166, 2011.
[37] S. F. Cotter and B. D. Rao, "Sparse channel estimation via matching pursuit with application to equalization," *IEEE Trans. Comm.*, vol. 50, pp. 374-377, 2002.
[38] G. Zhang and H. Dong, "Experimental demonstration of spread spectrum communication over long range multipath channels," *Applied Acoustics*, vol. 73, pp. 872-876, 2012.
[39] G. Zhang, J. M. Hovem, H. Dong, S. Zhou, and S. Du, "An efficient spread spectrum pulse position modulation scheme for point-to-point underwater acoustic communication," *Applied Acoustics*, vol. 71, pp. 11-16, 2010.
[40] K. Grythe, J. E. Hakegard, T. A. Myrvoll, and T. A. Reinen, "The Trondheim harbour: Acoustic propagation measurements and communication capacity," in *Proc. MTS/IEEE OCEANS 2008*, pp. 1-9, Quebec, 2008.
[41] E. M. Sozer, M. Stojanovic, and J. G. Proakis, "Underwater acoustic networks," *IEEE J. Ocean. Eng.*, vol. 25, pp. 72-83, 2000.
[42] H. Jens M., *Marine Acoustics: The Physics of Sound in Underwater Environments*. Los Altos: Peninsula Publishing, 2010.
[43] J. M. Hovem, S. Yan, X. Bao, and H. Dong, "Modeling underwater communication links," in *Proc. The Second International Conference on Sensor Technologies and Applications (SENSORCOMM '08)*, pp. 679-686, Cap Esterel, France, 2008.
[44] B. S. Sharif, J. Neasham, O. R. Hinton, and A. E. Adams, "A computationally efficient Doppler compensation system for underwater acoustic communications," *IEEE J. Ocean. Eng.*, vol. 25, pp. 52-61, 2000.
[45] A. Baggeroer, "Acoustic telemetry—An overview," *IEEE J. Ocean. Eng.*, vol. 9, pp. 229-235, 1984.
[46] K. F. Scussel, J. A. Rice, and S. Merriam, "A new MFSK acoustic modem for operation in adverse underwater channels," in *Proc. MTS/IEEE OCEANS '97*, vol. 1, pp. 247-254, Halifax, 1997.
[47] D. George, R. Bowen, and J. Storey, "An adaptive decision feedback equalizer," *IEEE Trans. Comm. Tech.*, vol. 19, pp. 281-293, 1971.
[48] P. Hursky, "Point-to-point underwater acoustic communications using spread-spectrum passive phase conjugation," *J. Acoust. Soc. Am.*, vol. 120, pp. 247, 2006.
[49] T. C. Yang and Y. Wen-Bin, "Performance analysis of direct-sequence spread-spectrum underwater acoustic communications with low signal-to-noise-ratio input signals," *J. Acoust. Soc. Am.*, vol. 123, pp. 842-855, 2008.

[50] P. Blomgren, P. Kyritsi, A. D. Kim, and G. Papanicolaou, "Spatial focusing and intersymbol interference in multiple-input-single-output timer reversal communication systems," *IEEE J. Ocean. Eng.*, vol. 33, pp. 341-355, 2008.
[51] M. Stojanovic, "Efficient processing of acoustic signals for high-rate information transmission over sparse underwater channels," *Phys. Comm.*, vol. 1, pp. 146-161, 2008.
[52] G. Zhang and H. Dong, "Joint passive-phase conjugation with adaptive multichannel combining for coherent underwater acoustic communications," *Applied Acoustics*, vol. 73, pp. 433-439, 2012.
[53] M. Stojanovic, "Retrofocusing techniques for high rate acoustic communications," *J. Acoust. Soc. Am.*, vol. 117, pp. 1173-1185, 2005.
[54] G. Zhang and H. Dong, "Experimental research on adaptive multichannel equalization for underwater communications," in *Proc. 2011 IEEE Instrumentation and Measurement Technology Conference (I2MTC)*, pp. 1-5, Hangzhou, 2011.
[55] G. Zhang, J. M. Hovem, H. Dong, and L. Liu, "Coherent underwater communication using passive time reversal over multipath channels," *Applied Acoustics*, vol. 72, pp. 412-419, 2010.
[56] G. Zhang, J. M. Hovem, H. Dong, and P. A. van Walree, "A novel probe processing method for underwater communication by passive-phase conjugation," in *Proc 2011 IEEE International Conference on Acoustics, Speech and Signal Processing (ICASSP)*, pp.2700-2703, Prague, 2011.
[57] S. Mallat, *A Wavelet Tour of Signal Processing*, 2 ed: Academic Press, 1999.
[58] http://www.sounddevices.com/products/722.htm.
[59] http://www.ntnu.edu/marine/gunnerus.
[60] http://www.chelsea.co.uk/.
[61] http://www.rme-audio.de/en_products_octamic_2.php.
[62] http://www.rme-audio.de/en_products_fireface_400.php.
[63] J. M. Cramer, R. A. Scholtz, and M. Z. Win, "Spatio-temporal diversity in ultra-wideband radio," in *Proc. 1999 IEEE Wireless Communications and Networking Conference (WCNC)*, vol. 2, pp. 888-892, New Orleans, 1999.
[64] S. E. Cho, S. Hee Chun, and W. S. Hodgkiss, "Successive interference cancellation for underwater acoustic communications," *IEEE J. Ocean. Eng.*, vol. 36, pp. 490-501, 2011.
[65] S. E. Cho, H. C. Song, and W. S. Hodgkiss, "Successive interference cancellation for time-reversed underwater acoustic channels," in *Proc MTS/IEEE OCEANS 2009*, pp. 1-7, Biloxi, 2009.
[66] S. E. Cho, H. C. Song, and W. S. Hodgkiss, "Successive interference cancellation for time-varying underwater acoustic channels," in *Proc. MTS/IEEE OCEANS 2010*, pp. 1-4, Seatle, 2010.
[67] A. Song, M. Badiey, V. K. McDonald, and T. C. Yang, "Time reversal receivers for high data rate acoustic multiple-input-multiple-output communication," *IEEE J. Ocean. Eng.,* vol. 36, pp. 525-538, 2011.
[68] R. Otnes and T. H. Eggen, "Underwater acoustic communications: Long-term test of turbo equalization in shallow water," *IEEE J. Ocean. Eng.*, vol. 33, pp. 321-334, 2008.

[69] P. A. van Walree and G. Leus, "Robust underwater telemetry with adaptive Turbo multiband equalization," *IEEE J. Ocean. Eng.*, vol. 34, pp. 645-655, 2009.

[70] C. Jun Won, T. J. Riedl, K. Kyeongyeon, A. C. Singer, and J. C. Preisig, "Adaptive linear Turbo equalization over doubly selective channels," *IEEE J. Ocean. Eng.*, vol. 36, pp. 473-489, 2011.

[71] T. Jun, Y. R. Zheng, X. Chengshan, and T. C. Yang, "Robust MIMO underwater acoustic communications using Turbo block decision-feedback equalization," *IEEE J. Ocean. Eng.,* vol. 35, pp. 948-960, 2010.

Selected Papers

Paper 1: Spatial Diversity in Multichannel Processing for Underwater Acoustic Communications

Guosong Zhang and Hefeng Dong

In Ocean Engineering, vol. 38, pp. 1611-1623, 2011.

The thesis author had the original idea for this paper. The co-authors participated in scientific discussions.

Ocean Engineering 38 (2011) 1611–1623

Contents lists available at ScienceDirect

Ocean Engineering

journal homepage: www.elsevier.com/locate/oceaneng

Spatial diversity in multichannel processing for underwater acoustic communications

Guosong Zhang*, Hefeng Dong

Department of Electronics and Telecommunications, Norwegian University of Science and Technology (NTNU), NO-7491 Trondheim, Norway

ARTICLE INFO

Article history:
Received 6 April 2011
Accepted 30 July 2011
Editor-in-Chief: A.I. Incecik

Keywords:
Spatial diversity
Adaptive multichannel processing
Passive time reversal
Passive-phase conjugation
Decision feedback equalizer
Underwater acoustic communication

ABSTRACT

This paper discusses spatial diversity for underwater communications and presents a passive-phase conjugation (PPC) based multichannel equalizer. Multichannel processing involves taking advantage of multiple receivers distributed in space to take advantage of spatial diversity. The multichannel decision feedback equalizer (DFE) uses multiple nonlinear adaptive filters to remove intersymbol interference (ISI), and its complexity increases with time spread plus the number of receiving channels. Passive time reversal realized by the passive-phase conjugation (PPC) approach refocuses time delayed arrivals at the receiving array, where spatial diversity is obtained by the multichannel combining. The property of refocusing can be used to mitigate ISI for underwater communications, and only one single channel equalizer is required to remove residual ISI. PPC achieves pulse compression for time delayed arrivals, where the number of taps is significantly reduced for a PPC based equalizer. Based on temporal diversity obtained by pulse compression, the proposed structure improves the performance of time reversal communications by adaptive diversity combining. Three receiver structures are evaluated by processing real data collected in an experiment, which was conducted in a range-dependent acoustic channel over a range of 4 km. Results have demonstrated superior performance of the proposed receiver structure.

1. Introduction

The underwater acoustic channel is characterized by the extended time-varying multipath due to acoustic propagation in a temporal variant wave guide (Catipovic, 1990). Complex oceanographic phenomena, such as turbulence, internal waves, a moving sea surface, and sound speed gradients impact stable underwater acoustic communications. High-rate coherent communications have been researched (Kilfoyle and Baggeroer, 2000), where adaptive channel equalizations are required to remove intersymbol interference (ISI). Adaptive multichannel equalization has been proposed by Stojanovic et al. (1992), where a multichannel decision feedback equalizer (DFE) plus carrier-phase tracking is used to remove ISI. With multiple receivers distributed in space, spatial diversity is exploited by the multichannel processing (Stojanovic, 1994; Stojanovic et al., 1993, 1994). Since the number of taps for an adaptive channel equalizer is determined by the time spread (Proakis, 2001), the computational load for a multichannel DFE becomes intractable with an increasing number of taps plus a large number of receiving channels.

A time reversal mirror refocuses time delayed arrivals at the intended depth, and this property is used to reduce ISI for communications (Dowling, 1994; Edelmann et al., 2002; Kuperman et al., 1998). Instead of two-way transmission involving two arrays, passive time reversal communications realized by the passive-phase conjugation (PPC) approach decrease the instrumentation using only one receiving array plus one-way transmission (Gomes et al., 2008; Rouseff et al., 2001; Song et al., 2006b; Yang, 2005). PPC processing can be treated as match-filtering of the received signal. For the passive time reversal method, spatial diversity is used to suppress ISI by low complex multichannel combining (Song et al., 2006a). ISI cannot be eliminated but is mitigated, where the channel impulse response cannot be converted into a Dirac function. In a time-varying underwater channel, the refocusing degrades with elapsed time. It is a rule of thumb that only one adaptive channel equalizer with a reduced number of taps removes residual ISI after refocusing and tracks channel variations. In terms of output signal-to-noise ratio (SNR), the theoretical performance of time reversal communications has been discussed in Stojanovic (2005), but it is difficult to precisely predict the performance in a real ocean due to interchannel correlations and residual ISI. As discussed by Yang (2004), the multichannel DFE achieves superior performance over the PPC method, as the multichannel DFE exploits spatial diversity by adaptive multichannel combining.

* Corresponding author. Tel.: +47 73590465; fax: +47 73591412.
E-mail address: Guosong.Zhang@iet.ntnu.no (G. Zhang).

0029-8018/$ - see front matter © 2011 Elsevier Ltd. All rights reserved.
doi:10.1016/j.oceaneng.2011.07.023

The complexity of adaptive multichannel DFE increases with the number of taps, which is determined by the time spread in the communication channel. In order to reduce the complexity, a PPC based equalizer of adaptive multichannel diversity combining is presented in this paper. PPC processing is conducted prior to adaptive equalization, where the number of taps is significantly reduced because of pulse compression for the time delayed arrivals. In a real ocean, since interchannel correlations exist among the receivers of different input SNRs, the adaptive scheme has advantage to exploit spatial diversity. Based on a previous output mean square error (MSE), the coefficients for the multichannel combining are updated to minimize current output MSE. By comparison, the passive time reversal method uses spatial diversity without considering the output.

In this paper, three receiver structures of a multichannel DFE (McDFE), passive time reversal communications realized by PPC plus one single channel DFE (PPC–DFE) and a PPC based multichannel DFE (PPC–DFE) are assessed by off-line processing real data collected in a recent experiment. In Trondheim harbor, the sea trial was carried out in a depth fluctuated environment over a range of 4 km.

This paper is organized as follows. Section 2 introduces the structure of multichannel DFE. In Section 3, the passive time reversal communications is briefly reviewed, and the PPC based multichannel DFE is presented. The field experiment is introduced in Section 4. In Section 5, the off-line processing results are presented and analyzed, and the performance of the three structures is shown. Finally, Section 6 summaries the work.

2. Adaptive multichannel equalization

The communication information consists of a sequence of symbols denoted as $I[m]$, and each symbol occupies a duration of T. The transmitted signal $s(t)$, which has a carrier frequency f_c is expressed as

$$s(t)=\mathrm{Re}\left\{\sum_m I[m]g(t-mT)e^{j2\pi f_c t}\right\}, \tag{1}$$

where $\mathrm{Re}\{\bullet\}$ denotes the real part of a complex number, and $g(t)$ is the pulse shape function for each symbol such that

$$g(\tau)=\begin{cases}1, & \text{for } 0\le\tau<T\\ 0, & \text{otherwise}\end{cases}. \tag{2}$$

At the kth receiver, the received signal $r_k(t)$ is demodulated to be a baseband signal $v_k(t)$ such as

$$v_k(t)=\sum_m I[m]h_k(t-mT)e^{j\theta_k(t)}+w_k(t), \tag{3}$$

where $h_k(t)$ represents the channel impulse response, $w_k(t)$ is a band-limited noise, and $\theta_k(t)$ denotes a frequency shift caused by a Doppler shift. In a multipath channel, there is ISI, which causes errors in high rate communications.

The objective of adaptive channel equalization is to remove ISI. In the deconvolution process, a linear equalizer exaggerates noise where there are spectral nulls. DFE has a nonlinear structure, which is determined by the channel physics (Yang, 2004). Based on the minimum mean square error (MSE) criterion, DFE achieves a superior performance over the linear equalizer. In an underwater environment due to boundary reflections, time-varying fading occurs in communications. It is intractable to pre-deploy a receiver in order to avoid deep fading. It is practical to use multiple independent receivers that are distributed in space, where the probability of deep fading is decreased, since the receivers provide spatial diversity (Proakis, 2001). Spatial diversity is used by multichannel processing to achieve stable communications. A multichannel DFE takes advantage of spatial diversity to achieve robust channel equalization.

Fig. 1 shows the diagram of an adaptive multichannel DFE. The baseband signal is converted to N samples per symbol for digital signal processing, and carrier-phase tracking is implemented on a symbol-by-symbol basis using a second order digital phase-locked loop (DPLL) proposed in Stojanovic et al. (1992, 1993). $\hat{\theta}_k[n]$ is the estimate of the phase offset $\theta_k[n]$. The recursive least squares (RLS) algorithm updates tap weights with respect to minimize output MSE, where the RLS algorithm is preferred for its fast convergence rate (Haykin, 2001).

When estimating the nth symbol, let the kth channel feed-forward filter tap weight vector be

$$a'_k[n]=\{a^k_1[n],\ldots,a^k_{N_{ff}}[n]\}^*, \tag{4}$$

where the number of feed-forward taps is N_{ff} and * denotes complex phase conjugation. For down-sampling at a random initial instant, a $T/2$ spaced (2 samples per symbol) DFE is sufficient to correct synchronization errors for the signal, which has a bandwidth of $1/T$ (George et al., 1971). The input samples to the feed-forward filter of N_{ff} taps are written as a vector

$$v_k[n]=\{v_k[nT],v_k[nT-T/2],\ldots,v_k[n-N_{ff}T/2]\}^T. \tag{5}$$

The tap coefficient vector for the feedback filter is written as

$$b'[n]=\{b_1[n],\ldots,b_{N_{fb}}[n]\}^*, \tag{6}$$

where the number of feedback taps is N_{fb}, and the vector is updated at the symbol rate $1/T$. The input vector to the feedback filter is

$$d[n]=\{\hat{I}[n-1],\ldots,\hat{I}[n-N_{fb}]\}^T, \tag{7}$$

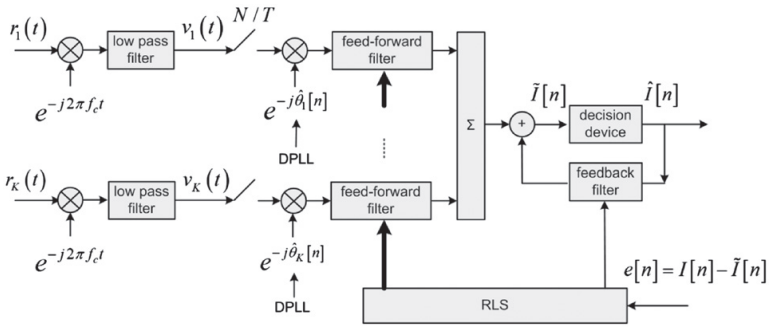

Fig. 1. Receiver structure of a multichannel DFE. There are N samples per symbol in baseband digital signal processing.

and $\hat{I}[n]$ is a decided output, which is the closest symbol to the estimated symbol $\tilde{I}[n]$. $\tilde{I}[n]$ is obtained by combining the K-channel estimates

$$\tilde{I}[n]=\{a'_1[n],\ldots,a'_K[n],-b'[n]\}\begin{Bmatrix} v_1[n]e^{-j\hat{\theta}_1[n]} \\ \vdots \\ v_K[n]e^{-j\hat{\theta}_K[n]} \\ d[n] \end{Bmatrix}=c'[n]u[n]. \tag{8}$$

$\hat{\theta}_k[n]$ corrects the phase offset of the current symbol, which is going to be fed into the feed-forward filter, and it is updated by the second order DPLL.

The estimation error is defined as

$$e[n]=I[n]-\tilde{I}[n], \tag{9}$$

where $I[n]$ is the training symbol in the training mode. $I[n]$ is replaced by $\hat{I}[n]$ in iterations of tracking mode. The coefficients of the K feed-forward filters are jointly updated by the RLS algorithm to minimize the output MSE

$$J_{MSE}[n]=E\{|e[n]|^2\}=E\{|I[n]-\tilde{I}[n]|^2\}, \tag{10}$$

where $|e[n]|$ denotes the absolute value of $e[n]$. The instantaneous estimate of the gradient of $J_{MSE}[n]$ with respect to $\hat{\theta}_k[n]$ is

$$\Phi_k[n]=\mathrm{Im}\{a'_k[n]v_k[n]\{e[n]\}^*\}, \tag{11}$$

and $\mathrm{Im}\{\bullet\}$ denotes the imaginary part of a complex number. The second order DPLL updating equation is given by (Stojanovic et al., 1993)

$$\hat{\theta}_k[n+1]=\hat{\theta}_k[n]+K_1\Phi_k[n]+K_2\sum_{m=0}^{n}\Phi_k[m],\quad k=1,\ldots,K, \tag{12}$$

where K is the number of receiving channels, and K_1 is the proportional tracking constant and K_2 is the integral tracking constant. As suggested by Stojanovic (2008), $K_2=K_1/10$ is chosen to achieve good performance, and this carrier-phase tracking method has been widely used in coherent communications (Edelmann et al., 2005; Gomes et al., 2008; Song et al., 2008; Yang, 2007).

Since the adaptive channel equalizer is an adaptive filter to deconvolve the channel impulse response, the number of taps for the filter is determined by the time spread. In each iteration for the RLS algorithm to update $a'_k[n]$ and $b'_k[n]$, the arithmetic operations for McDFE are performed on the order of $\{(N_{ff}+N_{fb})K\}^2$ (Haykin, 2001). The computational load increases with the number of taps plus the number of receiving channels, and it becomes intractable in a channel of extended time spread. Besides, the number of training symbols increases with the number of taps, where the efficiency in communications is decreased.

3. PPC approach

The passive time reversal communications can be realized by PPC processing. The PPC approach refocus time delayed arrivals at the receiving array, where ISI caused by multipath is significantly reduced, and this property is used for communications. ISI caused by multipath is mitigated by temporal focusing, and spatial diversity is obtained by spatial focusing. The single channel output of refocusing $z(t)$ is written as

$$\begin{aligned} z(t)&=\sum_{k=1}^{K}h_k(-t)\otimes v_k(t)\\ &=\sum_{k=1}^{K}h_k(-t)\otimes\sum_m I[m]h_k(t-mT)e^{j\theta_k(t)}+\sum_{k=1}^{K}h_k(-t)\otimes w_k(t)\\ &=\sum_m I[m]\sum_{k=1}^{K}h_k(-t)\otimes h_k(t-mT)e^{j\theta_k(t)}+\varsigma(t)\\ &=\sum_m I[m]\sum_{k=1}^{K}Q_k(t-mT)e^{j\bar{\theta}_k(t)}+\varsigma(t)\\ &=\sum_m I[m]Q(t-mT)e^{j\bar{\theta}_k(t)}+\varsigma(t), \end{aligned} \tag{13}$$

where $Q(t)$ is the autocorrelations of the channel impulse response summed over the K-channels, $\bar{\theta}_k(t)$ is the carrier frequency shift after K-channel combining, $\varsigma(t)$ is a filtered noise, and $\otimes$ denotes convolution. In each channel, the time reversed impulse response $h_k(-t)$ is used as a filter to achieve pulse compression $Q_k(t)$, which denotes the autocorrelation of $h_k(t)$.

The Fourier transform of $Q(t)$ is

$$\begin{aligned} Q(\omega)&=FT\left\{\sum_{k=1}^{K}h_k(-t)\otimes h_k(t)\right\}=\sum_{k=1}^{K}H_k^*(\omega)H_k(\omega)\\ &=\sum_{k=1}^{K}|H_k(\omega)|^2=\sum_{k=1}^{K}Q_k(\omega), \end{aligned} \tag{14}$$

where $H_k(\omega)$ denotes the Fourier transform of the impulse response $h_k(t)$. $Q(\omega)$ represents a frequency response averaged over the independent $\{Q_k(\omega)\}$, and it can remove spectral nulls and peaks, which could occur in a single channel $Q_k(t)$ function. By multichannel combining shown in Eq. (14), spatial diversity is exploited by passive time reversal to suppress ISI. Since $Q(\omega)$ is bandwidth limited, the main lobe plus side lobes of $Q(t)$ could cause residual ISI. As discussed by Yang (2004), the side lobe level of $Q(t)$ decreases with an increasing number of receivers, and the side lobes cannot be eliminated. In Eq. (13), residual ISI caused by $Q(t)$ is removed by an adaptive channel equalizer.

The receiver structure for passive time reversal communications is shown in Fig. 2, and it is realized by PPC plus a single channel DFE. A single channel DPLL is used to track the phase offset caused by $e^{j\bar{\theta}_k(t)}$. Since ISI is mitigated by refocusing, the

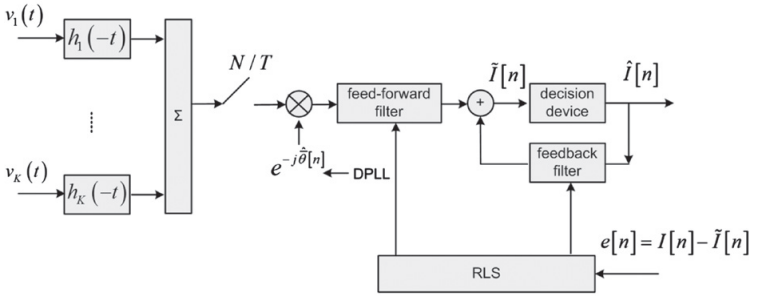

Fig. 2. Receiver structure for passive time reversal communications.

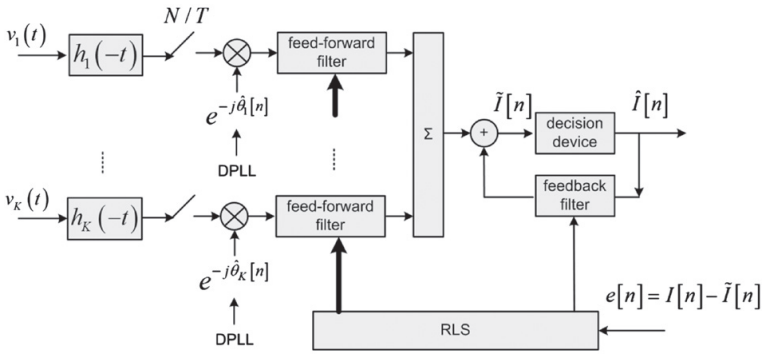

Fig. 3. Receiver structure of a PPC based multichannel DFE.

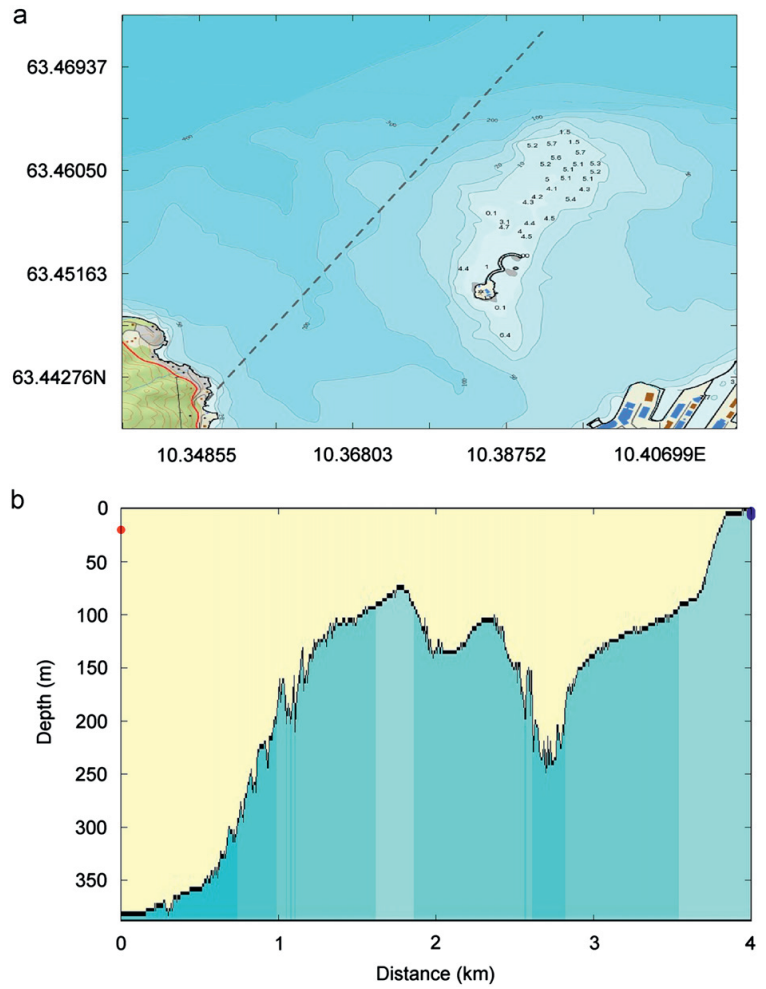

Fig. 4. (a) Experimental area in Trondheim harbor. The dash line is the communication track. (b) Depth profile in the communication direction. The red dot on the left denotes the transmitter position, and the blue dot on the right denotes the receiving array. (For interpretation of the references to color in this figure legend, the reader is referred to the web version of this article.)

number of taps for the feed-forward and feedback filters is significantly reduced, where the computational load for the RLS algorithm is reduced. In a time-varying channel, the refocusing degrades with time, and the DFE also tracks the channel variation.

It is discussed by Yang (2004) that DFE achieves superior performance over PPC, where one receiver is used for analysis, as the minimum output MSE satisfies

$$J_{\min}^{PPC} \geq J_{\min}^{DFE}. \tag{15}$$

Due to interchannel correlations in a real ocean, there is lack of literature for theoretical analysis of the inequality for multichannel scenarios. The inequality has been proved by numerical simulations and real data processing results (Yang, 2004), where 11 receivers (with an element spacing of 5 m in simulations) were used in communications at a carrier frequency of 750 Hz, and an McDFE achieves better performance than PPC–DFE. The performance improvement of PPC–DFE is attributed to spatial diversity exploitation.

For practical purposes, a small number of hydrophones are preferred. In order to improve the performance of PPC–DFE, adaptive spatial diversity combining is investigated. The structure of PPC–McDFE is shown in Fig. 3. Prior to the multichannel equalization, pulse compression is conducted to reduce the number of taps for equalization, where the complexity of the multichannel DFE is reduced. The RLS algorithm jointly updates the coefficients for the feed-forward filters in order to minimize output MSE. *K*-channel independent DPLLs are implemented for carrier-phase tracking. Comparing with the structure shown in Fig. 2, where multichannel combining is conducted prior to equalization, adaptive diversity combining is performed by PPC–McDFE to obtain an estimate. Spatial diversity is exploited in the same way of McDFE shown in Fig. 1.

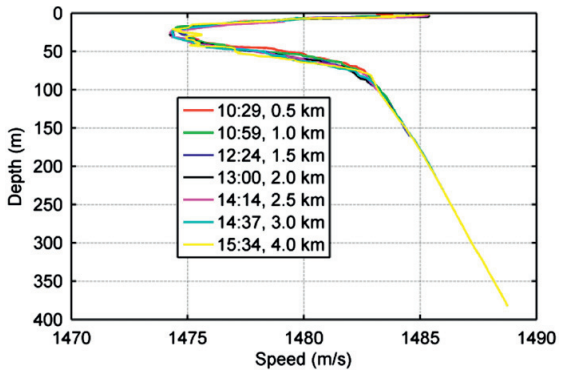

Fig. 5. Sound speed profiles measured at different distances to the receiving array.

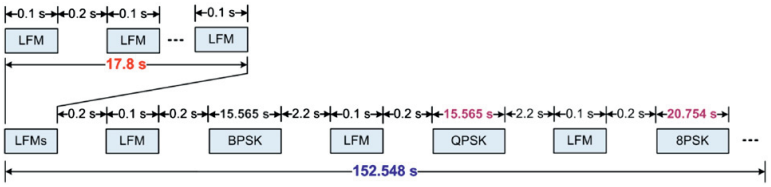

Fig. 6. One period of the transmitted signal.

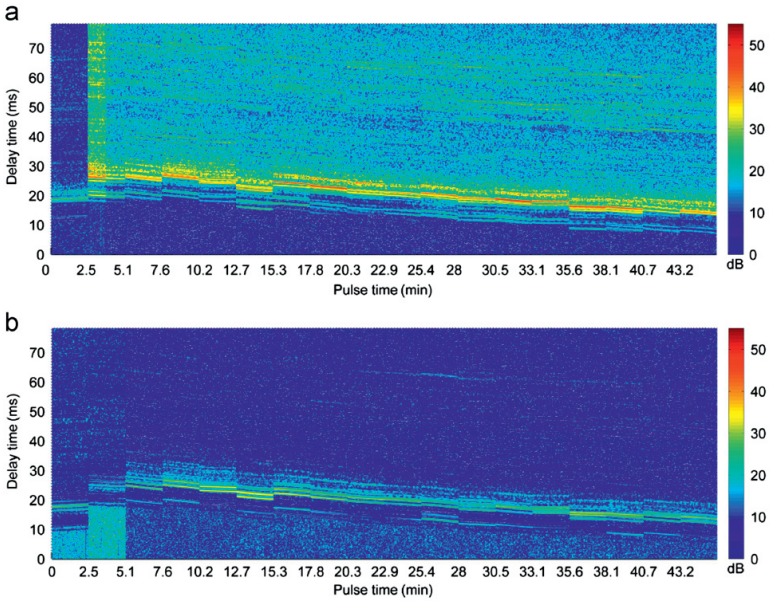

Fig. 7. Impulse response measurements in the 45 min experiment. (a) Hydrophone No. 2 and (b) hydrophone No. 5.

For a receiving array deployed in a time-varying ocean, since it is unfeasible to predict interchannel correlations, it is preferred that spatial diversity could be exploited by an adaptive scheme, which updates the diversity combining coefficients to minimize output MSE. In order to decrease the computational load for the RLS algorithm, PPC–McDFE provides an alternative as a receiver structure of low complexity, since the number of taps is significantly reduced by pulse compression. The three receiver structures shown in Figs. 1–3 are assessed by off-line real data processing.

4. The experiment

The communication experiment was conducted on June 30, 2010, in Trondheim harbor in Norway. The experimental area is shown in Fig. 4(a). The shallow region, which is less than 20 m, extends about 100 m offshore, and the sea depth varies from tens of meters near the island Munkholmen (in the center of the figure) to hundreds of meters. Fig. 4(b) shows that the depth along the communication track changes from 10 m to 380 m. The red dot denotes the position of the transmitter in a distance of 4 km to a cross receiving array (CRA). The transmitter used a hemispherical acoustic transducer suspended at a depth of 20 m from the NTNU research vessel R/V Gunnerus. The CRA of 10 hydrophones is near-shore deployed in a water depth of 10 m, and it consists of a vertical receiving array of 6 hydrophones (hydrophone No. 1–6) with 1 m element spacing and a horizontal receiving array of 4 hydrophones (hydrophone No. 7–10) with 1.5 m element spacing. Hydrophone No. 1 is 1.5 m above the bottom, and hydrophones No. 7–10 are 4 m above the bottom. The dynamic positioning system of R/V Gunnerus was activated to reduce drifting.

The experiment was conducted on a windy and rainy day. In order to monitor the environmental variations in the trial, sound speed profiles were measured by the R/V Gunnerus. Fig. 5 shows the sound speed profiles measured at different distances to the receiving array. In the communication track, there was a sound channel at the depth of 20 m during the trials. The array was deployed in the shallow region at a depth which was different from the transmitter depth, and the received signal experienced time-varying fading due to reflections in the acoustic propagation.

In the experiment, one period of the transmitted signals shown in Fig. 6 was repeatedly transmitted for about 45 min. The carrier frequency of the transmitted signals was 12 kHz. LFM denotes a 0.1 s linear frequency modulation (LFM) chirp with a Hanning window, and its effective bandwidth is 2.2 kHz. The 60-chirp signal is used to measure the channel response of 18 s within each period. The data symbols are generated by binary phase shift keying (BPSK), quadrature phase shift keying (QPSK) modulations and 8 phase shift keying (8PSK), and the symbol rate is $1/T=1$ kilosymbols/s. The LFM chirp is used as both a channel probe signal and a shaping pulse for PPC communications, so the received probe signal is immediately used for PPC processing. The received waveforms were recorded with a sampling frequency of 96 kHz for off-line processing in the laboratory.

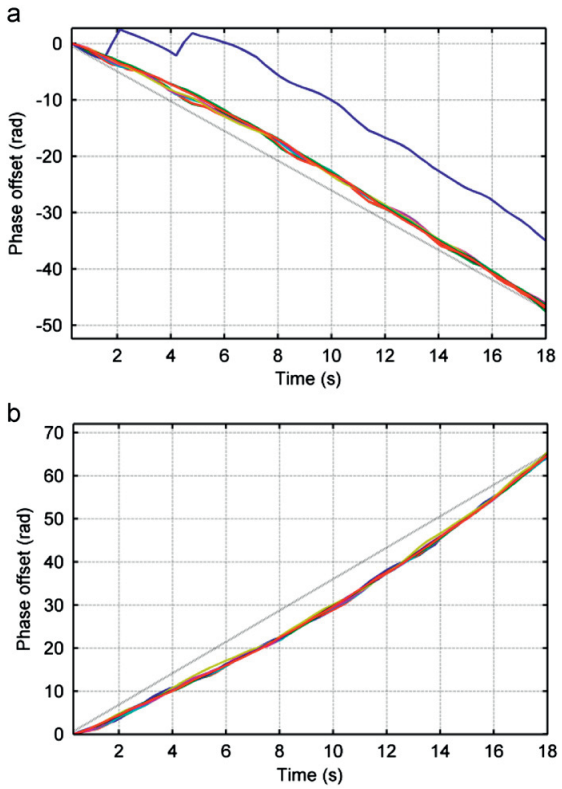

Fig. 8. Phase offset measurements in two periods. (a) The first period and (b) the tenth period.

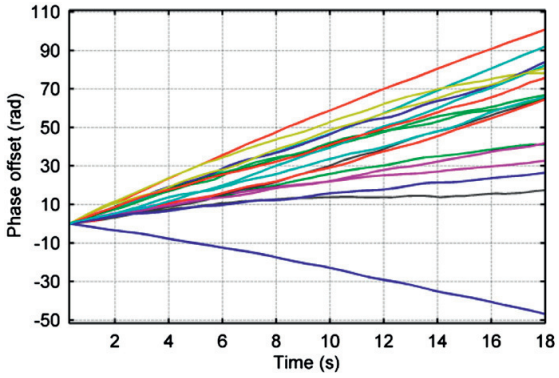

Fig. 9. Mean phase offset measurement in the 45 min experiment.

Table 1
Receiver parameters for McDFE.

Parameters	Description	Value
F_s	Sampling frequency (kHz)	96
f_c	Carrier frequency (kHz)	12
R	The symbol rate (kilosymbols/s)	1
N	Over sampling factor	2
N_{ff}	The number of feed-forward filter taps	40
N_{fb}	The number of feedback filter taps	40
N_t	The number of training symbols	720
λ	RLS forgetting factor	0.99
K_1	Proportional tracking constant in PLL	0.01
K_2	Integral tracking constant in PLL	0.001

5. Results and analysis

This section shows channel measurements, communication results, and performance of the three receiver structures.

5.1. Channel measurements

By taking advantage of the correlation property of the LFM chirp, the channel impulse response is measured using the replica correlation method. Fig. 7 shows two overview examples of the channel response that the 18-second channel response is measured every 152.548 s, where the hydrophones are 2.5 m and 5.5 m above the sea bottom, respectively. The response changes with time and the hydrophone position, and time delayed arrivals span more than 10 ms. The magnitude variations indicate that the receiving SNR changes with time and hydrophone position. Temporal dilation is observed in the first period, temporal compression of different rates is observed in the rest of 17 periods, as the arrivals are not aligned in delay time due to relative movement between the transmitter and the receiver (Sharif et al., 2000). Since the rate of compression or dilation caused by Doppler shift is time variant, it indicates that the carrier frequency shift changes with time in the trial.

The carrier frequency shift is measured using the cross-correlation method given in Zhang and Dong (2011), where the first received chirp is used to correlate with the following received chirps. The phase offset of cross-correlation between two received chirps is measured, and the frequency shift is estimated by the slope of the phase offset. Fig. 8 shows the phase offset measurements of 10 receiving hydrophones. Among the

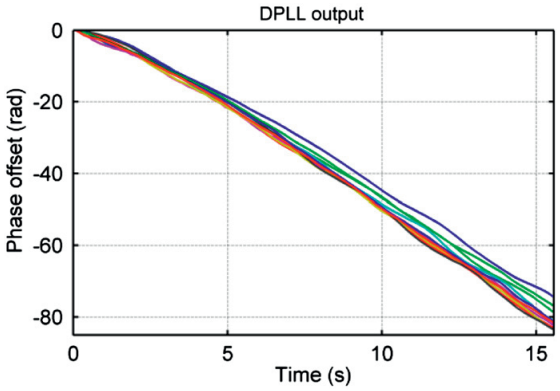

Fig. 11. Output of 10 DPLLs in the first period.

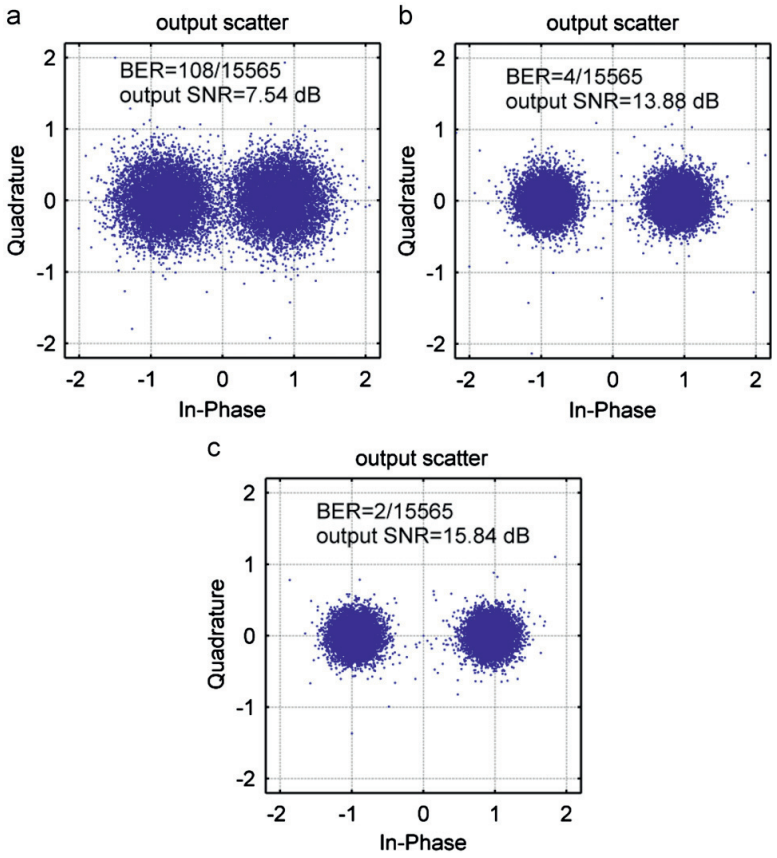

Fig. 10. Performance of McDFE for various numbers of hydrophones. (a) Hydrophone No. 1–4, (b) hydrophone No. 1–6, and (c) hydrophone No. 1–10.

hydrophones, there is little difference in terms of the slope of the phase offset. The slope is not constant within 18 s due to time-varying Doppler shift. In approximation, the slope in the first period is about −2.70 rad/s, which is equivalent to a frequency shift of −0.42 Hz; the slope in Fig. 8(b) is about 3.60 rad/s, which is equivalent to a frequency shift of 0.57 Hz. A negative frequency shift correlates with the response measurement in the first period shown in Fig. 7, where dilation caused by the reverse movement is observed.

The mean phase offset measurement for 18 periods is shown in Fig. 9, where 10 hydrophones are used. The slope changes with period. Only one negative frequency shift is observed. In calculation, the equivalent frequency shift changes from 0.16 Hz to 0.88 Hz in the rest of 17 periods. It is shown that time variant Doppler shift existed in the experiment, where the phase offset measurement correlates with the impulse measurement shown in Fig. 7. It is unfeasible to preset a carrier frequency in demodulation, and the method of DPLL is implemented to realize carrier-phase tracking.

5.2. The communication results

Since the transmitted communication signal was pulse-shaped by the LFM chirp of 0.1 s, McDFE has to remove ISI caused by the chirp plus the channel impulse response. The parameters for McDFE are listed in Table 1. The feed-forward filters span 20 symbol intervals, where there are two samples per symbol in digital signal processing. Fig. 10 shows the receiver performance for BPSK. The number of hydrophones is increased from 4 to 10, the bit error rate (BER) is decreased from 6.94e−3 to 1.28e−4, and the output SNR calculated by (1−MSE)/MSE (Proakis, 2001) is increased from 7.54 dB to 15.84 dB. The performance in terms of

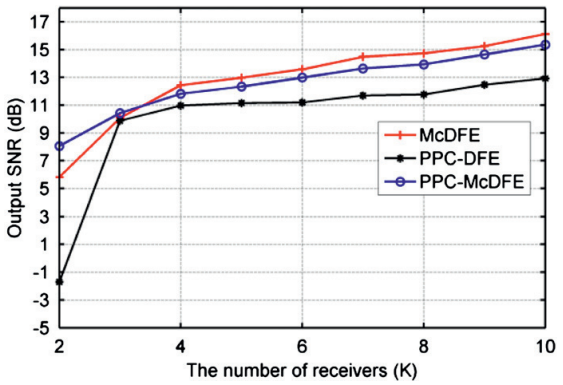

Fig. 13. Performance in terms of output SNR as a function of the number of receivers.

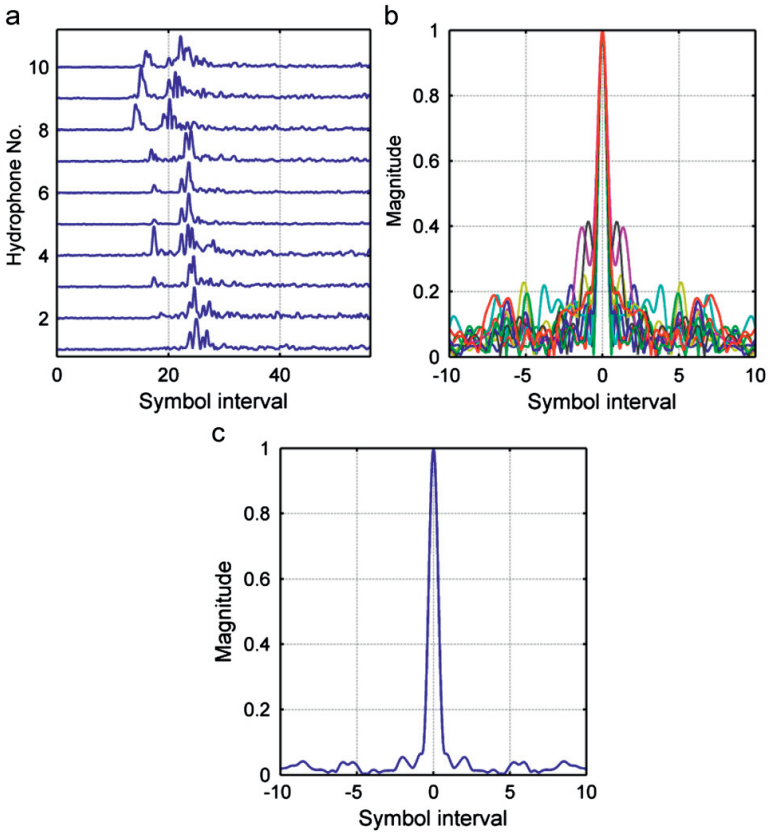

Fig. 12. (a) Channel responses estimated by the LFM chirp, (b) normalized magnitude of $\hat{Q}_k(t)$ functions over 10 receiving channels, and (c) normalized magnitude of $\hat{Q}(t)$ function.

output SNR is improved with an increasing number of receivers, as spatial diversity is better exploited using more independent receivers. $K=10$ receiving channels are used in the following analysis.

Fig. 11 shows the DPLL output in BPSK communication of the first period. There is little difference among the receivers in terms of the slope of the phase offset, and the mean slope is -5.13 rad/s, which is equivalent to a frequency shift of -0.81 Hz. The negative frequency shifts obtained by DPLLs correlate with the measurement shown in Fig. 8(a). In order to deconvolve the channel impulse response, the number of taps for McDFE increases with the time spread. With a large number of taps, the computational load for the RLS algorithm is intractable in practice where the number of receiving channels becomes large. PPC communications take advantage of pulse compression to reduce the complexity of an adaptive channel equalizer.

Fig. 12 shows an example of ISI mitigation by pulse compression. As shown in Fig. 12(a), the multipath pattern changes with hydrophone, and the time spread varies from 5 to 15 symbol intervals. The complexity of conventional adaptive channel equalizers increases with the time spread. Pulse compression acts as match-filtering, which mitigates ISI by taking advantage of temporal diversity. Fig. 12(b) shows the normalized $\hat{Q}_k(t)$ functions, where $\hat{Q}_k(t)$ is the estimate of $Q_k(t)$. The time delayed arrivals are compressed within the main lobe width of 1 symbol interval, and there are side lobes. In two receiving channels, the side lobe magnitude is more than 40% of the main lobe magnitude. The side lobes change with receiving channel, as they are determined by the channel physics—the channel impulse response. Fig. 12(c) shows the normalized $\hat{Q}(t)$ function, where $\hat{Q}(t)$ is the estimate of $Q(t)$. $\hat{Q}(t)$ is obtained by

$$\hat{Q}(t)=\frac{1}{10}\sum_{k=1}^{10}\hat{Q}_k(t) \tag{16}$$

Comparing with a single channel $\hat{Q}_k(t)$, the side lobe level of $\hat{Q}(t)$ is reduced, because $\{\hat{Q}_k(t)\}$ are uncorrelated. After temporal focusing, spatial diversity is used by passive time reversal to reduce residual ISI caused by the side lobes, and residual ISI is removed by a single channel DFE shown in Fig. 2.

Since ISI is mitigated by pulse compression, the number of tabs for an adaptive channel equalizer is reduced. For both PPC–DFE and PPC–McDFE, the numbers of feed-forward and feedback filter taps are $N_{ff}=8$ and $N_{fb}=2$, respectively, where the number of training symbols is $N_t=72$, and the RLS algorithm is configured the same as McDFE shown in Table 1. Fig. 13 shows the performance in terms of output SNR as a function of the number of receivers K. The output SNR increases with the number of receiving channel, since more receivers are used to exploit spatial diversity. With a reduced number of taps, PPC–McDFE achieves similar performance of McDFE. PPC–DFE achieves the poorest performance when $K\geq 2$, and it obtains an output SNR of 3.20 dB less than McDFE, where 10 receivers are used.

The results for BPSK and QPSK of 18 periods are shown in Fig. 14. The output SNR changes with time due to the time variant input SNR, which is shown by the magnitude variation of the

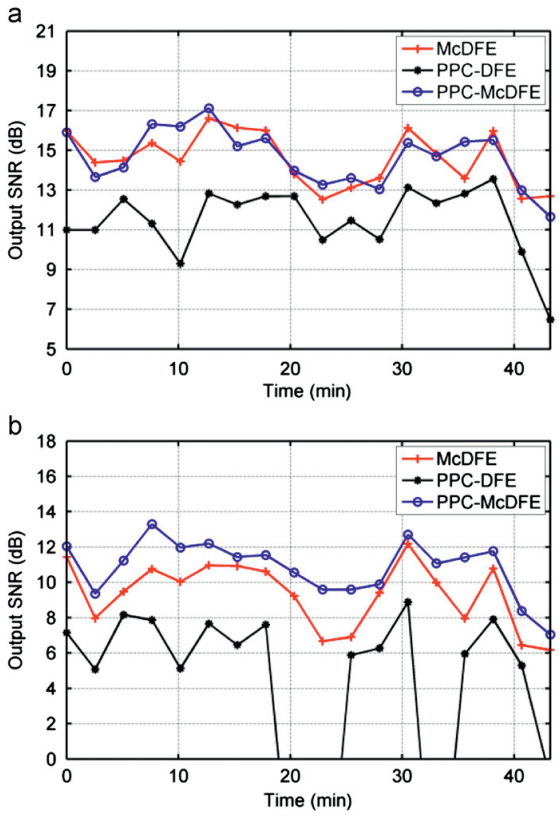

Fig. 14. Performance in terms of output SNR. (a) BPSK and (b) QPSK.

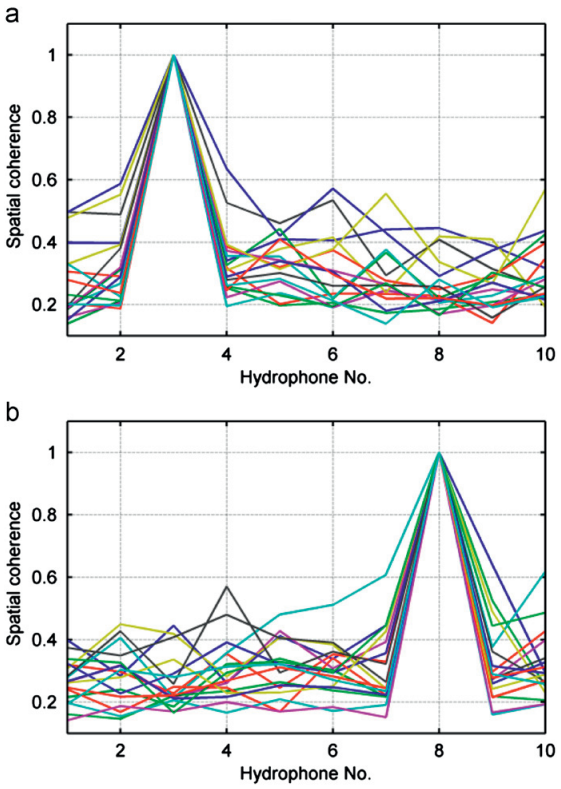

Fig. 15. Spatial coherence measured as a function of the receiver index. The reference hydrophone is: (a) $k=2$ and (b) $k=8$.

response measurements shown in Fig. 7. PPC–DFE achieves the poorest performance for both BPSK and QPSK, and it fails to recover the information in 4 periods for QPSK. PPC–McDFE achieves similar performance of McDFE for BPSK, and it achieves superior performance for QPSK. PPC–McDFE improves the performance of PPC–DFE, and the improvement changes with time. In calculation, the improvement changes from 1.28 dB to 6.90 dB for BPSK.

The improvement by PPC–McDFE originates from spatial diversity exploited by adaptive multichannel combining. Interchannel correlations exist among the receivers of the receiving array. The interchannel correlation between the kth and lth receivers is measured by the spatial coherence, which is given by

$$\psi(k,l)=\frac{|r_k(-t)\otimes r_l(t)|_{\max}}{\sqrt{|r_k(-t)\otimes r_k(t)|_{\max}|r_l(-t)\otimes r_l(t)|_{\max}}} \tag{17}$$

where $|r_k(-t)\otimes r_l(t)|_{\max}$ denotes the maximum absolute value of the correlation between $r_k(t)$ and $r_l(t)$, and $r_k(t)$ is the received signal of the kth hydrophone. Fig. 15 shows two examples of the spatial coherence measurement in 18 periods, where k is fixed as a reference and l is changed from 1 to 10. It is shown that the receiving channels are not independent and interchannel correlations change with time. Time-variant spatial diversity attributes to the improvement variation of PPC–McDFE.

In order to show the advantage of pulse compression, PPC–DFE and PPC–McDFE are tested using $N_{ff}=2$ and $N_{fb}=1$, where the number of training symbols is $N_t=24$ and the RLS is configured as shown in Table 1. The feed-forward filter taps span one symbol interval. Fig. 16 shows the performance of PPC–DFE and PPC–McDFE, respectively. Both structures with a minimal number of tabs have succeeded in recovering the distorted information. As shown in Fig. 16(a), PPC–DFE achieves a BER of 1.25e−2 with a mean output MSE of −10.89 dB. Its performance is improved by PPC–McDFE

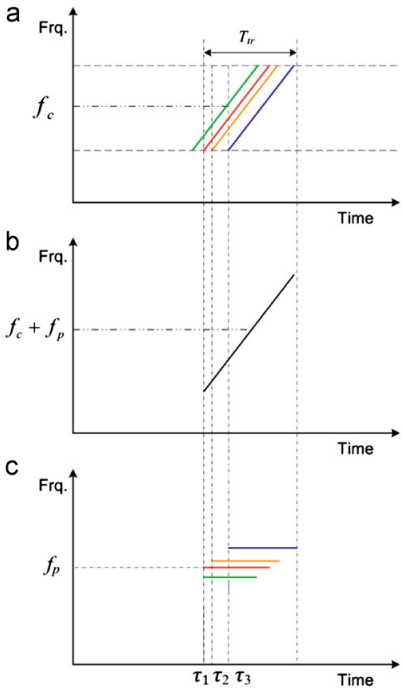

Fig. 17. Illustration of despreading. (a) 4 multipath arrivals of a central frequency f_c, (b) replica LFM chirp of a central frequency f_c+f_p, and (c) output of frequency components. (For interpretation of the references to color in this figure, the reader is referred to the web version of this article.)

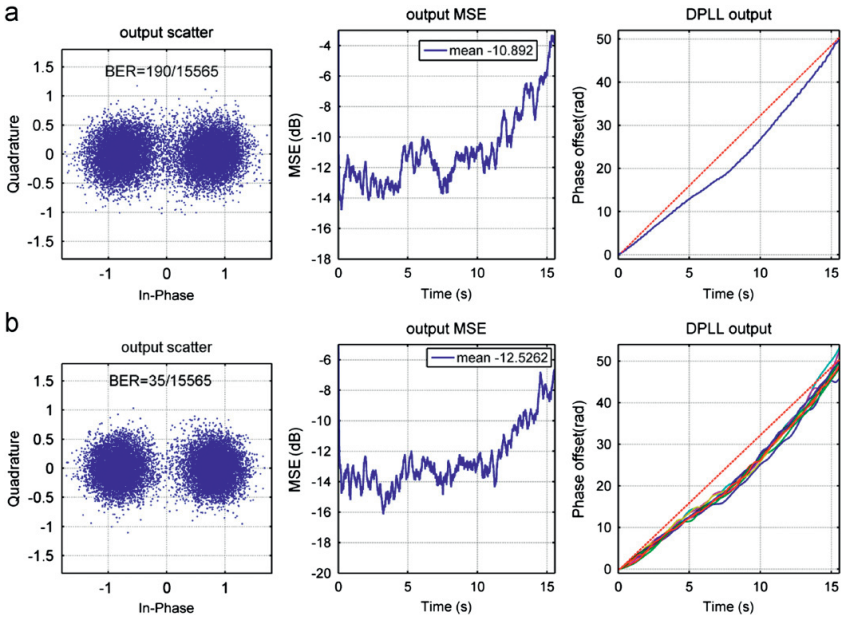

Fig. 16. Performance for BPSK. (a) PPC–DFE and (b) PPC–McDFE.

shown in Fig. 16(b), where BER is decreased to 2.24e−3 with a mean output MSE of −12.52 dB. The phase offset of PPC–DFE is the mean of 10-DPLL output of PPC–McDFE. The slope of the phase offset is not constant within 15.565 s, and it is approximate 3.21 rad/s, which is equivalent to a frequency shift of 0.51 Hz. Spatial diversity contributes the superior performance of PPC–McDFE, as the information of the output MSE is used in the diversity combining.

In a real ocean, since receivers are deployed with interchannel correlations (Yang, 2007) plus different input SNRs due to acoustic propagation, the scheme of adaptive multichannel combining is superior to obtain spatial diversity. PPC–McDFE takes advantage of temporal diversity by pulse compression, and it exploits spatial diversity with considering a previous output MSE to adjust diversity combining in order to minimize current output MSE.

5.3. Improvement from the probe processing

In this paper, the LFM chirp is used as both a shape pulse and a channel probe signal. As discussed by Song et al. (2010), there is minimal difference between using the two kinds of shape pulses—a LFM chirp and a root-raised cosine filter. Comparing with the method using a root-raised cosine filter (Flynn et al., 2004; Song et al., 2008), where the least square algorithm is used to estimate the channel response, the method using the chirp as a shaping pulse is of low complexity in realization. The received probe signal, which is immediately used for PPC processing is further processed to improve the receiver performance (Zhang et al., 2011).

The time delayed LFM chirp arrivals do not overlap in the frequency domain. The arrivals can be converted into constant frequencies by dispreading (Kebkal and Bannasch, 2002). Fig. 17 shows the despreading process. There are 4 arrivals illustrated by different colors shown in Fig. 17(a), where the arrivals are truncated with a time window T_{tr} and multiply with the replica chirp of time duration T_{tr}. As shown in Fig. 17(b), the frequency sweeping rate of the replica chirp is the same as the probe signal, but the carrier frequency is different from the probe signal. The received probe signal multiplies with the replica chirp, the double frequency part is filtered out using a low pass filter, and then the arrivals are converted into frequency components shown in Fig. 17(c). The frequencies can be selected by narrow band pass filtering, where the broadband noise is also suppressed, and afterwards the selected frequencies are converted into chirp arrivals by spreading on the replica chirp again.

Fig. 18 shows examples of the received probe processing, where the filtering bandwidth for the arrival selection is 1.2 kHz, which is equivalent to select the arrivals within 0.02 s. In the three examples, it is shown that the noise level is reduced and some late arrivals are excluded. Fig. 19 shows an example of the improvement by the probe processing. The BER is decreased from 3.53e−2 to 1.08e−2, as the output SNR is increased by 2.23 dB. The improvement is attributed to noise suppression and multipath selection, where the arrivals outside 0.02 s are

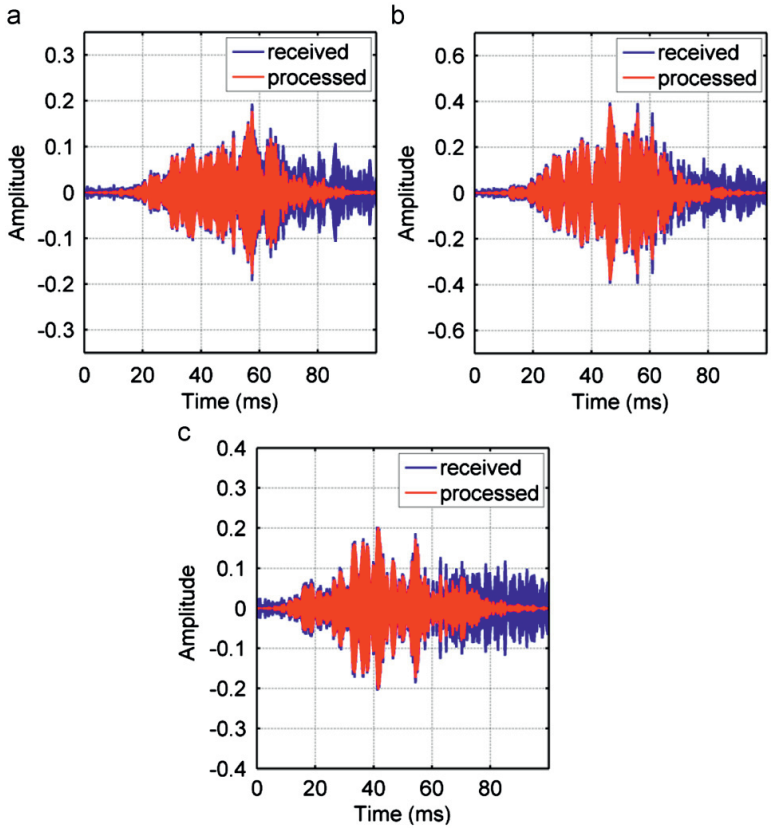

Fig. 18. Received and processed probe signals. (a) Hydrophone No. 1, (b) hydrophone No. 4, and (c) hydrophone No. 7.

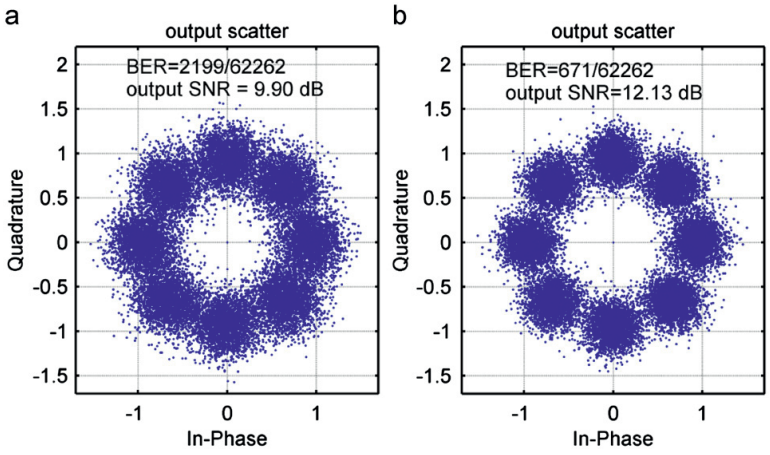

Fig. 19. Performance for 8PSK. (a) Without the probe processing and (b) with the probe processing.

excluded. With a LFM chirp as the shape pulse for PPC communications, it is of low complexity to estimate the channel for PPC processing, and the performance can be further improved by selecting the arrivals from the received probe signal.

6. Summary

Using multiple receivers distributed in space, spatial diversity is exploited by multichannel processing to achieve stable performance in a time-varying channel. Passive time reversal refocuses time delayed arrivals at the receiving array, where spatial diversity is used to suppress ISI for communications, and the property of refocusing reduces the number of taps for adaptive channel equalization. For practical purposes, it is preferred that good performance could be obtained with a small number of receivers. We have investigated three types of receiver structures, which are assessed by the real data collected in a range-dependent channel where the depth changes from 10 m to 380 m. The receiver performance is evaluated in terms of BER, output SNR and output MSE. The proposed PPC based multichannel DFE displays improved performance for the structure based on passive time reversal, and it also displays a reduced complexity for the conventional multichannel DFE.

The computational load of the RLS algorithm increases with the number of taps for an adaptive channel equalizer. Pulse compression is used by the PPC approach to reduce the number of taps for equalization. Since the time delayed arrivals is compressed within one symbol interval, the PPC based methods recover distorted information with a minimal number of taps, which span only one symbol interval. In the experimental assessment, PPC–McDFE with a reduced number of taps approximates the performance of McDFE, and it achieves superior performance over the passive time reversal communications. Based on temporal diversity obtained by PPC processing, PPC–McDFE performs adaptive diversity combining to exploit spatial diversity, where the output MSE is minimized.

Finally, with a LFM chirp as a shape pulse, the performance of PPC–McDFE is improved by processing the received probe signal, where the time delayed arrivals are selected and the noise from the received probe signal is suppressed. The improvement in terms of output SNR is shown for 8PSK communication, where the arrivals within 0.02 s are selected. It is flexible to select the arrivals by adjusting the filtering bandwidth.

Acknowledgment

The author would like to thank Jens M. Hovem for discussions, Ph.D. students Yan Jiang, Zhongxi Chao, technical engineer Tim Cato Netland, and the crew of the R/V Gunnerus for the help in conducting the experiments.

References

Catipovic, J.A., 1990. Performance limitations in underwater acoustic telemetry. IEEE Journal of Oceanic Engineering 15 (3), 205–216.
Dowling, D.R., 1994. Acoustic pulse compression using passive phase-conjugate processing. The Journal of the Acoustical Society of America 95 (3), 1450–1458.
Edelmann, G.F., Akal, T., Hodgkiss, W.S., Seongil, K., Kuperman, W.A., Hee Chun, S., 2002. An initial demonstration of underwater acoustic communication using time reversal. IEEE Journal of Oceanic Engineering 27 (3), 602–609.
Edelmann, G.F., Song, H.C., Kim, S., Hodgkiss, W.S., Kuperman, W.A., Akal, T., 2005. Underwater acoustic communications using time reversal. IEEE Journal of Oceanic Engineering 30 (4), 852–864.
Flynn, J.A., Ritcey, J.A., Rouseff, D., Fox, W.L.J., 2004. Multichannel equalization by decision-directed passive phase conjugation: experimental results. IEEE Journal of Oceanic Engineering 29 (3), 824–836.
George, D., Bowen, R., Storey, J., 1971. An adaptive decision feedback equalizer. IEEE Transactions on Communication Technology 19 (3), 281–293.
Gomes, J., Silva, A., Jesus, S., 2008. Adaptive spatial combining for passive time-reversed communications. The Journal of the Acoustical Society of America 124 (2), 1038–1053.
Haykin, S., 2001. Adaptive Filter Theory. Prentice Hall, Upper Saddle River, New Jersey.
Kebkal, K.G., Bannasch, R., 2002. Sweep-spread carrier for underwater communication over acoustic channels with strong multipath propagation. The Journal of the Acoustical Society of America 112 (5), 2043–2052.
Kilfoyle, D.B., Baggeroer, A.B., 2000. The state of the art in underwater acoustic telemetry. IEEE Journal of Oceanic Engineering 25 (1), 4–27.
Kuperman, W.A., Hodgkiss, W.S., Song, H.C., Akal, T., Ferla, C., Jackson, D.R., 1998. Phase conjugation in the ocean: experimental demonstration of an acoustic time-reversal mirror. The Journal of the Acoustical Society of America 103 (1), 25–40.
Proakis, J.G., 2001. Digital Communications. McGraw-Hill, New York.
Rouseff, D., Jackson, D.R., Fox, W.L.J., Jones, C.D., Ritcey, J.A., Dowling, D.R., 2001. Underwater acoustic communication by passive-phase conjugation: theory and experimental results. IEEE Journal of Oceanic Engineering 26 (4), 821–831.
Sharif, B.S., Neasham, J., Hinton, O.R., Adams, A.E., 2000. A computationally efficient Doppler compensation system for underwater acoustic communications. IEEE Journal of Oceanic Engineering 25 (1), 52–61.
Song, A., Badiey, M., Song, H.C., Hodgkiss, W.S., Porter, M.B., the KauaiEx, G., 2008. Impact of ocean variability on coherent underwater acoustic communications

during the Kauai experiment (KauaiEx). The Journal of the Acoustical Society of America 123 (2), 856–865.
Song, H.C., Hodgkiss, W.S., Kuperman, W.A., Higley, W.J., Raghukumar, K., Akal, T., Stevenson, M., 2006a. Spatial diversity in passive time reversal communications. The Journal of the Acoustical Society of America 120 (4), 2067–2076.
Song, H.C., Hodgkiss, W.S., Kuperman, W.A., Stevenson, M., Akal, T., 2006b. Improvement of time-reversal communications using adaptive channel equalizers. IEEE Journal of Oceanic Engineering 31 (2), 487–496.
Song, H.C., Kim, J.S., Hodgkiss, W.S., Kuperman, W.A., Stevenson, M., 2010. High-rate multiuser communications in shallow water. The Journal of the Acoustical Society of America 128 (5), 2920–2925.
Stojanovic, M., 1994. Coherent digital communications for rapidly fading channels with applications to underwater acoustics. The Journal of the Acoustical Society of America 96 (4), 2596.
Stojanovic, M., 2005. Retrofocusing techniques for high rate acoustic communications. The Journal of the Acoustical Society of America 117 (3), 1173–1185.
Stojanovic, M., 2008. Efficient processing of acoustic signals for high-rate information transmission over sparse underwater channels. Physical Communication 1 (2), 146–161.
Stojanovic, M., Catipovic, J., Proakis, J.G., 1992. An algorithm for multichannel coherent digital communications over long range underwater acoustic telemetry channels. In: Proceedings of the OCEANS '92, Mastering the Oceans Through Technology, pp. 577–582.
Stojanovic, M., Catipovic, J., Proakis, J.G., 1993. Adaptive multichannel combining and equalization for underwater acoustic communications. The Journal of the Acoustical Society of America 94 (3), 1621–1631.
Stojanovic, M., Catipovic, J.A., Proakis, J.G., 1994. Phase-coherent digital communications for underwater acoustic channels. IEEE Journal of Oceanic Engineering 19 (1), 100–111.
Yang, T.C., 2004. Differences between passive-phase conjugation and decision-feedback equalizer for underwater acoustic communications. IEEE Journal of Oceanic Engineering 29 (2), 472–487.
Yang, T.C., 2005. Correlation-based decision-feedback equalizer for underwater acoustic communications. IEEE Journal of Oceanic Engineering 30 (4), 865–880.
Yang, T.C., 2007. A study of spatial processing gain in underwater acoustic communications. IEEE Journal of Oceanic Engineering 32 (3), 689–709.
Zhang, G., Dong, H., 2011. Experimental assessment of a multicarrier underwater acoustic communication system. Applied Acoustics 72 (12), 953–961.
Zhang, G., Hovem, J.M., Dong, H., Walree, P.A.v., 2011. A novel probe processing method for underwater communication by passive-phase conjugation. In: Proceedings of the 2011 IEEE International Conference on Acoustics Speech and Signal Processing (ICASSP), pp. 2700–2703.

Paper 2: Experimental Assessment of a Multicarrier Underwater Acoustic Communication System

Guosong Zhang and Hefeng Dong

In Applied Acoustics, vol. 72, pp. 953-961, 2011.

The thesis author had the original idea for this paper. The co-authors participated in scientific discussions.

Applied Acoustics 72 (2011) 953–961

Contents lists available at ScienceDirect

Applied Acoustics

journal homepage: www.elsevier.com/locate/apacoust

Experimental assessment of a multicarrier underwater acoustic communication system

Guosong Zhang *, Hefeng Dong

Department of Electronics and Telecommunications, Norwegian University of Science and Technology (NTNU), NO-7491 Trondheim, Norway

ARTICLE INFO

Article history:
Received 29 November 2010
Received in revised form 7 June 2011
Accepted 8 June 2011
Available online 5 July 2011

Keywords:
Underwater acoustic communication
Passive-phase conjugation
Adaptive multichannel equalization
Decision feedback equalizer
Multicarrier communication

ABSTRACT

This paper presents a multicarrier communication system which transmits information on independent subcarriers to achieve an increased data rate. For this system, a passive-phase conjugation (PPC) based receiver structure is assessed by processing data collected in sea trials. Based on temporal diversity (pulse compression) exploited by PPC processing, an adaptive multichannel decision feedback equalizer is used to remove intersymbol interference, where spatial diversity is exploited by adaptive multichannel combination. The digital phase-locked loop (DPLL) technique is implemented for carrier-phase tracking. In the scenario of low input signal-to-noise ratios (SNRs), the receiver structure achieved superior performance using a common DPLL. In a depth-fluctuated environment, two sea experiments were conducted over ranges of 2 km and 4 km, respectively, and this communication system was assessed with a data rate of 4 kbps. In terms of mean square error, output SNR and bit error rate, this receiver structure has demonstrated its performance for the multicarrier communication system.

1. Introduction

Underwater acoustic communication is subject to the bandwidth limited acoustic channel [1], which is characterized by time-varying extended multipath patterns. For the concept of underwater acoustic networks [2], high-rate communications have been researched to increase the throughput of point-to-point communications. Examples include incoherent communications using orthogonal multiple frequency shift keying [3], coherent communications using time reversal [4–6], and orthogonal frequency-division multiplexing communications using orthogonal subcarriers [7]. For high rate communications, intersymbol interference (ISI) caused by multipath results in errors, and has to be removed by adaptive channel equalizers. Passive-phase conjugation (PPC) processing achieves pulse compression of time delayed arrivals [8], and this property is used to mitigate ISI for coherent communications, where the complexity of adaptive channel equalization is reduced [9]. In this paper, a multicarrier communication system is presented, for which a PPC receiver structure is tested.

On the mth subcarrier frequency f_m, a communication signal consists of a sequence of informational symbols denoted as $I_m[n]$, where each symbol occupies a duration T. The transmitted signal $s_m(t)$ is expressed as

$$s_m(t) = \mathrm{Re}\left\{ \sum_n e^{j2\pi f_m t} I_m[n] g(t - nT) \right\}, \tag{1}$$

where $\mathrm{Re}\{\bullet\}$ denotes the real part of a complex number, and $g(\tau)$ presents a pulse shape function that

$$g(\tau) = \begin{cases} 1, & \text{for } 0 \leqslant \tau < T \\ 0, & \text{otherwise} \end{cases}. \tag{2}$$

The transmitted signal $s(t)$ of N_C independent subcarriers is expressed as

$$s(t) = \sum_{m=1}^{N_C} s_m(t). \tag{3}$$

In order to reduce intercarrier interference caused by spectrum leakage, a raised-root cosine pulse shape is used to constrain the bandwidth of $s_m(t)$ to B_w. Then the frequency separation between two adjacent subcarriers is required to be

$$|f_m - f_{m+1}| \geqslant B_w. \tag{4}$$

Information modulated on the N_C subcarriers is recovered independently at the receiver.

In the kth receiving channel of the impulse response $h_k(t)$, the received signal can be written as

$$r_k(t) = h_k(t) \otimes s(t) + w_k(t), \tag{5}$$

where $\otimes$ denotes convolution, and $w_k(t)$ is a bandwidth limited noise. Using the time reversed channel response $h_k(-t)$, PPC

* Corresponding author.
E-mail address: guosong.zhang@iet.ntnu.no (G. Zhang).

0003-682X/$ - see front matter © 2011 Elsevier Ltd. All rights reserved.
doi:10.1016/j.apacoust.2011.06.004

processing acts as a matched filter for the received signal. The output of one channel PPC processing is

$$z_k(t) = h_k(-t) \otimes r_k(t) = h_k(-t) \otimes (h_k(t) \otimes s(t) + w_k(t)) = q_k(t) \otimes s(t) + \varsigma_k(t), \quad (6)$$

where $q_k(t)$ presents the autocorrelation of $h_k(t)$, and $\zeta_k(t)$ is a filtered noise. Since $h_k(t)$ is bandwidth limited, the main lobe width of $q_k(t)$ is determined by the bandwidth of $h_k(t)$, and the side lobes of $q_k(t)$ cause residual ISI. The side lobes of temporal focusing is suppressed by multichannel combination, e.g. the passive time reversal method exploits spatial diversity with a receiving array to mitigate ISI [10]. As discussed by Yang [10], ISI cannot be eliminated. However, residual ISI can be removed by an adaptive channel equalizer.

Multiple receivers distributed in space decrease the probability of deep fading in a time-varying channel [11], where spatial diversity is exploited for stable communications. For practical purposes, a small number of receivers are preferred in realization. Yang showed [10] that a multichannel decision feedback equalizer (DFE) achieves superior performance over the receiver structure based on passive time reversal, where up to 11 receivers are used in both numerical simulation and real data verification. With reduced complexity, a receiver structure of PPC based multichannel DFE [12] is used in this paper, and it achieves superior performance over the structure based on passive time reversal [13], where adaptive spatial combination exploits spatial diversity. The PPC based receiver structure is assessed for the multicarrier communication system.

The reminder of this paper is organized as follows. The receiver diagram of PPC based multichannel DFE is introduced in Section 2. Section 3 describes the setup for two experiments conducted in Trondheim harbor, Norway. Section 4 shows the channel measurements, including examples of channel response overview, spatial coherence and carrier frequency shift measurements. In Section 5, the off-line processed results are presented and discussed. Conclusions are given in Section 6.

2. The receiver structure

For passive time reversal communications, ISI is significantly mitigated by refocusing time delayed arrivals at the receiving array, and then only one adaptive channel equalizer with a reduced number of taps is required to remove residual ISI [5]. Fig. 1 shows the receiver structure based on passive time reversal. One channel output for adaptive channel equalization is obtained by the K-channel equal weight combination

$$z(t) = \sum_{k=1}^{K} h_k(-t) \otimes r_k(t) = \sum_{k=1}^{K} q_k(t) \otimes s(t) + \sum_{k=1}^{K} \varsigma_k(t) = q(t) \otimes s(t) + \varsigma(t), \quad (7)$$

where $q(t)$ is the autocorrelation of the impulse response functions summed over the K receivers, and $\zeta(t)$ denotes the noise. Residual ISI caused by $q(t)$ is removed by a single channel DFE, and carrier-phase tracking is realized by a second order digital phase-locked loop (DPLL) technique [14]. DPLL tracks carrier-phase on a symbol-by-symbol basis. Between the transmitter and the receivers, sampling frequency differences can exist in the instrumentation, time-varying Doppler shift due to relative movement causes the carrier frequency shift, and therefore it is necessary that DPLL is implemented to track the K-channel averaged frequency shift. The output error is expressed as

$$e_m[n] = I_m[n] - \tilde{I}_m[n], \quad (8)$$

where $\tilde{I}_m[n]$ denotes the estimate. $I_m[n]$ is replaced by the decided output $\hat{I}_m[n]$ in the tracking mode. Based on the minimum mean square error (MSE) criterion, tap coefficients of the feed-forward filter and the feedback filter are jointly updated by the recursive least squares (RLS) algorithm, which has a fast convergence rate with independence on the input data [15]. Since the receivers are independently distributed in space, spatial diversity is exploited by the multichannel combination. In a real ocean, time variant inter-channel correlation exists [16], and adaptive spatial combination is implemented to exploit spatial diversity in this paper.

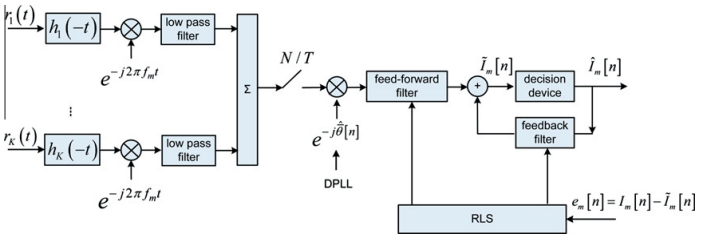

Fig. 1. The receiver structure of passive time reversal. There are N samples per symbol in baseband digital signal processing.

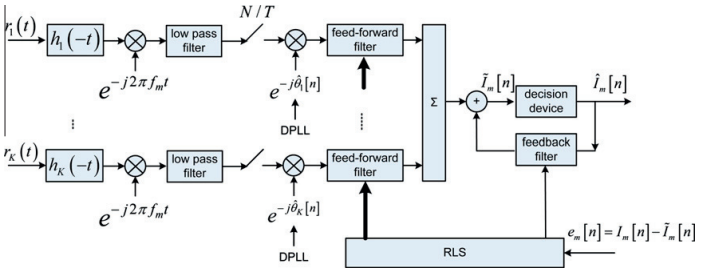

Fig. 2. The receiver structure of PPC based multichannel DFE.

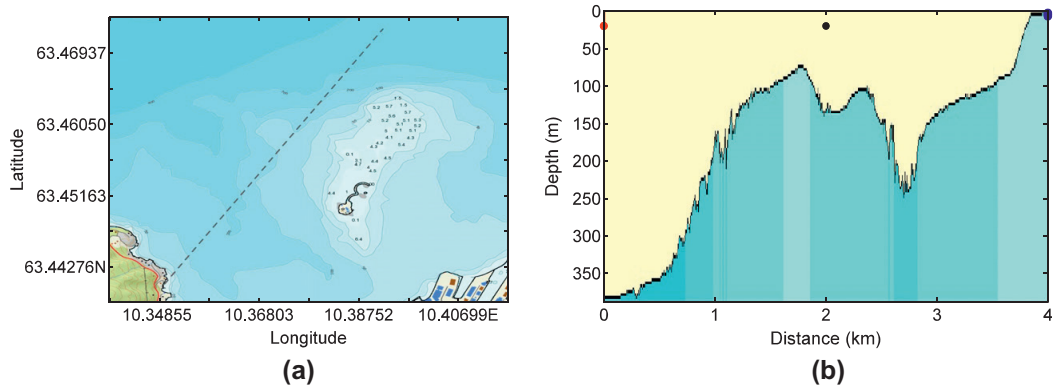

Fig. 3. (a) Experimental area in Trondheim harbor. The dash line denotes the communication track. (b) The depth profile in the communication track. The black and red dots denote the positions of the transmitter in Trial A and Trial B, and the blue dots to the right denote the receiving array. (For interpretation of the references to color in this figure legend, the reader is referred to the web version of this article.)

Fig. 2 shows the receiver structure of PPC based multichannel DFE. PPC processing is conducted prior to an adaptive multichannel DFE, and time delay spread is reduced by pulse compression. Then the number of taps for the feed-forward filters is decreased, and the computational load for the RLS algorithm which updates the K-channel tap coefficients is reduced. The tap coefficients and independent DPLLs are jointly updated to minimize the output MSE. Comparing with the multichannel combination of the structure shown in Fig. 1, adaptive spatial combination shown in Fig. 2 exploits spatial diversity. As discussed by Yang [16], no model can precisely predict the time variant spatial coherence in a real ocean. Interchannel correlation impacts the spatial diversity exploited by the $q(t)$ function, since spatial diversity is obtained regardless of the output. Based on a previous output MSE, adaptive spatial combination is performed to minimize current output MSE. The structure shown in Fig. 2 is tested by processing data collected in two recent sea experiments.

3. The experiments

The two experiments denoted as Trial A and Trial B were carried out on June 30, 2010, in Trondheim harbor in Norway. Fig. 3a shows the experimental area, where the sea depth varies from a few meters to hundreds of meters along the communication path. Fig. 3b shows that the depth profile in the communication track changes from 10 m to 380 m. The distances from the transmitter to a cross receiving array (CRA) of 10 hydrophones are 2 km (Trial A) and 4 km (Trial B), respectively. A hemispherical acoustic transducer is used by the transmitter, and its beam pattern is shown in Fig. 4. The transducer was suspended at a depth of 20 m from the NTNU research vessel R/V Gunnerus. The signals at an acoustic source level of 183 dB re 1 μPa @ 1 m were repeatedly transmitted for 45 min in each trial. The CRA was near-shore deployed in a water depth of 10 m. The CRA consisted of a vertical receiving array with six hydrophones (hydrophone Nos. 1–6) with 1 m element spacing and a horizontal receiving array of 4 hydrophones (hydrophone Nos. 7–10) with 1.5 m element spacing. Fig. 5 shows an example of the sensitivity of the hydrophones. The dynamic positioning system of R/V Gunnerus was activated to reduce drifting.

The information symbols were generated using quadrature phase-shift keying modulation with symbol rate of $1/T = 1$ kilo-symbols/s. Due to the bandwidth limitation of the transducer, two subcarrier frequencies $f_1 = 11$ kHz and $f_2 = 13$ kHz were used in the testing. Within a bandwidth of 4 kHz, the total data rate was 4 kilobits/s. Data signals $s_1(t)$ and $s_2(t)$ were pulse-shaped by a raised-root cosine filter, where the roll-off ratio was 1 to

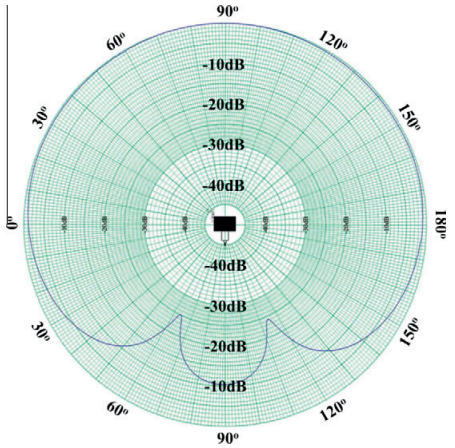

Fig. 4. Beam pattern of the transducer at 10 kHz. It is given by the manufacturer of Chelsea Technologies Group.

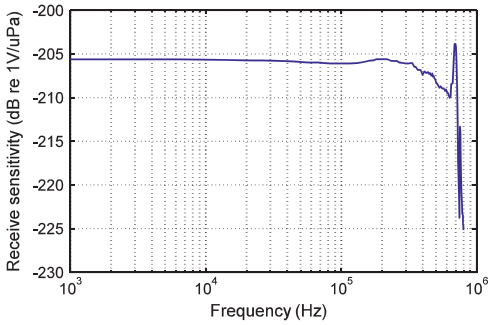

Fig. 5. Receive sensitivity of the hydrophones.

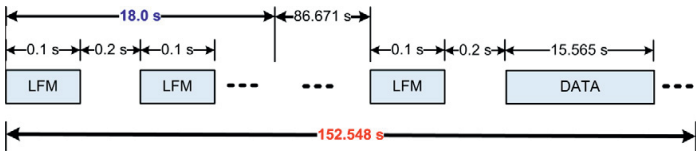

Fig. 6. One period of the transmitted signal.

constrain the signal bandwidth $B_w = 2$ kHz. The subcarrier frequency separation satisfied Eq. (4).

The signals shown in Fig. 6 were repeatedly transmitted with a period of 152.548 s for about 45 min. The channel measurement signal has duration of 18 s, and it consists of 60 Hanning-windowed linear frequency modulation (LFM) chirps. A data signal of 15.565 s transmits 62,260 bits. One chirp in advance to the data signal is used as the channel probe signal for PPC processing. The central frequency of the chirp is 12 kHz, and the effective bandwidth of the chirp is 2.2 kHz.

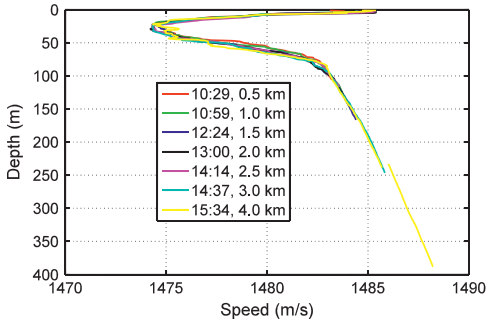

Fig. 7. Sound speed profiles measured at different distances to the receiving array.

4. The channel measurements

The trials were conducted on a windy and rainy day. In order to monitor the environmental variations in the communication track, sound speed profiles were measured by the R/V Gunnerus. Fig. 7 shows the sound speed profiles measured at different distances to the receiving array. There was a sound channel at the depth of 25 m during the trials.

In each period of 152.548 s, the channel impulse response of 18 s is measured by the signal consisting of 60 chirps. Fig. 8 shows overviews of the channel response measurements in the 45-min trials, where the replica correlation method is used. Time delayed arrivals span about 5 ms in Trial A as shown in Fig. 8a, and they extend more than 10 ms in Trial B as shown in Fig. 8b. In both trials, temporal compression/dilation is observed, as the arrivals are not aligned in delay time. The compression/dilation of different rates observed are caused by variant Doppler shifts due to relative movement between the transmitter and the receiver [17]. The dilation is only observed in the first transmission period of Trial

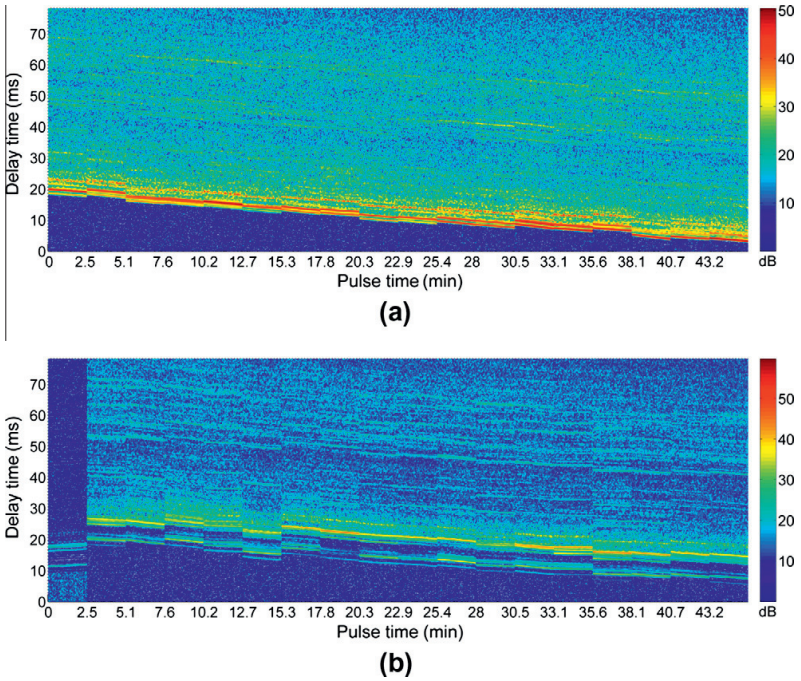

Fig. 8. The channel response measured at a depth of 4.5 m above the sea bottom. (a) Trial A. (b) Trial B.

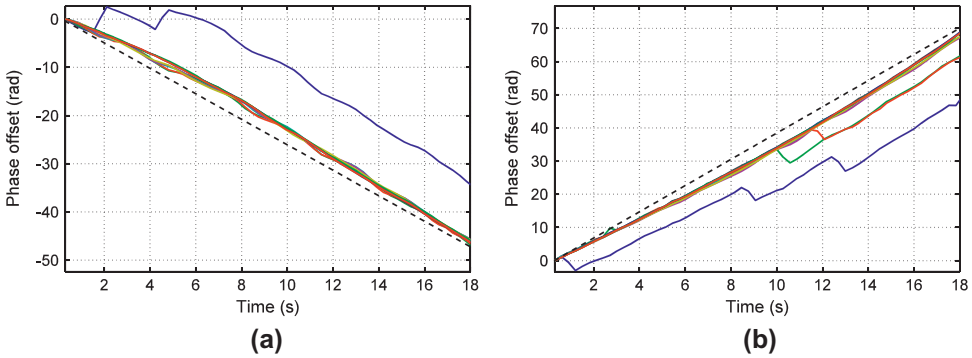

Fig. 9. The phase offset measurements in the first period of two trials. (a) Trial A. (b) Trial B.

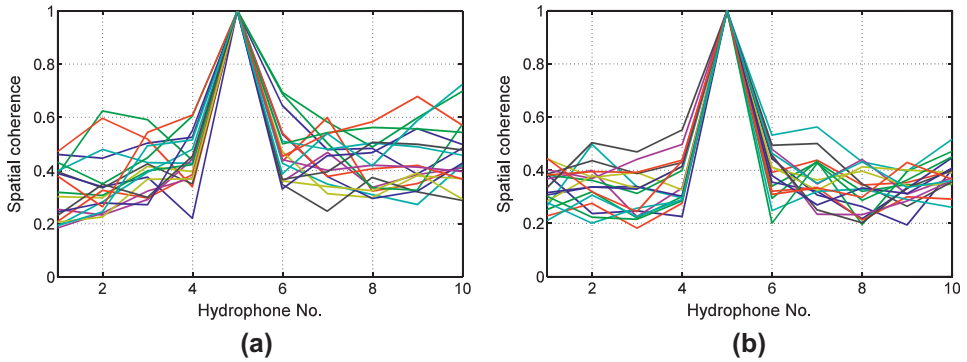

Fig. 10. The spatial coherence in 45 min. (a) Trial A. (b) Trial B.

Table 1
Receiver parameters.

Parameters	Description	Value
F_s	Sampling frequency	96 kHz
f_1	Subcarrier-1	13 kHz
f_2	Subcarrier-2	11 kHz
R	The symbol rate on both subcarriers	1 kilosymbol/s
N	Over sampling factor	4
N_{ff}	The number of feed forward filter taps	12
N_{fb}	The number of feedback filter taps	2
N_t	The number of training symbols	60
λ	RLS forgetting factor	0.999
K	The number of channels	10
K_1	Proportional tracking constant in DPLL	0.01
K_2	Integral tracking constant in DPLL	0.001

B, where the compression occurs in the other periods. The Doppler shift of the carrier frequency is measured using the method of cross-correlation between two received chirps.

For the kth receiving channel, the $(l+1)$th received chirp $r_k^p(t,l)$ is written as

$$r_k^p(t,l) = e^{j\theta_k(t+lT_p)} p(t) \otimes h_k(t, lT_p) + w_k(t,l), \quad 0 \leqslant l < 60, \tag{9}$$

where $p(t)$ is the chirp transmitted with a period of $T_p = 0.3$ s, $\theta_k(t + lT_p)$ is the phase offset, $h_k(t, lT_p)$ presents the channel impulse response at lT_p, and $w_k(t, l)$ denotes a bandwidth limited noise. The

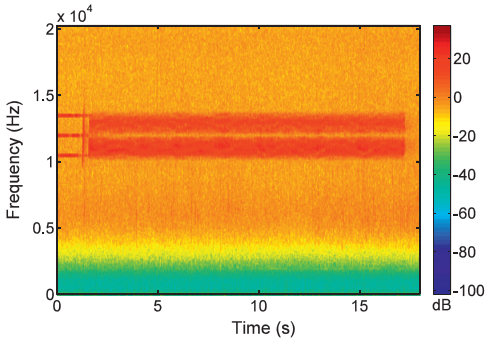

Fig. 11. The spectrogram of the received communication signal.

cross-correlation between the 1st and $(l+1)$th received chirps is defined as

$$\begin{aligned}\rho_k(l) &= \int_0^{T_p} r_k^p(t,0)^* r_k^p(t,l)dt \\ &= \int_0^{T_p} e^{j(\theta_k(t+lT_p)-\theta_k(t))}|p(t)|^2 h_k(t,0)^* h_k(t,lT_p)dt \\ &\quad + \int_0^{T_p} w_k(t,0)^* w_k(t,l)dt,\end{aligned} \tag{10}$$

where $(\bullet)^*$ denotes the complex conjugation. In a static channel, it is simplified to

$$\rho_k(l) = \int_0^{T_p} e^{j(\theta_k(t+lT_p)-\theta_k(t))}|p(t)|^2|h_k(t,0)|^2dt + \sigma_w, \quad (11)$$

where σ_w denotes the cross-correlation of the noises. The phase offset $\theta_k(t)$ caused by a carrier frequency shift Δ_k can be written as

$$\theta_k(t) = 2\pi\Delta_k t + \phi_k, \quad (12)$$

where Δ_k denotes the carrier frequency shift and ϕ_k is the initial phase. Eq. (11) is changed into

$$\rho_k(l) = \int_0^{T_p} e^{j2\pi\Delta_k lT_p}|p(t)|^2|h_k(t,0)|^2dt + \sigma_w = Ce^{j2\pi\Delta_k lT_p} + \sigma_w, \quad (13)$$

where C is an integration constant. Since there is no correlation between $w_k(t,0)$ and $w_k(t,l)$, the phase interference from σ_w is neglected. The phase offset caused by Δ_k is given by

$$\varphi_k(lT_p) = phase(\rho_k(l)) \approx 2\pi\Delta_k(lT_p). \quad (14)$$

Fig. 9a and b shows two examples of phase offset measurements in Trial A and Trial B, respectively. There is little difference in both examples in terms of the slope of phase offset, and the

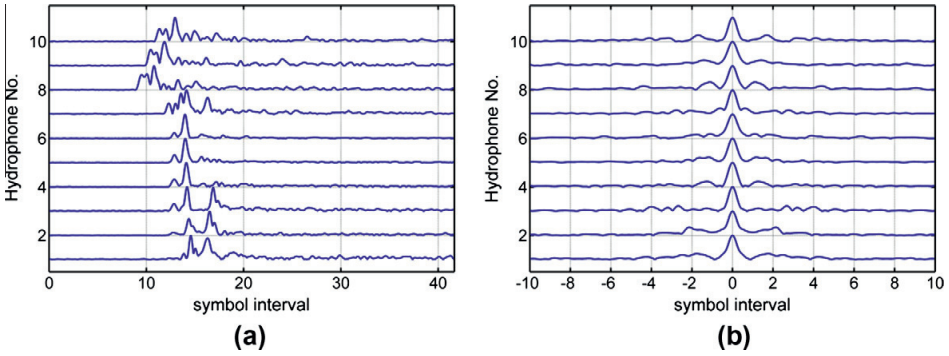

Fig. 12. (a) The channel response estimated by the received LFM chirp. (b) Pulse compression.

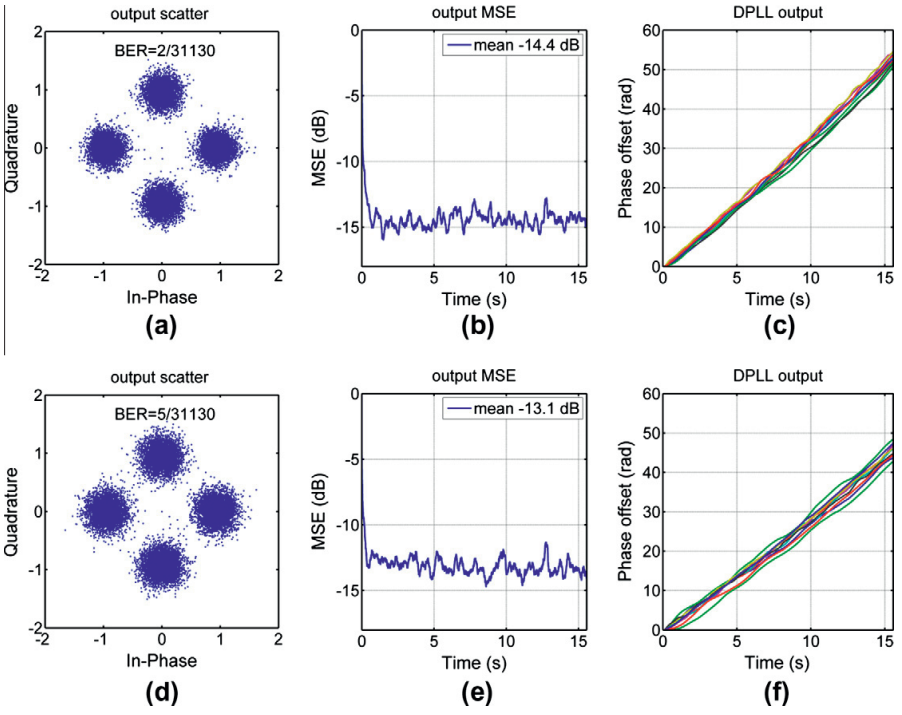

Fig. 13. The receiver performance. (a–c) Subcarrier-1. (d–f) Subcarrier-2.

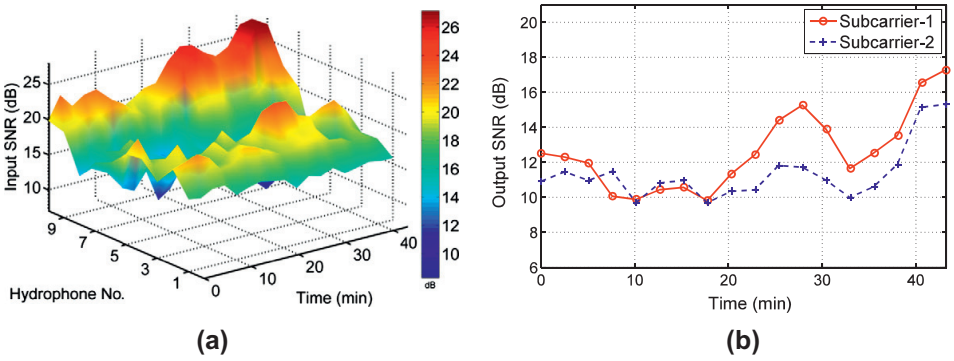

Fig. 14. The input SNR and the receiver performance in the 45-min trial. (a) The input SNRs among 10 hydrophones. (b) The performance in terms of output SNR.

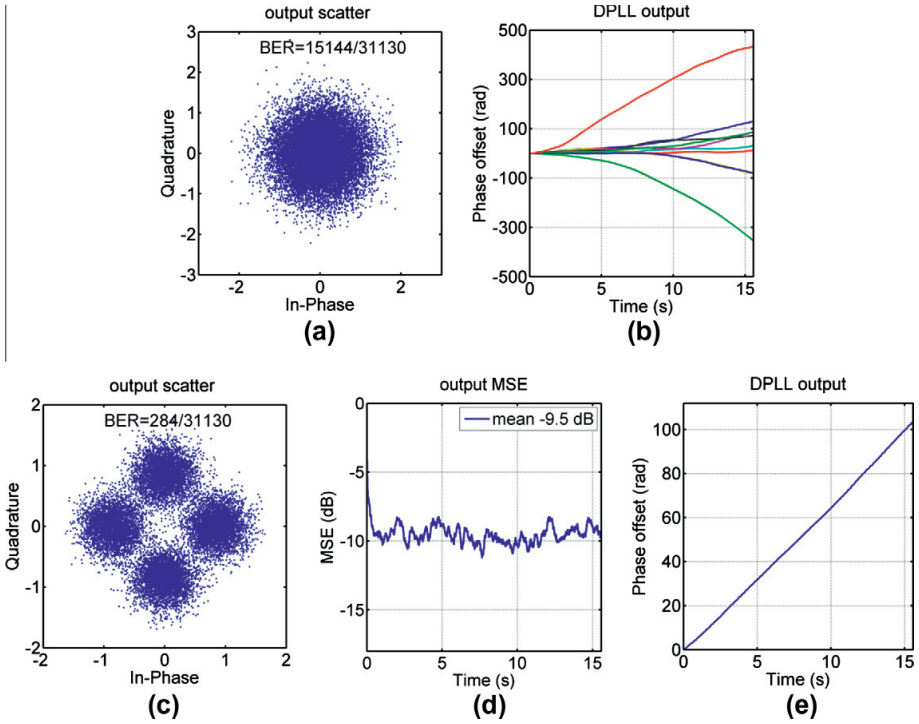

Fig. 15. The receiver performance with different phase tracking modes. (a and b) 10-DPLL. (c–e) 1-DPLL.

slopes are indicated by the dotted lines. In Fig. 9a, the slope of phase offset is about 3.9 rad/s, which is equivalent to a frequency shift of 0.60 Hz. In Fig. 9b, an equivalent frequency shift of −0.41 Hz is observed. A negative frequency shift correlates with the channel measurement, where temporal dilation is only observed in the first period, as shown in Fig. 8b. Since Doppler shift changes in a time-varying channel, it is necessary to implement DPLL to track the carrier frequency shift.

Interchannel correlation between two receivers is measured by spatial coherence. The spatial coherence between the kth and ith receiving channel is calculated by

$$\psi(k,i)=\frac{|r_k(-t)\otimes r_i(t)|_{\max}}{\sqrt{|r_k(-t)\otimes r_k(t)|_{\max}|r_i(-t)\otimes r_i(t)|_{\max}}}, \tag{15}$$

where $|r_k(-t)\otimes r_i(t)|_{\max}$ denotes the maximum absolute value of $r_k(-t)\otimes r_i(t)$. The spatial coherence measured in the trials is shown in Fig. 10. It is shown that the spatial coherence changes with time. In Trial A, there are several periods in which spatial coherence between two different hydrophones is more than 0.6. In Trial B, spatial coherence is less than 0.6. The interchannel correlation decreased in Trial B. Thus the adaptive spatial combination has advantage to exploit time-varying spatial diversity.

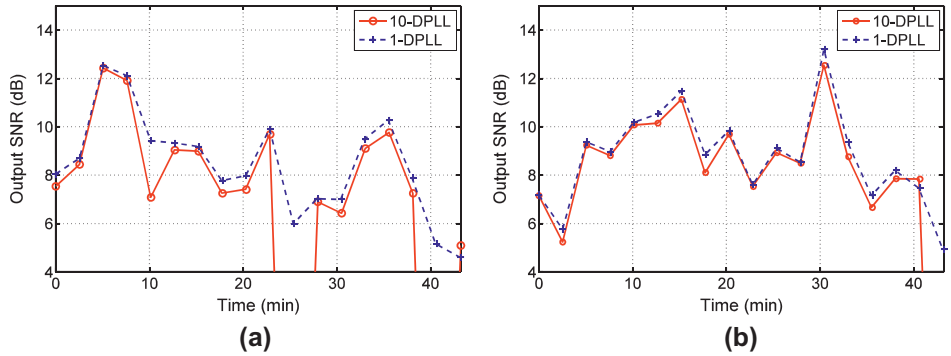

Fig. 16. The receiver performance in terms of output SNR. (a) Subcarrier-1. (b) Subcarrier-2.

5. Results and analysis

The parameters for the receiver structure are given in Table 1. The number of taps for the multichannel DFE is chosen in an *ad hoc* manner in the signal processing, and the forgetting factor λ is empirically chosen for the presented results. For the DPLL technique proposed by Stojanovic [18], the integral tracking constant K_2 is chosen as $K_2 = K_1/10$ in order to achieve good performance, where K_1 is the proportional tracking constant. A $T/4$ spaced (four samples per symbol) multichannel DFE is used, and the taps of the feed-forward filters spans three symbols as the number of taps for the feed-forward filters is $N_{ff} = 12$.

5.1. Trial A

Fig. 11 shows a spectrogram of the received communication signal. Intercarrier interference is reduced by pulse-shaping, and the signal on each carrier is independent. Using an LFM chirp as the channel probe signal, the received chirp is immediately used for PPC processing [19], where the complexity for channel estimation is reduced.

Fig. 12 shows an example of ISI mitigation by pulse compression. As shown in Fig. 12a, the multipath pattern changes with the hydrophone, and the time spread changes from 2 to 8 symbol intervals. Fig. 12b shows that the time delayed arrivals are compressed within one symbol interval with side lobes. Based on pulse compression, the number of taps for the multichannel DFE is significantly reduced to remove residual ISI.

Fig. 13 shows the receiver performance for the received signal within the first period. Fig. 13a and d shows the scatters of the soft output. The bit error rates (BERs) on both subcarriers are 6.4e−5 and 1.6e−4, respectively. Information is correctly recovered with the output MSEs shown in Fig. 13b and e, where the mean MSEs of −14.4 dB and −13.1 dB are achieved. The 10-channel DPLL output is shown in Fig. 13c and f. There is little difference in terms of the slope of phase offset, where the equivalent carrier frequency shifts are 0.51 Hz and 0.46 Hz. The DPLL output validates the channel measurement within the first period as shown in Fig. 9a, where an equivalent carrier frequency shift of 0.60 Hz is observed.

To calculate the input SNR, noise power is calculated after the received signal interval, and the signal-plus-noise power is calculated within the signal interval. Fig. 14a shows the input SNR measurement. The input SNR changes with receiving channel and time. Hydrophone No. 10 obtains the highest input SNR through the trial, and the lowest SNR which occurs in hydrophone No. 6 is 8.3 dB. Fig. 14b shows the receiver performance in terms of output SNR given by (1-MSE)/MSE [11]. The output SNR changes with time due to the time variant input SNR. The output SNR increases with increased input SNRs. The lowest output SNRs are 9.8 dB and 9.6 dB achieved on both subcarriers. In total, 560,340 bits were transmitted, and BERs of 1.1e−4 and 2.1e−4 are achieved on both subcarriers, respectively.

5.2. Trial B

DPLL corrects phase rotations of the received symbols prior to adaptive channel equalization. Fig. 15 shows that the receiver performance is deteriorated without correct carrier-phase tracking, where BER is 4.9e−1, because the DPLLs lost tracking as shown in Fig. 15b. As discussed above, there is slight difference in terms of Doppler shift among the 10 receiving channels, and therefore the receiver structure can use a common DPLL given by

$$\bar{\theta}[n] = \frac{1}{10}\sum_{i=1}^{10}\hat{\theta}_i[n]. \tag{16}$$

Fig. 15c shows that BER is significantly reduced to 9.0e−3, where Fig. 15d shows that a mean output MSE of −9.5 dB is achieved. Fig. 15e shows that the averaged slope of phase offset is 6.6 rad/s, which is equivalent to a frequency shift of 1.1 Hz. One common DPLL given by Eq. (16) is used in the following analysis.

Fig. 16 shows the receiver performance in terms of output SNR. For both subcarriers, there are some periods that the receiver

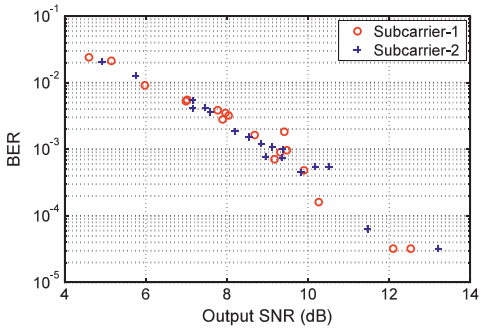

Fig. 17. The receiver performance in terms of BER.

structure using 10-DPLL fails to recover the transmitted information. Consequently, the structure using 1-DPLL achieves superior performance with improved output SNRs. The transmission source level was kept the same in both trials, but the propagation distance was increased to 4 km in Trial B, and the received SNRs were decreased because of an increased propagation loss. With low input SNRs, one common DPLL decreases the probability of losing carrier-phase tracking. Fig. 17 shows the receiver performance in terms of BER, which changes with the time variant output SNR. The poorest BER of 2.4e−2 occurs on subcarrier-1, where the output SNR is 4.6 dB. BER is decreased by an increased output SNR, which is limited by the input SNR.

6. Conclusion

A multicarrier communication system is presented and assessed through field trials. Higher data rate can be achieved by increasing the number of subcarriers. Due to the bandwidth limitation of the acoustic transducer, two subcarriers were used in the 45-min experimental testing. In processing data collected at two distances to the receiving array, the receiver structure of PPC based multichannel DFE has demonstrated its performance. Both temporal diversity and spatial diversity are exploited by this structure.

From the channel measurements and DPLL output, it is evident that time-varying Doppler shift existed in the trials. Carrier-phase tracking by the DPLL technique corrects phase rotations of the input symbols prior to adaptive equalization. The performance of the adaptive multichannel equalizer is deteriorated by the carrier-phase tracking loss, and it is improved by using a common DPLL which updates an averaged phase offset correction for all the receiving channels.

Acknowledgements

The authors would like to thank technical engineer Tim Cato Netland, PhD students Zhongxi Chao and Yan Jiang, and the crew of the R/V Gunnerus for the help in conducting the experiments. The authors also thank Anders Løvstad for his comments.

References

[1] Kilfoyle DB, Baggeroer AB. The state of the art in underwater acoustic telemetry. IEEE J Ocean Eng 2000;25:4–27.
[2] Sozer EM, Stojanovic M, Proakis JG. Underwater acoustic networks. IEEE J Ocean Eng 2000;25:72–83.
[3] Scussel KF, Rice JA, Merriam S. A new MFSK acoustic modem for operation in adverse underwater channels, MTS/IEEE OCEANS '97 1997;1:247–54.
[4] Kuperman WA, William SH, Hee Chun S, Akal T, Ferla C, Darrell RJ. Phase conjugation in the ocean: experimental demonstration of an acoustic time-reversal mirror. J Acoust Soc Am 1998;103:25–40.
[5] Song HC, Hodgkiss WS, Kuperman WA, Stevenson M, Akal T. Improvement of time-reversal communications using adaptive channel equalizers. IEEE J Ocean Eng 2006;31:487–96.
[6] Song HC, Hodgkiss WS, Kuperman WA, Akal T, Stevenson M. High-frequency acoustic communications achieving high bandwidth efficiency. J Acoust Soc Am 2009;126:561–3.
[7] Baosheng L, Jie H, Shengli Z, Ball K, Stojanovic M, Freitag L, et al. MIMO-OFDM for high-rate underwater acoustic communications. IEEE J Ocean Eng 2009; 34:634–44.
[8] Dowling DR. Acoustic pulse compression using passive phase-conjugate processing. J Acoust Soc Am 1994;95:1450–8.
[9] Yang TC. Correlation-based decision-feedback equalizer for underwater acoustic communications. IEEE J Ocean Eng 2005;30:865–80.
[10] Yang TC. Differences between passive-phase conjugation and decision-feedback equalizer for underwater acoustic communications. IEEE J Ocean Eng 2004;29:472–87.
[11] Proakis JG. Digital communications. New York: McGraw-Hill; 2001.
[12] Zhang G, Hovem JM, Dong H. Passive-phase conjugation based adaptive multichannel equalization for underwater acoustic communications. Acta Acustica united with Acustica; submitted for publication.
[13] Zhang G, Hovem JM, Dong H. Experimental assessment of adaptive spatial combination for underwater acoustic communications. In: The fifth international conference on sensor technologies and applications, SENSORCOMM 2011, Nice/Saint Laurent du Var, France; in press.
[14] Stojanovic M, Catipovic J, Proakis JG. Adaptive multichannel combination and equalization for underwater acoustic communications. J Acoust Soc Am 1993; 94:1621–31.
[15] Haykin S. Adaptive filter theory. Upper Saddle River, New Jersey: Prentice Hall; 2001.
[16] Yang TC. A study of spatial processing gain in underwater acoustic communications. IEEE J Ocean Eng 2007;32:689–709.
[17] Sharif BS, Neasham J, Hinton OR, Adams AE. A computationally efficient Doppler compensation system for underwater acoustic communications. IEEE J Ocean Eng 2000;25:52–61.
[18] Stojanovic M. Efficient processing of acoustic signals for high-rate information transmission over sparse underwater channels. Phys Commun 2008;1:146–61.
[19] Song HC, Kim JS, Hodgkiss WS, Kuperman WA, Stevenson M. High-rate multiuser communications in shallow water. J Acoust Soc Am 2010;128: 2920–5.

Paper 3: Joint Passive-phase Conjugation with Adaptive Multichannel Combining for Coherent Underwater Acoustic Communications

Guosong Zhang and Hefeng Dong

In Applied Acoustics, vol. 73, pp. 433-439, 2012

The thesis author had the original idea for this paper. The co-authors participated in scientific discussions.

Applied Acoustics 73 (2012) 433–439

Contents lists available at SciVerse ScienceDirect

Applied Acoustics

journal homepage: www.elsevier.com/locate/apacoust

Technical Note

Joint passive-phase conjugation with adaptive multichannel combining for coherent underwater acoustic communications

Guosong Zhang *, Hefeng Dong

Department of Electronics and Telecommunications, Norwegian University of Science and Technology (NTNU), Trondheim 7491, Norway

ARTICLE INFO

Article history:
Received 24 April 2011
Received in revised form 14 September 2011
Accepted 8 November 2011
Available online 30 November 2011

Keywords:
Passive-phase conjugation
Passive time reversal
Adaptive multichannel combining
Decision feedback equalizer
Underwater acoustic communication

ABSTRACT

This paper presents a receiver structure which exploits spatial diversity by adaptive multichannel combining, which improves the performance of passive time reversal communications realized by passive-phase conjugation (PPC). PPC processing achieves pulse compression for the time delayed arrivals at the receiver, and this property is used for coherent communications to reduce the computational load. The presented structure takes advantage of pulse compression and performs adaptive multichannel combining, where the number of taps for adaptive multichannel processing is significantly reduced in order to decrease the computational load. With a previous output mean square error (MSE), the adaptive combining minimizes current output MSE, where spatial diversity is exploited by the adaptive combining. This structure improves performance of the passive time reversal approach, even though the taps for combining span one symbol interval. The performance improvement is demonstrated by a set of real data collected in a recent sea experiment, which was conducted in a range dependent acoustic channel over a range of 4 km.

1. Introduction

Underwater acoustic communication is limited by the time-varying underwater acoustic channel, which is characterized by the time variant multipath structure due to boundary reflections and refractions in the acoustic propagation [1]. The time delayed arrivals due to multipath propagation can be refocused at the receiver by passive time reversal, which is realized by the passive-phase conjugation (PPC) method [2]. PPC processing achieves pulse compression which mitigates intersymbol interference (ISI) for coherent communications [3]. Pulse compression reduces the complexity for equalizing the channel effects. As discussed by Yang [4], the main lobe width of pulse compression is determined by the signal's bandwidth, there are also side lobes, which cause residual ISI. After the temporal focusing, it has become popular that only a single channel decision feedback equalizer (DFE) is required to remove residual ISI [5–7]. This scheme shows potential for high rate communications of both single user [8] and multiuser scenarios [9–11].

In this paper, a method is introduced to improve the performance of passive time reversal approach. It is realized by PPC coupled with a single channel DFE (PPC–DFE). The equal weight multichannel combining is performed by passive time reversal, where spatial diversity is exploited without considering inter-channel correlations plus output MSEs. Based on pulse compression, the presented structure with a reduced number of taps performs the adaptive combining to minimize the output mean square errors (MSEs), and it is denoted as PPC coupled multichannel DFE (PPC–McDFE). The presented receiver structure achieves better performance, attributed to exploiting spatial diversity. Since there is lack of a model which precisely predicts the acoustic channel for the high frequency scenario (e.g., 11–13 kHz), a field experiment was conducted to collect data for off-line processing in the Lab. Presented results have demonstrated that improvement is obtained even though the taps span one symbol interval.

This paper is organized as follows. Section 2 introduces the structure PPC–McDFE, and shows the difference from PPC–DFE. Section 3 describes the experiment and presents the results and analysis of coherent acoustic communications over a range of 4 km. Conclusions are given in Section 4.

2. The receiver structures

The underwater acoustic channel is characterized by time-varying multipath patterns, which can be caused by bottom reflections, moving sea surface reflections, and transmission through the internal waves [7]. An adaptive channel equalizer is required to deconvolve the channel effects for coherent communications. Conventional signal processing applies the minimum MSE criterion to determine the tap coefficients for the equalizer. The number of

* Corresponding author.
E-mail addresses: guosong.zhang@iet.ntnu.no, guosong.zhang@hotmail.com (G. Zhang).

0003-682X/$ - see front matter © 2011 Elsevier Ltd. All rights reserved.
doi:10.1016/j.apacoust.2011.11.001

taps is determined by the channel physics—multipath, and it is usually obtained by an *ad hoc* procedure and adjusted according to the output error. Frequently, one gets poor performance due to ignoring the time spread in the channel.

The concept of PPC processing is similar to match-field processing [2]. PPC processing uses a filter of the channel response, and achieves temporal focusing for multipath arrivals. The compression at the receiver suppresses the multipath, and reduces the span of taps for adaptive channel equalization. Spatial diversity originates from spatially distributed receivers, and it is exploited by passive time reversal communications to mitigate ISI, where the fixed equal weight multichannel combining is performed prior to the adaptive channel equalization. As pointed out in [12], there is no model that could precisely predict the spatial coherence in a real ocean. In reality, it is unfeasible to deploy receivers which are independent. Without knowing interchannel correlations plus input signal-to-noise ratios (SNRs) among the receivers, we prefer adaptive multichannel combining to exploit the spatial diversity in order to obtain better performance.

2.1. Passive time reversal structure

The communication information consists of a sequence of symbols denoted as $I[n]$, and each symbol occupies a duration of T. The baseband data signal $s(t)$ can be expressed as

$$s(t) = \sum_n I[n] g(t - nT), \tag{1}$$

where $g(t)$ is the pulse shape function for each symbol such that

$$g(\tau) = \begin{cases} 1, & \text{for } 0 \leqslant \tau < T \\ 0, & \text{otherwise} \end{cases}. \tag{2}$$

In a multipath channel, the received communication signal of the ith receiver can be written as

$$r_i(t) = h_i(t) \otimes s(t) + w_i(t), \tag{3}$$

where $h_i(t)$ represents the channel impulse response, and $w_i(t)$ is a band-limited noise, and $\otimes$ denotes convolution. PPC processing can be seen as match-filtering the received signal. The output of match-filtering of the ith receiving channel is expressed as

$$\begin{aligned} z_i(t) &= h_i(-t) \otimes r_i(t) \\ &= h_i(-t) \otimes (h_i(t) \otimes s(t) + w_i(t)) \\ &= h_i(-t) \otimes h_i(t) \otimes s(t) + h_i(-t) \otimes w_i(t) \\ &= Q_i(t) \otimes s(t) + \varsigma_i(t), \end{aligned} \tag{4}$$

where $Q_i(t)$ is the autocorrelation of the impulse response $h_i(t)$ and $\varsigma_i(t)$ is a filtered noise. $Q_i(t)$ is a function that the main lobe width is determined by the bandwidth of $h_i(t)$ and there are side. Since $Q_i(t)$ is not a *Dirac* function, side lobes of $Q_i(t)$ cause ISI. ISI can be mitigated by time reversal refocusing. With the equal weight combining over the K receivers, one channel output of the focusing is given by

$$z(t) = \sum_{i=1}^{K} z_i(t) = \sum_{i=1}^{K} Q_i(t) s(t) + \sum_{i=1}^{K} \varsigma_i(t) = Q(t) \otimes s(t) + \varsigma(t), \tag{5}$$

where $Q(t)$ denotes the total response of autocorrelations $\{Q_i(t)\}$ summed over the K receiving channels, and $\varsigma(t)$ represents a filtered noise.

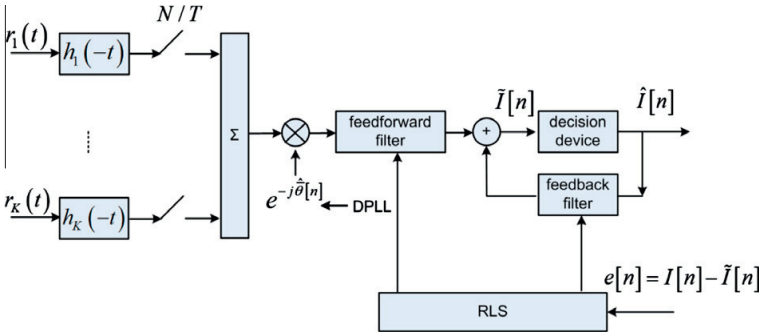

Fig. 1. The diagram of PPC coupled with a single DFE (N samples per symbol for digital signal processing).

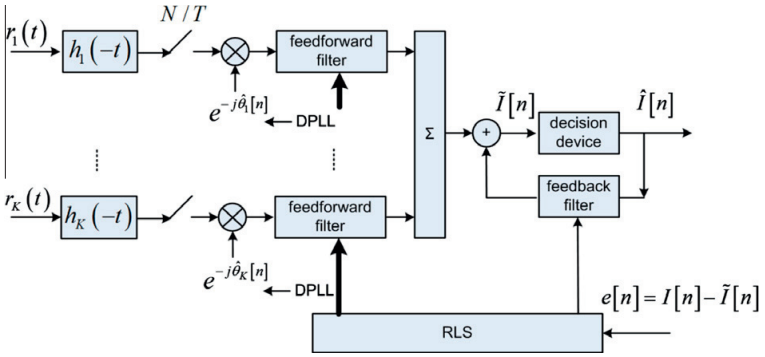

Fig. 2. The diagram of PPC coupled with a multichannel DFE.

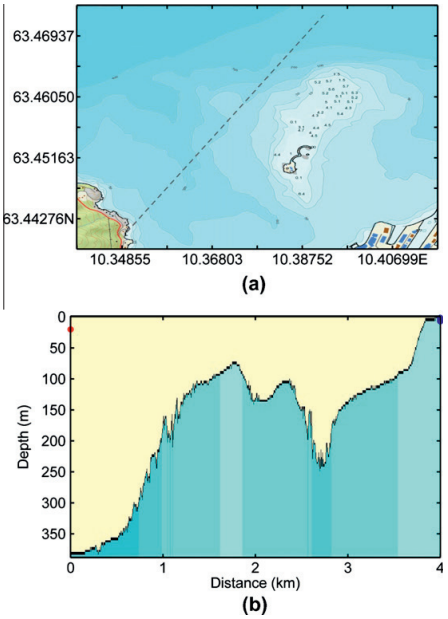

Fig. 3. (a) The experimental areal in Trondheim harbor. (b) The depth profile in the communication track. The left red dot denotes the transmitter, and the right blue dot denotes the receiving array.

The Fourier transform of the $Q(t)$ function can be written as

$$Q(\omega) = \sum_{i=1}^{K} H_i^*(\omega) H_i(\omega) = \sum_{i=1}^{K} |H_i(\omega)|^2, \quad (6)$$

where the superscript * denotes complex conjugation and $H_i(\omega)$ is the Fourier transform of $h_i(t)$, and $|H_i(\omega)|$ means the absolute value of $H_i(\omega)$. $H_i(\omega)$ is frequency selective, and it may have spectral peaks and nulls. The total frequency response $Q(\omega)$ is smoothed by the averaging over K independent receivers. Spatial diversity is exploited to mitigate ISI in the combining process shown in Eq. (5). With an increasing number of independent receivers, $Q(t)$ approximates a *sinc* function [4], and the side lobes of $Q(t)$ could result in residual ISI which is removed by a single channel equalizer.

Table 1
Receiver parameters.

Parameters	Description	Value
F_s	Sampling frequency	96 kHz
f_c	Carrier frequency	12 kHz
R	The symbol rate	1 kilosymbols/s
N	Over sampling factor	2
N_{ff}	The number of feed forward filter taps	2 or 8
N_{fb}	The number of feedback filter taps	1 or 2
N_t	The number of training symbols	72
N_c	The maximum number of receiving channels	10
λ	RLS forgetting factor	0.999
K_1	Proportional tracking constant in PLL	0.01
K_2	Integral tracking constant in PLL	0.001

Fig. 1 shows the passive time reversal receiver structure, which is realized by PPC coupled with a single channel DFE. In cascade with the refocusing process, a single channel DFE with a reduced number of taps is applied to remove residual ISI. The DFE also tracks the variations, since the refocusing degrades with elapsed time in a time-varying acoustic channel. Since the performance of DFE is sensitive to the carrier-phase offset, a second order digital phase-locked loop (DPLL) [13] is used to track the carrier-phase on a symbol-by-symbol basis. With a fast convergence rate without dependence on the input data, a recursive lease squares (RLS) algorithm is used to update the tap weights to minimize output MSE.

2.2. The presented structure

The presented receiver structure referred as PPC–McDFE is shown in Fig. 2. In this receiver structure, the adaptive multichannel combining replaces the equal weight combining of passive time reversal, at a cost of an increased number of taps of the feed-forward filters, and there are K independent DPLLs for each receiver. PPC processing acts as match-filtering, and it is conducted prior to adaptive multichannel equalization, where the number of taps is significantly reduced by pulse compression. The tap coefficients of the feed-forward filters are jointly updated to minimize output MSE. A small number of taps is preferred to reduce the computational load in iterations of the RLS algorithm. As shown in Fig. 1, PPC–DFE exploits spatial diversity prior to the performance of adaptive channel equalization. The proposed structure exploits spatial diversity by adaptive multichannel combining, which is updated based on a previous output MSE to minimize current output MSE. The superior performance originates from spatial diversity

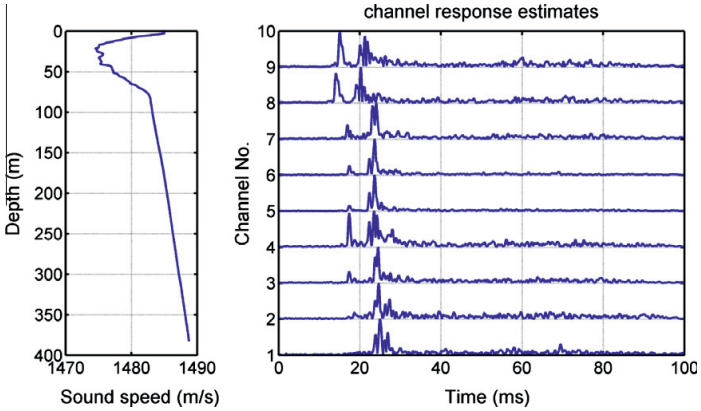

Fig. 4. The estimated channel responses (the right panel) conditioned by the sound speed profile (the left panel) measured during the trial.

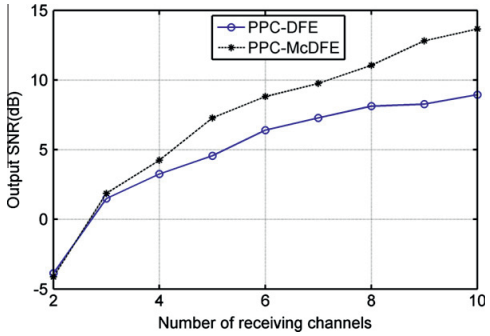

Fig. 5. The performance in terms of output SNR versus the number of receiving channels.

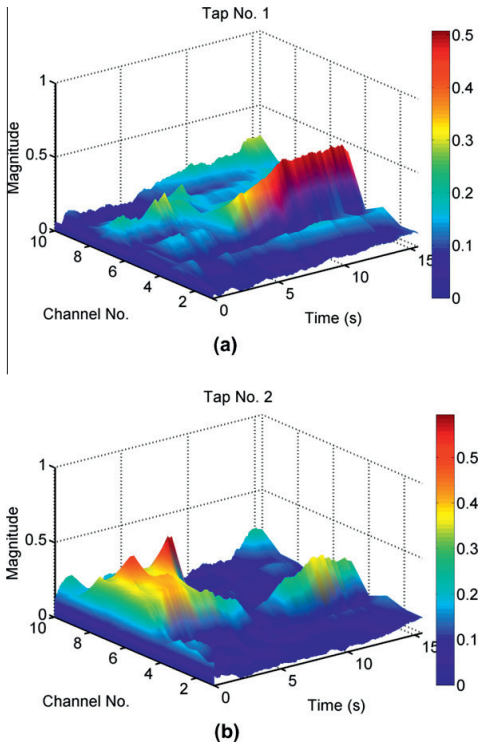

Fig. 6. The evolution of feed-forward tap coefficients within 15.565 s. (a) The tap No. 1. (b) The tap No. 2.

exploited by the adaptive combining, and it is demonstrated by the real data processing.

2.3. The carrier-phase synchronization

The carrier-phase offset is caused by the frequency shift, and it has to be corrected before feeding the samples into the DFE, whose performance could be degraded by the phase rotated symbols. The frequency shift can be caused by two factors. One is Doppler shift due to the relative movement between the transmitter and the

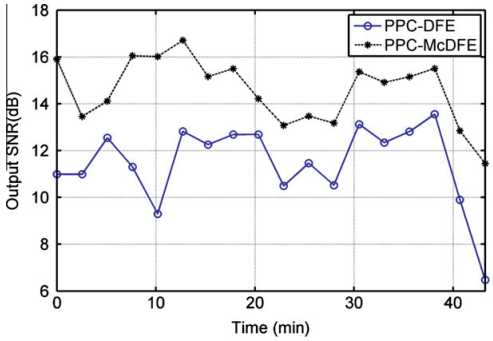

Fig. 7. Output SNR of 18 periods within 45 min.

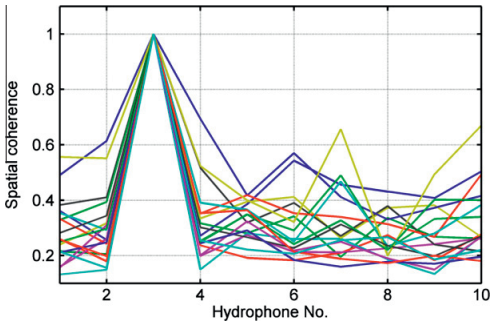

Fig. 8. The spatial coherence measured in the 45-min trial.

receivers. For example, a frequency shift can be observed by acoustic reflection from the moving sea surface. The other is from the oscillators of instrumentation, where there is the sampling frequency difference between the transmitter and the receivers.

In the ith receiving channel of PPC–McDFE, a second order DPLL tracks the carrier-phase given by

$$\hat{\theta}_i[n+1] = \hat{\theta}_i[n] + K_1\Phi_i[n] + K_2\sum_{m=0}^{n}\Phi_i[m], \tag{7}$$

where $\Phi_i[n]$ is the output MSE gradient with respect to $\hat{\theta}_i[n]$, K_1 is the proportional tracking constant, and K_2 is the integral tracking constant. It is suggested that K_2 is equal to $K_1/10$ for achieving good performance [14]. The expression for $\Phi_i[n]$ is written as

$$\Phi_i[n] = \mathrm{Im}\left\{a_i' v_i[n] e^{-j\hat{\theta}_i[n]} e^*[n]\right\}, \tag{8}$$

where $a_i' = \left[a_1^i, \ldots, a_{N_{ff}}^i\right]^*$ is the feed-forward filter tap weight vector, $v_i[n]$ is a vector of input baseband samples for the feed-forward filter. $e[n]$ is the estimation error, which is defined as

$$e[n] = I[n] - \widetilde{I}[n], \tag{9}$$

where $\widetilde{I}[n]$ is the soft output of multichannel DFE. In the training mode, $I[n]$ is the transmitted symbol. In the tracking mode, the decision output $\widehat{I}[n]$ replaces $I[n]$ to obtain the estimation error. For PPC–DFE shown in Fig. 1, the single DPLL tracks the averaged frequency shifts of K receiving channels.

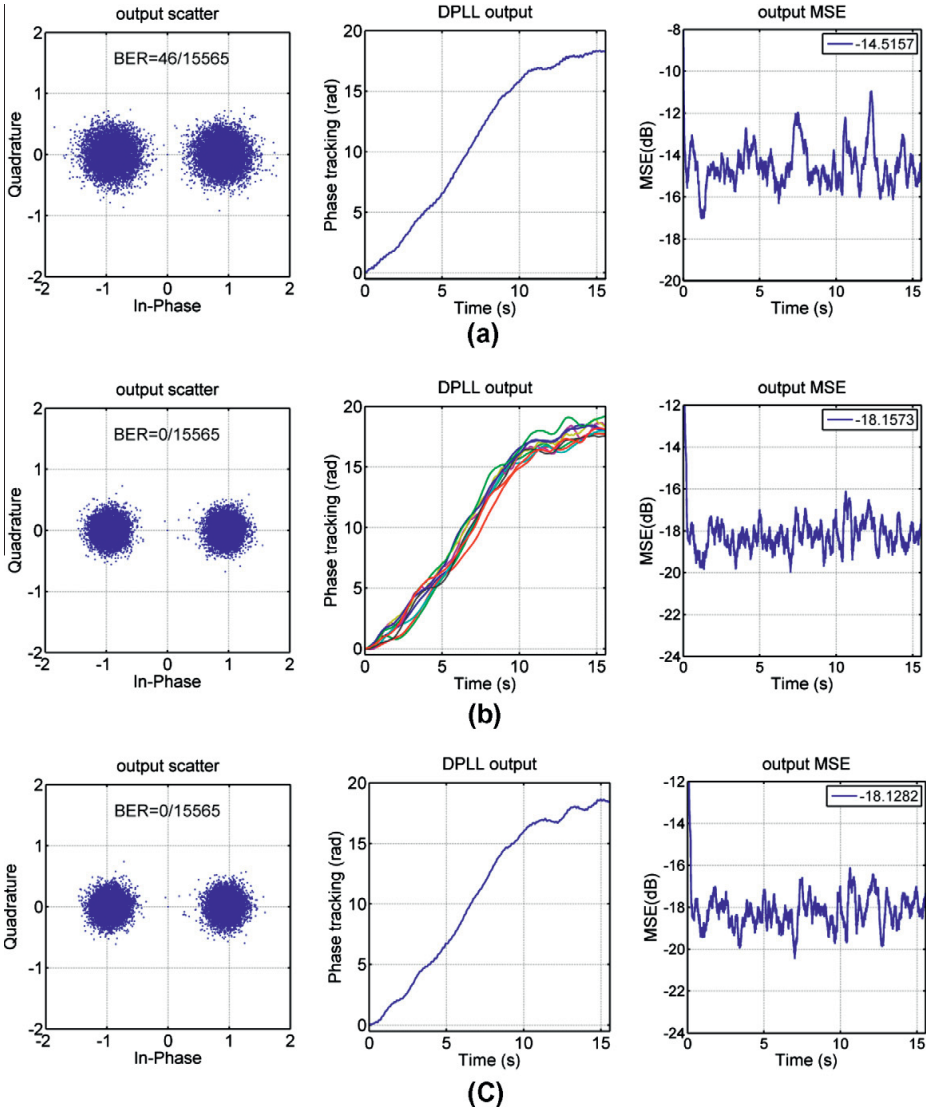

Fig. 9. The receiver performance. (a) PPC–DFE. (b) PPC–McDFE (10 DPLL). (c) PPC–McDFE (1 DPLL averaged of 10 DPLL).

3. The experiment and analysis

3.1. The experimental setup

The sea experiment was carried out on June 30, 2010, in Trondheim harbor, Norway. In the experimental area shown in Fig. 3a, the sea depth changes from a few meters to hundreds of meters. Fig. 3b shows that the depth profile in the communication track of 4 km changes from 380 m to 10 m. The red[1] dot denotes the position of the transmitter, which used a hemispherical acoustic source suspended at a depth of 20 m from the NTNU research vessel R/V Gunnerus. It was rainy and windy when the trial was conducted from 15:00 to 16:00, and the dynamic positioning system of R/V Gunnerus was activated to reduce drifting. A vertical receiving array of 6 hydrophones (channel Nos. 1–6) with 1 m element spacing and a horizontal receiving array of 4 hydrophones (channel Nos. 7–10) with 1.5 m element spacing were used. The deepest hydrophone of the vertical array, with number 1, was about 1.5 m above the sea bottom. The horizontal array was deployed at the depth of 5.5 m. The two arrays formed a cross receiving array (CRA) in a water depth of 10 m.

In the 45-min trial, one period signal at the carrier frequency of 12 kHz was repeatedly transmitted every 152.548 s. Within each period, there were a channel probe signal of 0.1 s and a data signal of 15.565 s. In order to decrease the impact from the probe signal, there was 0.2 s silence between the probe signal and the data

[1] For interpretation of color in Fig. 3, the reader is referred to the web version of this article.

signal. The probe signal was a linear frequency modulation chirp with a Hanning window, resulting in an effective bandwidth of 2.2 kHz, and it was also used as a shaping pulse for a binary phase shift keying (BPSK) signal. For simplicity, the received chirp is immediately used as the channel response estimate for PPC processing [11]. The BPSK signal was transmitted at a symbol rate of 1 kilosymbols/s. The received waveforms of 18 periods were recorded at a sampling frequency of 96 kHz for off-line processing in the laboratory.

3.2. The analysis

Fig. 4 shows the sound speed profile and an example of the channel impulse response patterns at the receiving array, which were estimated by the received probe signal using the replica correlation method. The measured sound speed profile shows that there was a sound channel at a depth about 20 m during the trial. The multipath pattern varies with channels, and it changes from 5 symbol intervals in the channel Nos. 1–10 symbol intervals in the channel No. 10. As the array was deployed in shallow water with a depth which was different from that for the transmitter, it received acoustic rays reflected from the surface and bottom. The multipath pattern changed with time in the 45-min trial, resulting in time-varying fading.

Both the receiver structures are configured with the parameters in Table 1. There are two samples per symbol in the digital signal processing. In order to compare with the equal weight combining, the taps of feed-forward filters span one symbol interval. With $N_{ff} = 2$ and $N_{fb} = 1$, Fig. 5 shows the performance of the first period versus the number of receiving channels, where output SNR is given by $(1 - \mathrm{MSE})/\mathrm{MSE}$ [15]. The performance improves with the increasing number of receivers. PPC–McDFE achieves a superior performance over PPC–DFE using up to 10 receiving channels, where the improvement gains 5 dB when using 10 channels. In reality due to the instrumentation and environmental conditions, for instance at different depths, the input SNRs are different among the channels, and the PPC–McDFE obtains spatial diversity by jointly updating the combining coefficients to maximize output SNR. Fig. 6 shows the evolution of tap coefficients within 15.565 s. The coefficients are not equal among channels and change with time evolution. The taps for channel No. 5 have large weights, and this is attributed to that fact that the channel No. 5 exhibits the highest temporal coherence within 15.565 s. In reality, it is impossible to deploy the receivers independently, which is preferred by PPC–DFE, and adaptive combining exploits spatial diversity based on the spatial coherence.

The number of taps is then increased to $N_{ff} = 8$ and $N_{fb} = 2$. Fig. 7 shows the performance using 10 receiving channels in the 45-min trial. Comparing with the output SNRs of the 1st period using 10 channels in Fig. 5, the output SNRs improve about 2 dB for both structures attributed to an increasing number of taps, which raises the computational load. PPC–McDFE achieves superior performance through the trial, there is a minimum 1.5 dB gain obtained in the 9th period, and there is a maximum 6.7 dB gain obtained in the 5th period. As the CRA was deployed in shallow water near the shore, the received signals experienced time-variant fading, and the improvement changes with periods due to the variation of interchannel correlations.

Spatial coherence measures the strength of interchannel correlation between two receivers, and it can be calculated by

$$\psi(m,l) = \frac{|r_m(-t) \otimes r_l(t)|_{\max}}{\sqrt{|r_m(-t) \otimes r_m(t)|_{\max} |r_l(-t) \otimes r_l(t)|_{\max}}}, \tag{10}$$

where $|r_m(-t) \otimes r_l(t)|_{\max}$ denotes the maximum absolute value of cross-correlation between the two signals $r_m(t)$ and $r_l(t)$, and $r_m(t)$ represents the signal received by the mth hydrophone. Fig. 8 shows the spatial coherence measurement in the 18 periods, where $m = 3$ and l is changed from 1 to 10. It is shown that interchannel correlation exists and changes with time during the trial. Since it is intractable to predict time variant spatial coherence, it is preferred to exploit spatial diversity by adaptive combining.

PPC–McDFE uses independent DPLLs to track frequency shifts that occurred in the receiving channels, whereas the passive time reversal method shown in Fig. 1 uses only one DPLL to track an averaged frequency shift. In order to prove that the improvement gain originates from the adaptive combining, the independent DPLLs are replaced with a common DPLL which updates the averaged value of phase-offset corrections given by

$$\bar{\hat{\theta}}[n] = \frac{1}{10} \sum_{i=1}^{10} \hat{\theta}_i[n]. \tag{11}$$

As an example, the received data of the 6th period is analyzed with $N_{ff} = 8$ and $N_{fb} = 2$ to compare the performance as shown in Fig. 9. As shown by the output MSE of the right panel, PPC–DFE achieves the poorest performance, and there is little difference for PPC–McDFE between using 1 DPLL and 10 DPLL. The DPLL output in Fig. 9a is similar to the DPLL output in Fig. 9c, which is the mean of the DPLL output in Fig. 9b. Therefore, the improvement gain originates from the adaptive diversity combining. This conclusion applies also to other received periods.

4. Conclusions

A modified receiver structure is proposed for underwater communications, and it is demonstrated by a sea experiment. The results of communications at high frequency in a range dependent channel over a range of 4 km are presented. Using up to 10 receivers, the proposed receiver structure achieves superior performance over the structure based on passive time reversal, where there is superiority even though the filter taps span one symbol interval. The improvement is attributed to spatial diversity exploited by the adaptive multichannel combining. Since it is intractable to predict time-variant interchannel correlations and input SNRs among the receivers distributed in a real oceanic environment, it is preferred that spatial diversity is exploited by the adaptive multichannel processing. Presented results have demonstrated that the improvement of passive time reversal communications is obtained.

Acknowledgment

The author would like to thank the crew of R/V Gunnerus and the engineer Tim Cato Netland for the help in data collection, and the NTNU Professor Emeritus Jens M. Hovem for discussions.

References

[1] Kilfoyle DB, Baggeroer AB. The state of the art in underwater acoustic telemetry. IEEE J Oceanic Eng 2000;25:4–27.
[2] Dowling DR. Acoustic pulse compression using passive phase-conjugate processing. J Acoust Soc Am 1994;95:1450–8.
[3] Rouseff D, Jackson DR, Fox WLJ, Jones CD, Ritcey JA, Dowling DR. Underwater acoustic communication by passive-phase conjugation: theory and experimental results. IEEE J Oceanic Eng 2001;26:821–31.
[4] Yang TC. Differences between passive-phase conjugation and decision-feedback equalizer for underwater acoustic communications. IEEE J Oceanic Eng 2004;29:472–87.
[5] Yang TC. Correlation-based decision-feedback equalizer for underwater acoustic communications. IEEE J Oceanic Eng 2005;30:865–80.
[6] Song HC, Hodgkiss WS, Kuperman WA, Stevenson M, Akal T. Improvement of time-reversal communications using adaptive channel equalizers. IEEE J Oceanic Eng 2006;31:487–96.
[7] Song A, Badiey M, Song HC, Hodgkiss WS, Porter MB, t. K. Group. Impact of ocean variability on coherent underwater acoustic communications

during the Kauai experiment (KauaiEx). J Acoust Soc Am 2008;123:856–65.
[8] Song HC, Hodgkiss WS, Kuperman WA, Akal T, Stevenson M. High-frequency acoustic communications achieving high bandwidth efficiency. J Acoust Soc Am 2009;126:561–3.
[9] Song HC, Roux P, Hodgkiss WS, Kuperman WA, Akal T, Stevenson M. Multiple-input–multiple-output coherent time reversal communications in a shallow-water acoustic channel. IEEE J Oceanic Eng 2006;31:170–8.
[10] Song HC, Hodgkiss WS, Kuperman WA, Akal T, Stevenson M. Multiuser communications using passive time reversal. IEEE J Oceanic Eng 2007;32:915–26.
[11] Song HC, Kim JS, Hodgkiss WS, Kuperman WA, Stevenson M. High-rate multiuser communications in shallow water. J Acoust Soc Am 2010;128:2920–5.
[12] Yang TC. A study of spatial processing gain in underwater acoustic communications. IEEE J Oceanic Eng 2007;32:689–709.
[13] Stojanovic M, Catipovic J, Proakis JG. Adaptive multichannel combining and equalization for underwater acoustic communications. J Acoust Soc Am 1993;94:1621–31.
[14] Stojanovic M. Efficient processing of acoustic signals for high-rate information transmission over sparse underwater channels. Phys Commun 2008;1:146–61.
[15] Proakis JG. Digital communications. New York: McGraw-Hill; 2001.

Paper 4: Experimental Demonstration of Spread Spectrum Communication over Long Range Multipath Channels

Guosong Zhang and Hefeng Dong

In Applied Acoustics, vol. 73, pp. 872-876, 2012

The thesis author had the original idea for this paper. The co-authors participated in scientific discussions.

Applied Acoustics 73 (2012) 872–876

Contents lists available at SciVerse ScienceDirect

Applied Acoustics

journal homepage: www.elsevier.com/locate/apacoust

Experimental demonstration of spread spectrum communication over long range multipath channels

Guosong Zhang *, Hefeng Dong

Department of Electronics and Telecommunications, Norwegian University of Science and Technology (NTNU), Trondheim 7491, Norway

ARTICLE INFO

Article history:
Received 11 October 2011
Received in revised form 28 February 2012
Accepted 6 March 2012
Available online 6 April 2012

Keywords:
Spread spectrum
Cyclic code shift keying
Pulse position modulation
Underwater acoustic communication
Passive-phase conjugation
Time reversal

ABSTRACT

This paper presents a spread spectrum scheme, which is designed for long range underwater acoustic communications of low signal-to-noise ratios. This scheme uses two maximum length sequences, which are overlapped in time. One is used as a time reference, and the other applies code cyclic shift keying (CCSK) to carry information. Compared with conventional spread spectrum techniques, CCSK achieves a higher spectral efficiency, and this property is of significance in spread spectrum communications. With the help of a time reference, performance impairment from timing errors for CCSK is reduced, as each CCSK symbol has its own time reference. For this scheme, three receiver structures are presented, and they are: (1) correlation receiver, (2) passive-phase conjugation receiver, and (3) time reversal receiver structures. A recent sea experiment was carried out in a range dependent channel over a distance of 10 km. By real data processing, performance of the three receiver structures are compared and discussed. The presented results demonstrate the feasibility of this spread spectrum scheme.

1. Introduction

Long range underwater acoustic communication at high frequencies is challenging due to the increased attenuation at higher frequencies. Direct sequence spread spectrum (DSSS) technique provides aspreading gain to achieve communications of low signal-to-noise ratios (SNRs) [1]. In the past, DSSS has been demonstrated in underwater acoustic communications [2–6]. For DSSS communications, intersymbol interference caused by multipath arrivals has been addressed by Stojanovic et al. [3,7], where adaptive channel equalizations have been applied to phase coherent signals at high SNRs. Simple DSSS schemes have been focused to reduce the complexity of receivers. Pulse position modulation is used by Hursky et al. [8], and differential phase modulation is proposed by Yang et al. [6], where passive-phase conjugation (PPC) processing is used to take advantage of the pulse compression. The spectral efficiency of the two simple schemes is low. Cyclic code shift keying (CCSK) for spread spectrum, e.g. the Joint Tactical Information Distribution System [9,10], is of high spectral efficiency [2], but it suffers performance impairment from timing errors in underwater acoustic communications.

In this paper, we presented a modified CCSK scheme for spread spectrum communications at low input SNRs. One advantage of CCSK is that this modulation scheme increases spectral efficiency of conventional DSSS technique, and another advantage is its simple demodulation using cyclic correlation, which is easily realized by fast Fourier transform (FFT). Being different from [2,9], where one code was used for CCSK, two codes of low cross-correlation are used in this paper. One code is used as a time reference, and the other is CCSK modulated to carry information. Instead of merely delaying used by the position modulation in [8], the code for modulation is cyclic shifted relative to the reference. At the receiver, the information is recovered by measuring the relative shift between the two codes.

The codes of good auto-correlations and low cross-correlations are selected, and a correlation receiver structure can be used to recover the position modulated information. Due to multipath arrivals and cross-correlations without precise phase synchronizations, correct decisions are easily impaired in measuring the cyclic shifts. PPC processing achieves the pulse compression for time delayed arrivals [11]. The pulse compression also applies to the case of one receiving channel [6,8], where there are higher side lobes comparing with the scenarios of multiple receivers. At the receiver, knowledge of the channel required by PPC processing can be estimated using training symbols [12]. However, a single receiver cannot avoid deep fading in a time-varying acoustic channel.

With multiple receivers distributed in a oceanic environment, there is spatial diversity which could be exploited by the time reversal focusing [13]. Obtained spatial diversity contributes an enhanced output SNR plus low side lobes of the *Q*-function [14], which is the auto-correlations of channel impulse response summed over the receiving channels. After the focusing, a subsequent

* Corresponding author. Tel.: +47 73590465; fax: +47 73591412.
E-mail addresses: Guosong.Zhang@iet.ntnu.no (G. Zhang), Hefeng.Dong@iet.ntnu.no (H. Dong).

0003-682X/$ - see front matter © 2012 Elsevier Ltd. All rights reserved.
http://dx.doi.org/10.1016/j.apacoust.2012.03.002

conventional CCSK demodulator can be applied to recover information. Since there is lack of a model which precisely predicts underwater acoustic channels for high frequencies (e.g., 11–13 kHz), a sea experiment was conducted in Trondheim harbor, in Norway over a range of 10 km to demonstrate the modified CCSK scheme.

This paper is organized as follows. Section 2 introduces the spread spectrum scheme for communications. In Section 3, correlation receiver, PPC receiver, and time reversal receiver structures are given. The experimental setup and measurement are shown in Section 4. In Section 5, the off-line processing results are presented and analyzed, and the performance of the three structures is shown. Finally, Section 6 summaries the work.

2. The modulation

The present modulation uses two pseudo-random codes of equal length, where there are low cross-correlations between the two codes. For example, two maximum-length sequences (MLSs) of 127 chips can be used. Let c_1 of N chips represents the code which is used as time reference within each symbol, and let$[c_2]_m$ denote code c_2 which is cyclic shifted by m chips (or positions). The cyclic offset between the sequences is used to carry information. Within the time interval of one symbol, there are $\lfloor \log_2(N) \rfloor$ positions which are used to carry information. Fig. 1 illustrates the modulation scheme. c_1 provides timing for $[c_2]_m$ during demodulation, where the impact from timing error is reduced. The transmitted spread spectrum signal is written as:

$$S(t) = Re\{(c_1 + j[c_2]_m)g(t)e^{j0032\pi f_c t}\} \tag{1}$$

where f_c denotes the carrier frequency, and $g(t)$ is the pulse shape function or each chip of time duration T, that is,

$$g(\tau) = \begin{cases} 1, & \text{for } 0 \leqslant \tau < T \\ 0, & \text{othertwise} \end{cases} \tag{2}$$

The data rate is calculated as:

$$R = \frac{\lfloor \log_2(N) \rfloor}{NT} \tag{3}$$

For a fixed bandwidth of $1/T$, since the denominator NT increases much faster than the numerator$\lfloor \log_2(N) \rfloor$, N should be chosen as a tradeoff between the data rate and the spreading gain, which is determined by N. For the method proposed by Yang et al. [6], binary information is differential modulated between two consecutive symbols, and the data rate is about $1/NT$. Hence the presented scheme increases the spectral efficiency of DSSS. This scheme also avoids the issue of a high peak-to-average power ratio of the transmitted signal, which occurs in the method proposed by Hursky et al. in [8], and this property benefits the power efficiency in signaling.

3. The receiver structures

The receiver recovers transmitted information by taking advantage of the spreading gain to achieve communications at low input SNR. Three type receiver structures are briefly introduced and discussed.

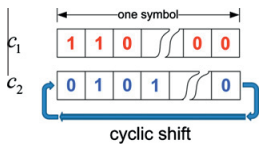

Fig. 1. The illustration of modulation.

3.1. Correlation receiver structure

In demodulation, the transmitted information is simply recovered by measuring the cyclic shift. The shift is estimated by measuring the distance between two main peaks of cyclic correlations, which can be realized by FFT processing. The MLS achieves a time resolution of T, which is one position. The method in [2] uses one code, and it suffers performance degradation due to timing errors. A time reference in each symbol benefits the shift estimation, since each information symbol is time synchronized by the reference code. Fig. 2 shows an example of the demodulation, where there are no multipath arrivals. As shown by the arrow, the shift estimate $\dot{m}$ is obtained by measuring the number of chips between two peaks.

c_1 and $[c_2]_m$ are not orthogonal without carrier-phase tracking, which is intractable in the scenarios of low input SNR, and thus there are cross-correlations between the two codes under non-coherent demodulation. For two MLSs of 127 chips used in the trial of Section 4, the maximal and minimal cross-correlations remain constant for the 64 positions, and the maximum is about 17% of the peak value of auto-correlation. The cross-correlations impact on the shift estimations. In presence of multipath arrivals, even though c_1 and $[c_2]_m$ convolve the same channel impulse response, there is interference for shift estimations due to the cross-correlations and pre-cursors of the impulse response.

A RAKE receiver recombines the multipath arrivals [4]. It requires phase information of the arrivals in order to align them in the combining process. Without explicit estimations of the phase information, pulse compression achieved by PPC processing recombines the time delayed arrivals, and it is simple in realization.

3.2. PPC receiver structure

The signal received at the ith receiving channel is written as:

$$r_i(t) = s(t) \otimes h_i(t) + w_i(t) \tag{4}$$

where $h_i(t)$ denotes the impulse response, $w_i(t)$ represents a bandwidth limited noise at the ith receiver, and $\otimes$ means convolution. The output of one channel PPC processing is

$$\begin{aligned} z_i(t) &= h_i(-t) \otimes r_i(t) = h_i(-t) \otimes h_i(t) \otimes s(t) + h_i(-t) \otimes w_i(t) \\ &= q_i(t) \otimes s(t) + \varsigma_i(t) \end{aligned} \tag{5}$$

where $q_i(t)$ is the auto-correlation of $h_i(t)$, and $\varsigma_i(t)$ is a filtered noise. The PPC structure is shown in Fig. 3, the channel can be estimated using training symbols. PPC processing is conducted prior to cyclic correlation. The purpose of PPC processing is to reduce impact of multipath arrivals, as the pulse compression provides a mean of recombining the arrivals. The recombining acts as a RAKE receiver [5,6], even in the scenario of a single receiver. Yang et al. [6] has tested the recombining in scenarios of low input SNR. Since the overlapped codes convolve the same channel response, only one copy channel estimation is required to take advantage of the pulse compression.

After cyclic correlation, the side lobes of $q_i(t)$ interfere in making a decision for the shift estimation, especially if there are high side lobes. As discussed by Yang [15], the peak-to-side lobe ratio of $q_i(t)$ is determined by the channel response $h_i(t)$. However, the ratio is decreased if multiple receiving channels are used to average the side lobes, which is given by

$$Q(t) = \sum_{i=1}^{K} q_i(t) \tag{6}$$

where K denotes the number of receiving channels. As multiple receivers are distributed in space, the side lobes of $\{q_i\}$ are

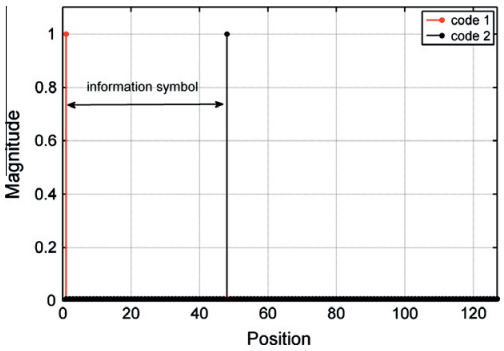

Fig. 2. The example of cyclic correlation demodulation.

uncorrelated because of spatial diversity, and therefore the peak-to-side lobe ratio is increased by the *K*-channel combining. In order to differentiate from the single channel scenario, we refer it as a time reversal structure.

3.3. Time reversal receiver structure

Time reversal has demonstrated its potential for high rate underwater communications [16–18]. The property of refocusing mitigates intersymbol interference (ISI) caused by multipath arrivals, and only one subsequent adaptive channel equalizer is needed to remove residual ISI. This refocusing principle can be applied to the modulation scheme presented in Section 2. Fig. 4 shows the diagram of the time reversal receiver structure for the spread spectrum scheme. There are two parts. One part is the combining of *K*-channel PPC processing, and the other is the cyclic correlation. Spatial diversity is exploited by the multichannel combining to reduce the side lobe level of the *Q*-function. In addition, the combining contributes an enhanced input SNR for the cyclic correlation. It is desirable to obtain an increased input SNR in long range communications.

4. The experiment

4.1. Experimental setup

The communication experiment was conducted on June 16, 2011, in Trondheim harbor in Norway shown in Fig. 5. The shallow region which is less than 20 m extends about 100 m offshore, and the sea depth varies from tens of meters to hundreds of meters. The red spot denotes the position of the transmitter in a distance of 10 km to a cross receiving array denoted by the black spot. The receiving array consisted of eight hydrophones, and it was near-shore deployed in a water depth of 10 m. The array consists of a vertical receiving array of four hydrophones (hydrophone No. 1–4) with 1 m element spacing and a horizontal receiving array of four hydrophones (hydrophone No. 5–8) with 1.5 m element spacing. Hydrophone No.1 was 0.5 m below the sea surface, and the depth of hydrophones No. 5–8 was 4.5 m. The transmitter used

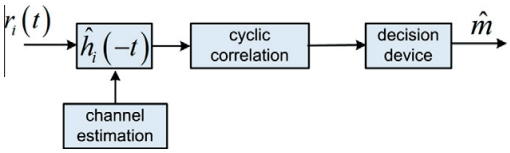

Fig. 3. The diagram of PPC receiver structure for one receiving channel.

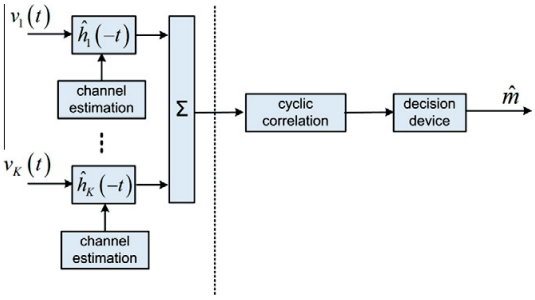

Fig. 4. The diagram of time reversal receiver structure.

a hemispherical acoustic transducer which was suspended at a depth of 20 m from the NTNU research vessel R/V Gunnerus. The dynamic positioning system was activated to reduce drifting during the trail.

In the experiment, the spread spectrum signal of 16.256 s was transmitted every 140.892 s for about 35 min, and the source level was 187 dB re 1 μPa at 1 m. The carrier frequency of the signal was 12 kHz. Two MLSs of 127 chips were used in modulation, and the chip rate was 1 kilo chips/s. Since 64 positions was used in each symbol, the data rate was 47.2 bits/s. A square root-raised cosine filter was used for pulse shaping, where the roll-off coefficient was 1, and therefore the bandwidth for the signal was 2 kHz. The received waveforms were recorded with a sampling frequency of 96 kHz for off-line processing in the laboratory.

4.2. The channel measurement

The sound speed profiles measured by the R/V Gunnerus are shown in Fig. 6. As indicated, there was a sound channel at the depth of 40 m during the trial and the water depth at the source location was about 90 m. It is shown that the depth changes along the communication track, and the sound speed profile changed with time and location, especially between 40 and 100 m depths.

Fig. 7 shows examples of the normalized channel impulse response with time evolution, where hydrophone No. 4 was 3.5 m below the sea surface. The least squares (LS) method [12] is used to estimate the response. As evident, the channel is time variant, and the input SNR of the 15th period is the lowest. Since the receiving array was deployed in the shallow region at a depth which was different from the transmitter depth of 20 m, the received signal experienced time-varying fading due to reflections in the acoustic propagation.

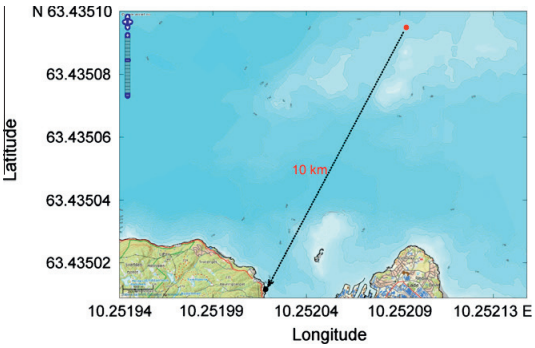

Fig. 5. The experimental area in Trondheim harbor.

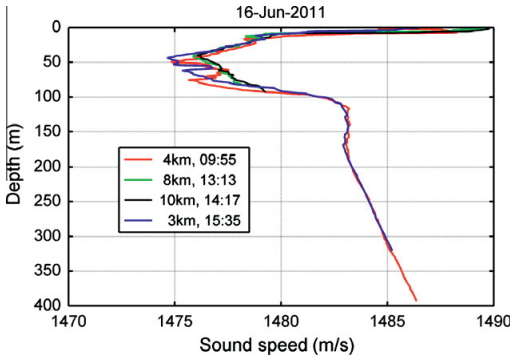

Fig. 6. Sound speed profiles measured at different distances to the receiving array.

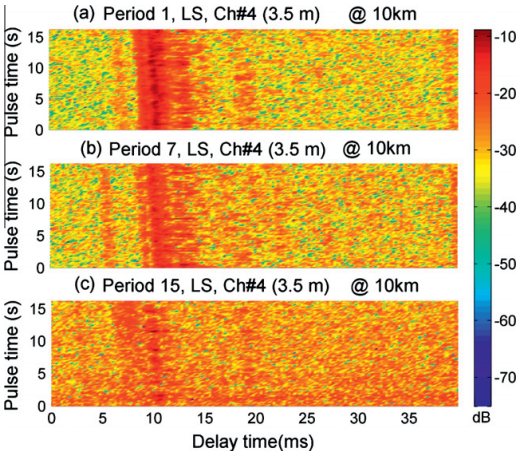

Fig. 7. Channel impulse response versus time evolution.

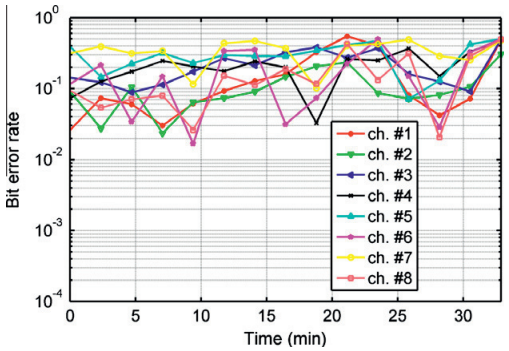

Fig. 8. Performance of the correlation receiver structure.

5. The results and analysis

The recorded signals of 15 periods are processed by the three receiver structures. For the correlation receiver structure, the performance in terms of bit error rate (BER) is shown in Fig. 8. The best performance is achieved in channel No. 6, with the lowest BER of 1.69e−2. During the 35 min, sometimes most information is correctly recovered. However, the BER plot shows that there is no stable communications in each individual receiving channel during the trial. Fig. 9 shows an example of matched filter output. Within 15.24 s, the correlation output changes with time, and time-varying response results in errors.

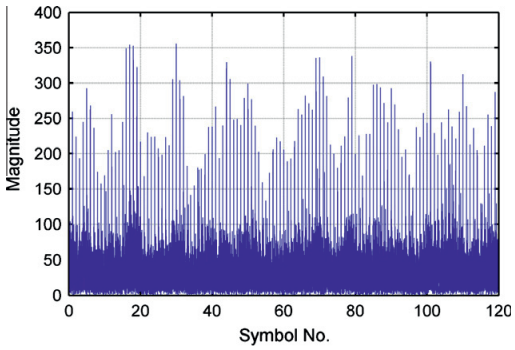

Fig. 9. Matched filter output of MLS c_1 in channel No. 1 (the 1st period).

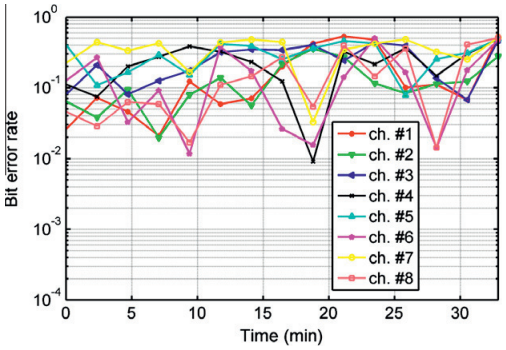

Fig. 10. Performance of the PPC receiver structure.

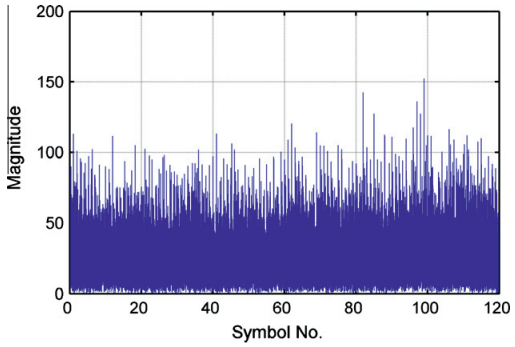

Fig. 11. Matched filter output of MLS c_1 in channel No. 1 (the 9th period).

The performance of the PPC receiver structure is shown in Fig. 10. Only one channel is used in PPC processing, and the channel response is estimated by the LS method. The lowest BER of 9.10e−3 is achieved in channel No. 4. In some periods, the PPC

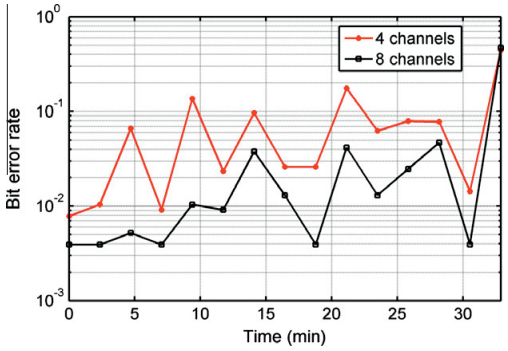

Fig. 12. Performance of the time reversal receiver structure.

processing improves the performance, e.g., the 5th and 9th periods. However, deep fading cannot be avoided using a single receiving channel. Fig. 11 shows another example of matched filter output in the case of deep fading, which results in errors. By the results presented above, it is suggested to exploit the spatial diversity using multiple receivers.

Two cases are tested in the multichannel scenarios. One uses four receiving channels of the vertical array, and the other uses eight receiving channels. Results of the time reversal receiver structure are shown in Fig. 12. The lowest BER achieved in both cases are 9.10e−3 and 3.90e−3, respectively. In 14 periods, BER is reduced with an increased number of receiving channels, and performance of the time reversal structure is improved by using more channels. Comparing the BERs shown in Figs. 10 and 12, the lowest BER using PPC structure is 9.10e−3, while the lowest BER using the time reversal structure with eight receiving channels is 3.90e−3. It is evident that spatial diversity is exploited by the time reversal focusing to improve the performance.

6. Conclusions and discussion

We have presented a spread spectrum scheme for long range communications. Since it is preferred to implement spectral efficient spread spectrum techniques, this scheme keeps the efficiency of CCSK, while the timing problem is solved by using a reference in each symbol. The code length should be chosen as a compromise between the spectral efficiency and the spreading gain, which is of significance in low SNR scenarios. Three type receiver structures are experimentally assessed. The time reversal receiver structure improves the performance with an increased number of receiving channels. The presented results have demonstrated that this scheme succeeded communications over a range dependent channel of 10 km.

Spread spectrum techniques are sensitive to relative movement during communications. The relative movement was not an issue in this sea trial, since the dynamic position system of R/V Gunnerus was activated to avoid drifting. However, with a reference code in each symbol, Doppler shift can be estimated using the ambiguity function method, and therefore this spread spectrum technique could be applied in communications of movement.

Acknowledgments

The authors would like to thank NTNU PhD candidates Yan Jiang and Qin Liu, the participants, technical engineer Tim Cato Netland and crew of R/V Gunnerus at NTNU for their help during the sea trial.

References

[1] Proakis JG. Digital communications. New York: McGraw-Hill; 2001.
[2] Ritcey JA, Griep KR. Code shift keyed spread spectrum for ocean acoustic telemetry. Presented at OCEANS 95 MTS/IEEE. Challenges of Our Changing Global Environment. Conference Proceedings; 1995.
[3] Stojanovic M, Proarkis JG, Rice JA, Green MD. Spread spectrum underwater acoustic telemetry. Presented at OCEANS 98. Conference Proceedings; 1998.
[4] Sozer EM, Proakis JG, Stojanovic R, Rice JA, Benson A, Hatch M. Direct sequence spread spectrum based modem for under water acoustic communication and channel measurements. Presented at OCEANS 99 MTS/IEEE. Riding the Crest into the 21st Century; 1999.
[5] Hursky P. Point-to-point underwater acoustic communications using spread-spectrum passive phase conjugation. J Acoust Soc Am 2006;120:247.
[6] Yang TC, Wen-Bin Y. Performance analysis of direct-sequence spread-spectrum underwater acoustic communications with low signal-to-noise-ratio input signals. J Acoust Soc Am 2008;123:842–55.
[7] Stojanovic M, Freitag L. Hypothesis-feedback equalization for direct-sequence spread-spectrum underwater communications. Presented at OCEANS 2000 MTS/IEEE. Conference and Exhibition; 2000.
[8] Paul H, Michael BP, Martin S, Vincent KM. Point-to-point underwater acoustic communications using spread-spectrum passive phase conjugation. J Acoust Soc Am 2006;120:247–57.
[9] Dillard GM, Reuter M, Zeiddler J, Zeidler B. Cyclic code shift keying: a low probability of intercept communication technique. Aerospace Electron Syst, IEEE Trans 2003;39:786–98.
[10] Chi-Han K, Robertson C, Kyle L. Performance analysis and simulation of cyclic code-shift keying. Presented at Military Communications Conference; 2008. [MILCOM 2008. IEEE, 2008].
[11] Dowling DR. Acoustic pulse compression using passive phase-conjugate processing. J Acoust Soc Am 1994;95:1450–8.
[12] Flynn JA, Ritcey JA, Rouseff D, Fox WLJ. Multichannel equalization by decision-directed passive phase conjugation: experimental results. IEEE J Ocean Eng 2004;29:824–36.
[13] Song HC, Hodgkiss WS, Kuperman WA, Higley WJ, Raghukumar K, Akal T, Stevenson M. Spatial diversity in passive time reversal communications. J Acoust Soc Am 2006;120:2067–76.
[14] Yang TC. Correlation-based decision-feedback equalizer for underwater acoustic communications. IEEE J Ocean Eng 2005;30:865–80.
[15] Yang TC. Temporal resolutions of time-reversal and passive-phase conjugation for underwater acoustic communications. IEEE J Ocean Eng 2003;28:229–45.
[16] Song HC, Hodgkiss WS, Kuperman WA, Akal T, Stevenson M. High-frequency acoustic communications achieving high bandwidth efficiency. J Acoust Soc Am 2009;126:561–3.
[17] Song HC, Kim JS, Hodgkiss WS, Kuperman WA, Stevenson M. High-rate multiuser communications in shallow water. J Acoust Soc Am 2010;128:2920–5.
[18] Song HC. Time reversal communication in a time-varying sparse channel. J Acoust Soc Am 2011;130:EL161–6.

Paper 5: Underwater Communications in Time-varying Sparse Channels Using Passive-phase Conjugation

Guosong Zhang, and Hefeng Dong

In Applied Acoustics, vol. 74, pp. 421-424, 2013

The thesis author had the original idea for this paper. The co-authors participated in scientific discussions.

Applied Acoustics 74 (2013) 421–424

Contents lists available at SciVerse ScienceDirect

Applied Acoustics

journal homepage: www.elsevier.com/locate/apacoust

Technical Note

Underwater communications in time-varying sparse channels using passive-phase conjugation

Guosong Zhang *, Hefeng Dong

Department of Electronics and Telecommunications, Norwegian University of Science and Technology (NTNU), Trondheim NO-7491, Norway

ARTICLE INFO

Article history:
Received 30 December 2011
Received in revised form 21 August 2012
Accepted 22 August 2012

Keywords:
Passive-phase conjugation
Matching pursuit
Underwater acoustic communication
Time reversal

ABSTRACT

Passive-phase conjugation (PPC) achieves the pulse compression for the time delayed arrivals. This property has been used in underwater acoustic communications. In a time-varying channel, the temporal focusing degrades with time evolution. The block-based approach is implemented to avoid the impact of channel variations. The basic idea is that the channel is assumed constant within each block of a short time interval, and the channel is updated using detected symbols in the previous block. Using real data collected in a recent sea trial, this paper investigates: (1) the communications using PPC processing, where the block-based approach is used, (2) the matching pursuit (MP) algorithm exploiting the channel sparseness. It is found that the MP algorithm improves performance of the communications using PPC processing.

1. Introduction

Underwater acoustic channels are often of extended time delay spread, time-varying, and sparse. Passive-phase conjugation (PPC) achieves temporal focusing (pulse compression) for time delayed arrivals [1]. In the scenarios of both a single receiver [2] and multiple receivers [3], this focusing property has been used for underwater acoustic communications with a low complex channel equalizer [4]. PPC processing requires the knowledge of the channel, which could be obtained by the probe signal or training symbols. The temporal focusing degrades with time evolution in time-varying channels. Song [5] has proposed the block-based approach to overcome the problems of channel variations. The channel remains time-invariant within each block of a short time interval, and the channel is updated on a block-by-block basis. For PPC processing in the current block, the channel is estimated using detected symbols in the previous block.

Since there is lack of a model which predicts the time-varying channel for high frequencies (e.g. 12–14 kHz), this paper investigates two PPC receiver structures using real data collected in a range dependent channel. The block-based approach is applied. As discussed by Song [6], the matching pursuit (MP) algorithm [7] could improve the performance of time reversal communication in a sparse channel. In this paper, the MP is experimentally assessed for communications where PPC processing is implemented. Being different from the conventional least squares (LSs) method, the MP algorithm estimates dominant arrivals instead of all the arrivals within a time interval. It is found that the MP algorithm improves the performance of communications using PPC processing.

2. The block-based receiver structures

Two receiver structures using PPC processing are shown in Fig. 1. The two structures differentiate in the way of multichannel combining. Fig. 1a shows the time reversal combining followed by a single channel decision feedback equalizer (DFE), and it is referred as PPC–DFE. Fig. 1b is a joint PPC and multichannel DFE, where temporal focusing is used to reduce the number of taps for the feed-forward filters in each receiving channel of a multichannel DFE, and it is referred as PPC–McDFE [8]. The carrier-phase tracking is implemented using the second order digital phase-locked loop (DPLL) [9], which operates on symbol-by-symbol basis to correct phase rotations. The recursive least squares (RLSs) algorithm is used to update the coefficients of feed-forward and feedback filters.

3. The experiment

3.1. The setup

The communication experiment was conducted on September 7, 2011, in Trondheim harbor in Norway. The transmitter was located at a distance of 3.7 km to a cross receiving array. The water depth in shallow region is less than 20 m and increases to 400 m, where the acoustic source was deployed at a depth of 40 m. The receiving array consisted of 12 hydrophones, and it was

* Corresponding author. Tel.: +47 7359 0465; fax: +47 7359 1412.
E-mail addresses: Guosong.Zhang@iet.ntnu.no (G. Zhang), Hefeng.Dong@iet.ntnu.no (H. Dong).

0003-682X/$ - see front matter © 2012 Elsevier Ltd. All rights reserved.
http://dx.doi.org/10.1016/j.apacoust.2012.08.008

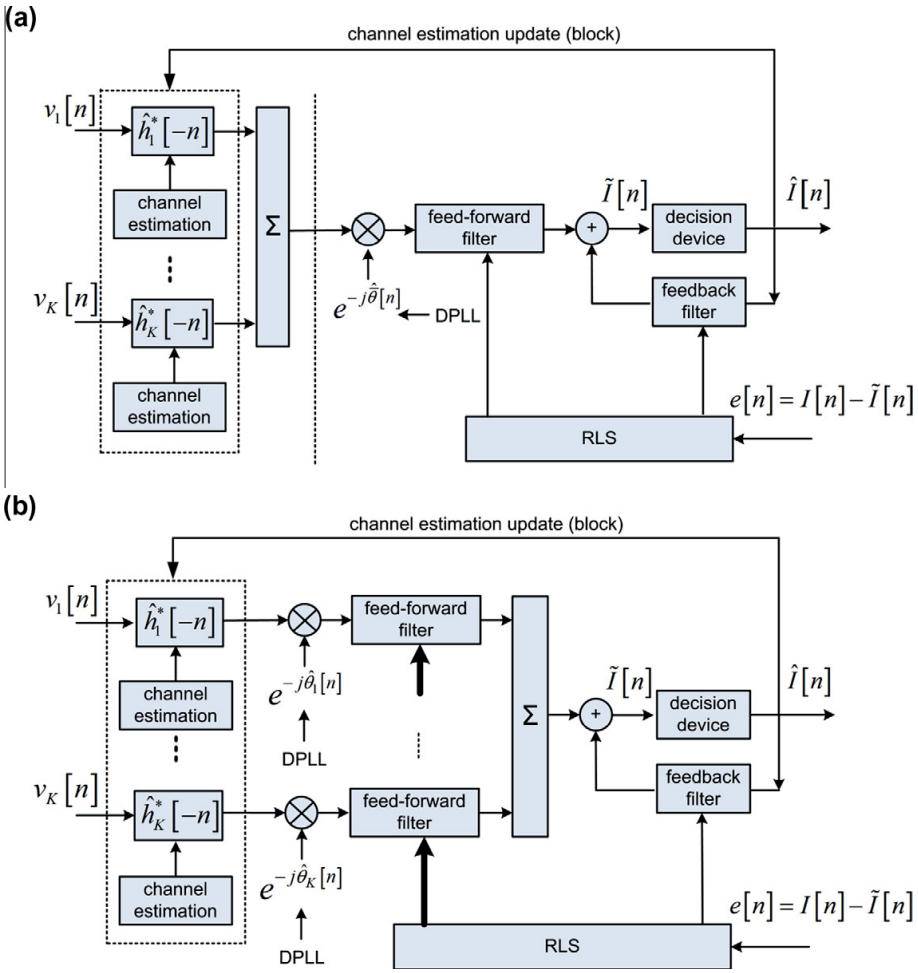

Fig. 1. Block diagram of the receiver structures. (a) PPC–DFE. (b) PPC–McDFE.

near-shore deployed in a water depth less than 10 m. The array consists of a vertical receiving array of 8 hydrophones (hydrophone No. 1–8) with 1 m element spacing and a horizontal receiving array of 4 hydrophones (hydrophone No. 9–12) with 1.5 m element spacing. Hydrophone No. 1 was located 0.5 m below the sea surface, and the depth of hydrophones No. 9–12 was 4.5 m. The transmitter used a hemispherical acoustic transducer suspended at a depth of 40 m from the NTNU research vessel R/V Gunnerus, and the dynamic positioning system was activated to reduce drifting during the trail.

In the experiment, the signals were repeatedly transmitted every 202.044 s for 15 periods, and the source level was about 187 dB re 1 μPa at 1 m. The carrier frequency of the transmitted signal was 12 kHz. The time durations of binary phase shift keying (BPSK) and quadrature phase shift keying (QPSK) modulated signals were the same as 15.565 s. In each period of 202.044 s, the QPSK signal were transmitted 20.265 s after the BPSK signal. A square root-raised cosine filter was used for pulse shaping, where the roll-off coefficient was 1. The symbol rate was 1 kilo-symbols/s, and therefore the signal's bandwidth was 2 kHz. The received waveforms were recorded to assess the receiver structures by off-line processing in the laboratory.

3.2. The channel measurements

Fig. 2 plots one example of the channel impulse response estimated by the least squares (LSs) method. It is indicated that the underwater channel is sparse of high time resolutions. The time interval between two parts of dominant arrivals is about 25 ms. Within each period of 15.565 s, it is seen that the dominant arrivals of large magnitude are slow time variant. In the time scale in terms of period, the channel changes with period. e.g., There is one group of concentrated arrivals in Fig. 2c, while there are two groups of concentrated arrivals in Fig. 2a and b. The channel impulse response within a time interval is estimated by LS method, and non-zero taps are obtained even though there are no real arrivals. Based on the channel sparseness in which only dominant arrivals represent the channel information, the MP algorithm [7] estimates the dominant arrivals within a time interval iteratively until a specified number of taps are selected.

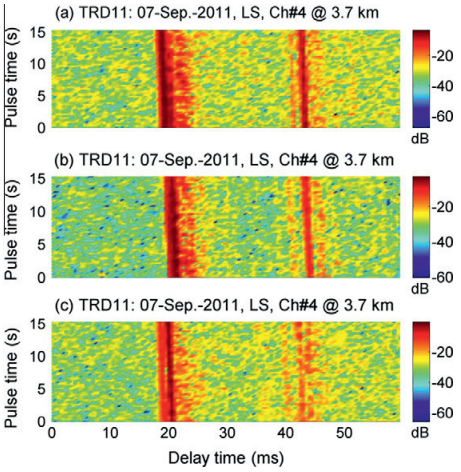

Fig. 2. The channel response at a depth of 3.5 m versus period: (a) the 1st period, (b) the 8th period and (c) the 15th period.

Table 1
Parameters used in the data processing of the two receiver structures.

Parameters	Description	Value
F_s	Sampling frequency at the receiver	96 kHz
f_c	Carrier frequency	12 kHz
R	Symbol rate	1 kilosymbol/s
M	Number of taps in the MP processing	4
N	Over sampling factor	2
T_{block}	Time duration of each block	1 s
N_{ff}	Number of feed-forward filter taps	8
N_{fb}	Number of feedback filter taps	2
Nt	Number of training symbols for DFE	72
λ	RLS forgetting factor	0.999
K	Number of receiving channels	12
K_1	Proportional tracking constant in PLL	0.01
K_2	Integral tracking constant in PLL	0.001

4. Performance comparison

In the 50 min trial, the collected data of 15 periods was processed by the two receiver structures shown in Fig. 1. The receiver parameters are given in Table 1. The time duration of each block is 1 s. Since PPC processing requires knowledge of the channel, the time duration in the channel estimation becomes important.

Firstly, the time interval is chosen from 25 ms to 45 ms, and the performance of PPC–DFE for BPSK is shown in Fig. 3. The performance of the channel estimation using the LS method decreases as the time interval increases. When it comes to the MP algorithm, the performance is the same regardless of the lengths of time intervals. The dominant arrivals shown in Fig. 2 span about 25 ms. With an impropriate time interval, the LS method introduces extra noise which degrades the performance, while the MP algorithm does not have this drawback because it only estimates the dominant arrivals. The performance of PPC–DFE is improved by using the MP algorithm. e.g., the output SNR for the 2nd period is increased by 1.7 dB compared with that using the LS method, where the time interval is 25 ms. In the following analysis, the time interval for channel estimations is 25 ms for both the LS and the MP methods.

Fig. 4 shows the performance comparison for BPSK and QPSK communications. Time variant channel results in variant output SNR. PPC–McDFE achieves superior performance regardless of the

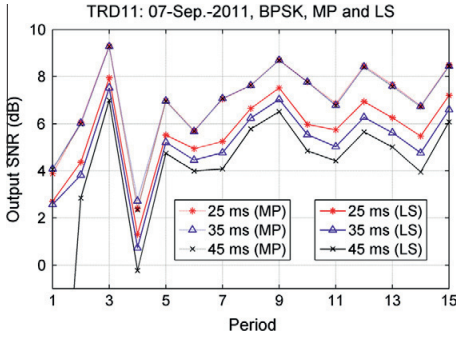

Fig. 3. Performance of PPC–DFE in terms of output SNR versus different time intervals.

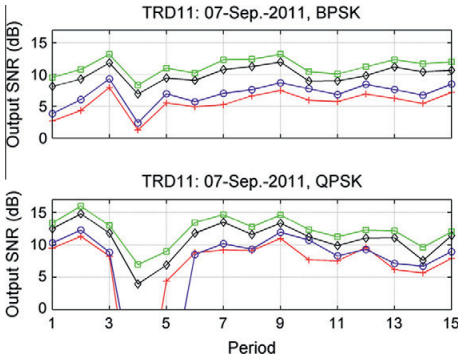

Fig. 4. Performance comparison in terms of output SNR. The up panel shows the performance for BPSK, and the bottom panel shows the performance for QPSK. PPC–DFE using LS (+), PPC–DFE using MP (○), PPC–McDFE using LS (◇), and PPC–McDFE using MP (□).

channel estimation method and the modulation scheme. For instance, in the 4th period of BPSK, the output SNR obtained by PPC–McDFE is 5.9 dB more than that of PPC–DFE, when the MP algorithm is used. The superior performance is attributed to the spatial diversity exploitation as discussed by Zhang et al. [8]. Using the MP algorithm, the performance is improved for both PPC–DFE and PPC–McDFE. In some periods shown of QPSK, the performance of PPC–McDFE is improved by more than 1 dB by using the MP algorithm instead of the LS method. The improvement from the MP processing is attributed to noise reduction, since only dominant arrivals are used in the pulse compression. Therefore the MP algorithm improves the performance of communications using PPC processing.

We have presented the assessment of communications using PPC processing. For both LS and MP channel estimation methods, PPC–McDFE has demonstrated its superior performance shown in Fig. 4. Processing gains are obtained by exploiting spatial diversity. Since interchannel correlations are intractable to be precisely predicted in a time variant oceanic environment, it is advantageous to make full use of spatial diversity, especially with a small number of receivers.

Acknowledgments

The author would like to thank NTNU Ph.D. candidate Bo Peng and Professor Jens M. Hovem and for discussions. The authors also

thank to all the participants and crew of R/V Gunnerus at NTNU for their help during the sea trial on 7th September 2011.

References

[1] Dowling DR. Acoustic pulse compression using passive phase-conjugate processing. J Acoust Soc Am 1994;95(3):1450–8.
[2] Hursky P, Porter MB, Siderius M, McDonald VK. Point-to-point underwater acoustic communications using spread-spectrum passive phase conjugation. J Acoust Soc Am 2006;120(1):247–57.
[3] Rouseff D, Jackson DR, Fox WLJ, Jones CD, Ritcey JA, Dowling DR. Underwater acoustic communication by passive-phase conjugation: theory and experimental results. IEEE J Ocean Eng 2001;26(4):821–31.
[4] Song HC, Hodgkiss WS, Kuperman WA, Stevenson M, Akal T. Improvement of time-reversal communications using adaptive channel equalizers. IEEE J Ocean Eng 2006;31(2):487–96.
[5] Song A, Badiey M, Song HC, Hodgkiss WS. Impact of ocean variability on coherent underwater acoustic communications during the Kauai experiment (KauaiEx). J Acoust Soc Am 2008;123(2):856–65.
[6] Song HC. Time reversal communication in a time-varying sparse channel. J Acoust Soc Am 2011;130(4):EL161–166.
[7] Cotter SF, Rao BD. Sparse channel estimation via matching pursuit with application to equalization. IEEE Trans Commun 2002;50(3):374–7.
[8] Zhang G, Dong H. Spatial diversity in multichannel processing for underwater acoustic communications. Ocean Eng 2011;38(14–15):1611–23.
[9] Stojanovic M, Catipovic J, Proakis JG. Adaptive multichannel combining and equalization for underwater acoustic communications. J Acoust Soc Am 1993;94(3):1621–31.

Paper 6: Experimental Assessment of Different Receiver Structures for Underwater Acoustic Communications over Multipath Channels

Guosong Zhang, Jens M. Hovem and Hefeng Dong

In Sensors, vol. 12, pp. 2118-2135, 2012

The thesis author had the original idea for this paper. The co-authors participated in scientific discussions.

Sensors **2012**, *12*, 2118-2135; doi:10.3390/s120202118

OPEN ACCESS

sensors

ISSN 1424-8220

www.mdpi.com/journal/sensors

Article

Experimental Assessment of Different Receiver Structures for Underwater Acoustic Communications over Multipath Channels

Guosong Zhang *, Jens M. Hovem and Hefeng Dong

Department of Electronics and Telecommunications, Norwegian University of Science and Technology (NTNU), Trondheim NO-7491, Norway; E-Mails: Jens.Hovem@iet.ntnu.no (J.M.H.); Hefeng.Dong@iet.ntnu.no (H.D.)

* Author to whom correspondence should be addressed; E-Mail: Guosong.Zhang@iet.ntnu.no; Tel.: +47-4622-0956; Fax: +47-7359-1412.

Received: 20 December 2011; in revised form: 1 February 2012 / Accepted: 3 February 2012 / Published: 14 February 2012

Abstract: Underwater communication channels are often complicated, and in particular multipath propagation may cause intersymbol interference (ISI). This paper addresses how to remove ISI, and evaluates the performance of three different receiver structures and their implementations. Using real data collected in a high-frequency (10–14 kHz) field experiment, the receiver structures are evaluated by off-line data processing. The three structures are multichannel decision feedback equalizer (DFE), passive time reversal receiver (passive-phase conjugation (PPC) with a single channel DFE), and the joint PPC with multichannel DFE. In sparse channels, dominant arrivals represent the channel information, and the matching pursuit (MP) algorithm which exploits the channel sparseness has been investigated for PPC processing. In the assessment, it is found that: (1) it is advantageous to obtain spatial gain using the adaptive multichannel combining scheme; and (2) the MP algorithm improves the performance of communications using PPC processing.

Keywords: underwater acoustic communication; time reversal; passive-phase conjugation; matching pursuit; decision feedback equalizer

1. Introduction

Coherent underwater acoustic communications are challenged by acoustic channels, which are often characterized as time-varying, dispersive, sparse, *etc*. [1]. Therefore, much of the recent research has

been focused on the development of channel equalizers to remove intersymbol interference (ISI) in multipath environments, especially for high-rate coherent communications.

One receiver cannot avoid deep fading in time-varying channels, and thus the equalizers fail to remove ISI. With multiple sensors exploiting spatial diversity, Stojanovic *et al.* [2] has proposed a multichannel decision feedback equalizer (McDFE). The disadvantage of McDFE is its complexity due to the computational load, which increases with the time spread of underwater channels. Therefore, it is difficult to apply McDFE in underwater channels of long time spread, especially using a large number of receiving hydrophones.

Another novel method is the time reversal mirror (TRM), originally proposed by Fink [3], which was later applied for underwater communications. The focusing of TRM results in a significant reduction of ISI for underwater communications, which has been demonstrated by Edelman *et al.* [4,5]. Two vertical hydrophone arrays and two-way transmission are required by TRM to achieve the focusing at the transmitter. During the transmission, the underwater channel is required to be constant.

An alternative technique for underwater communications is proposed by Rouseff *et al.* [6] to take advantage of the focusing at the receiver, commonly referred as passive time reversal or passive-phase conjugation (PPC). This method requires only one receiving array and one-way transmission. ISI cannot be eliminated by the focusing, and thus a subsequent channel equalizer is used to remove residual ISI [6–9], where a single channel decision feedback equalizer (DFE) is used. It is referred to as PPC-DFE in this paper. Spatial diversity is used by the focusing to suppress ISI. In a real oceanic environment, it is difficult to predict time variant spatial coherence [10], when interchannel correlations impact spatial focusing.

Stojanovic [11] has discussed the upper bound performance of time reversal communications, but it is very difficult to predict real performance of time reversal communications, as spatial coherence is neglected in the model. By numerical simulations and experimental demonstrations, Yang [12] has demonstrated that McDFE achieves superior performance over that of PPC-DFE. This leads to a receiver structure which uses adaptive multichannel combining after PPC processing in each individual channel.

Zhang *et al.* [13] have presented a receiver structure—joint PPC and McDFE (PPC-McDFE). This receiver structure involves temporal focusing (pulse compression by PPC processing) for time delayed arrivals [14], and thus the computational load of a subsequent McDFE is much reduced. It is well known that temporal focusing degrades with time evolution in time-varying channels. To counter for this degradation, the block-based approach proposed by Song [15] can be used to extend PPC-McDFE in time-varying channels.

PPC processing requires information of the channel characteristics, which can be estimated using training symbols. Underwater channels are often sparse, especially at the high-frequency regime, where there are a few dominant arrivals. The dominant arrivals can be estimated using the matching pursuit (MP) algorithm [16]. Song [17] has shown that the MP algorithm exploits the channel sparseness to improve the performance of PPC-DFE. It is an open question whether the MP algorithm can improve the performance of PPC-McDFE, in comparison with the conventional channel estimation method—the least squares (LS) method.

The above brief introduction shows that different approaches have been proposed and have been tested in field experiments. However, the experiments were conducted under different conditions, and it is therefore difficult to compare the performance of different receiver structures. This has motivated

the work of this paper. A recent field experiment was conducted to collect data over a range of 7.4 km, when three modulation schemes were used. Four data rates with a maximal data rate of 4 kilo-bits/s have been achieved. Using the same real data, we compare the performance of three receiver structures: McDFE, PPC-DFE, and PPC-McDFE. These structures are frequently discussed in the literature, and in the future we may extend the discussion to other structures and modulation schemes.

As required, information of the channel characteristics for PPC processing can be obtained by a channel probe signal or estimated using training symbols. For example, using a linear frequency modulation pulse (LFM) chirp as a channel probe signal, when the chirp is also used as a shaping pulse at the transmitter, the received LFM is immediately used for PPC processing. Alternatively, the channel is estimated using training symbols, when a root-raised-cosine pulse (RRC) is used as a shaping pulse. In this paper, we have also tested the scenario using the two shaping pulses.

The contributions of this paper include: (1) experimental assessment of the difference between two shaping pulses—LFM and RRC; (2) performance comparison of the McDFE, PPC-DFE, and PPC-McDFE structures; (3) evaluation of the block-based approach for PPC-McDFE; and (4) assessment of the MP algorithm for both PPC-DFE and PPC-McDFE, in which PPC processing is implemented in two modes—one block and multi-block.

This paper is organized as follows: Section 2 introduces the field experiment conducted in Trondheim harbor on 7 September 2011. Section 3 shows the receiver structures: (1) McDFE; (2) PPC-DFE; and (3) PPC-McDFE. Section 4 briefly introduces channel estimations for PPC processing, the LS method and the MP algorithm. In Section 5, the results are presented and discussed, and performance of the three structures is shown. Finally, Section 6 summarizes the work.

2. The Experiment

2.1. The Setup

The communication experiment was conducted on 7 September 2011, in Trondheim harbor (Norway), where the water depth varies from 10 m to 400 m. The transmitter was carried by the NTNU research vessel R/V Gunnerus, and it used a hemispherical acoustic transducer deployed at a depth of 20 m. The dynamic positioning system of R/V Gunnerus was activated during the trial to reduce drifting.

A cross receiving array of 12 hydrophones was deployed from a pier, where the water depth was about 10 m. The array consisted of a vertical array of eight hydrophones (hydrophones No. 1–8) with 1 m element spacing and a horizontal array with four hydrophones (hydrophones No. 9–12) with 1.5 m element spacing. Hydrophone No. 1 was located 0.5 m below the sea surface, and the depth of the horizontal array was 4.5 m. The range between the source and the receiving array was 7.4 km.

Digital modulations of phase shift keying (BPSK), quadrature phase shift keying (QPSK), and eight quadrature amplitude modulation (8QAM) were used. The carrier frequency of the transmitted signal was 12 kHz. A 0.1 s LFM chirp with a Hanning window was used for coarse time synchronization in each data packet, and its effective bandwidth was 2.2 kHz. When the LFM was used as the channel probe signal, it was also used as a shaping pulse. As a shaping pulse, the roll-off coefficient of RCC was 1.

Figure 1 shows the signals which were repeatedly transmitted every 202.044 s for 15 periods. The signals of the same modulations, but using different shaping pulses were transmitted continuously with a time gap of 2.2 s. The symbol rates were 1 kilo-symbols/s and 2 kilo-symbols/s, and the respective bandwidths were 2 and 4 kHz when the RRC was used. The received waveforms were recorded at a sampling frequency of 96 kHz for offline processing in the laboratory.

Figure 1. Block diagrams of the transmitted signals using different shaping pulses shown in the parentheses. [a] The symbol rate was 1 kilo-symbol/s; [b] The symbols rate was 2 kilo-symbol/s.

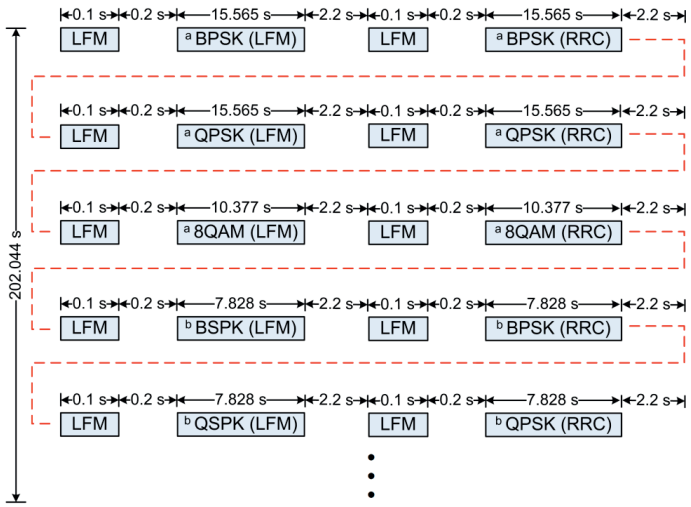

Figure 2. Measured SSP (the left panel) and the ray traces (the right panel) from a source on the left. The source was at a depth of 20 m.

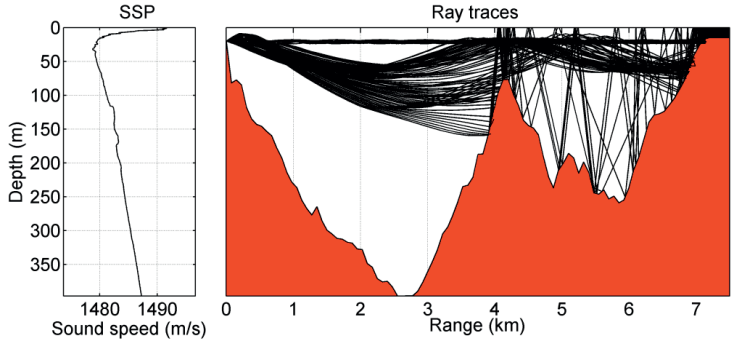

2.2. Channel Characterization and Measurements

Sound speed profile (SSP) measured by the R/V Gunnerus is shown by the left panel of Figure 2. The sound speed profile has a surface channel and a negative gradient down to about 50 m. At deeper depths, the sound speed increases nearly linearly. With the conditions of the SPP and the bathymetry, the PlaneRay ray-tracing program [18] is used to illustrate the acoustic propagation during the trial.

The right panel of Figure 2 shows that ray traces and the bathymetry from a source at 20 m depth to the receiving array located at a distance of 7.4 km. The sound propagation dominated by the sound channel at about 25 m and the positive gradient below 50 m. It is shown that there are several almost horizontal paths in the sound channel as well as several deep refracted paths, and all other possible ray paths are blocked by the seamount at 4 km.

Figure 3 shows the simulated responses to the vertical array with five hydrophones spanning the depth of 0.5 m to 4.5 m. The results are plotted as a function of reduced time, which is the actual travel time with the nominal gross travel time of 4.9333 seconds subtracted. The transmitted pulse used in the simulations was a short transient with 2 ms duration. There is a group of arrivals followed by a second group arriving about 40 ms later. This structure can be understood from the ray tracing with the first group is due to the sound channel paths and the second is the deep refracted paths. Each of the groups has several multipath contributions probably caused by a multitude of surface and bottom reflections occurring in shallow area near the receiving array.

Figure 3. Modeled channel impulse response calculated by the PlaneRay program to the vertical array with five hydrophones spanning the depth of 0.5 m to 4.5 m.

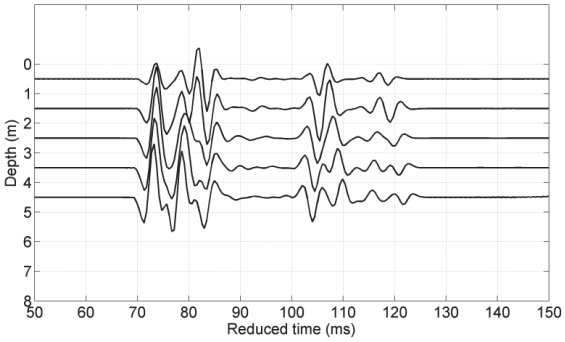

Figure 4. Channel response at different depths. (**a**) 1 m; (**b**) 3.5 m; (**c**) 4.5 m.

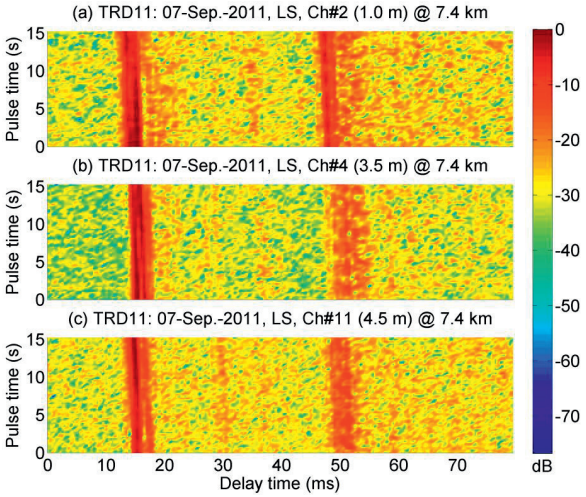

Figure 4 shows examples of channel response estimated using the LS method. Within the observations of 15 s, the responses varied with time. In each receiving channel, there are two groups of concentrated arrivals with a time span of 35 ms, and they correlate with the simulated results in Figure 3. It is evident that the channel is sparse. It is apparent that they are similar over the three water depths. In particular, the signals received in Ch #2 and Ch #4 are highly correlated, the correlation coefficient between these two channels is calculated to be 0.68.

3. The Receiver Structures

Generally, the receiver recovers distorted information by baseband signal processing, where multipath channels are often modeled as finite filters of multiple taps. In digitized form, the received signal at *k*th hydrophone can be written as:

$$V_k^n = \sum_{l=0}^{L-1} H_k^l I_{n-l} + W_k^n,\ k = 1,\ldots,K \tag{1}$$

where H_k^l denotes the *l*th tap of channel impulse response (CIR) H_k which spans L symbol interval, I_n is the *n*th symbol of a sequence $\{I_n\}$, and W_k^n represents a bandwidth limited noise. In a multipath channel, where $L \neq 1$, ISI caused by H_k results in errors. The objective of a channel equalizer is to remove the ISI.

Figure 5. Block diagram of McDFE using the RLS algorithm. There are *K* receiving channels. $\hat{\theta}_k^n$ denotes the estimate of phase offset θ_k^n at the *k*th receiving channel, $\hat{I}_n$ presents the soft estimate of I_n, and $\tilde{I}_n$ is the decided symbol which best matches $\hat{I}_n$.

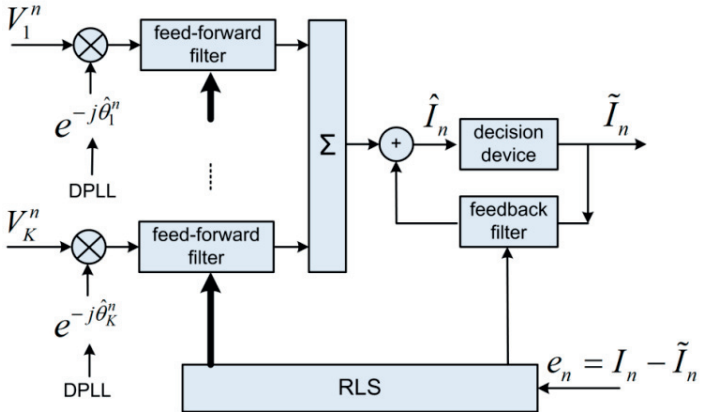

Figure 5 shows the block diagram of McDFE [2]. The tap coefficients of the *K*-channel feed-forward filters plus one channel feedback filter are jointly updated by the recursive least squares (RLS) algorithm for its fast rate of convergence [19]. The technique of a second order digital phase-locked loop (DPLL) is implemented for the carrier-phase tracking. The DPLLs $\left\{e^{-j\hat{\theta}_k^n}\right\}$ operate on a symbol-by-symbol basis to remove phase changes caused by the carrier frequency shift. In order to deconvolve H_k, the number of taps for the McDFE is determined by the time spread L, and it is usually chosen in an *ad hoc* manner. The computational load increases with L, and it may become

prohibitive, when a large number of hydrophones are used. Moreover, under the same channel conditions, the number of taps increases with the symbol rate.

Figure 6 shows the receiver structure of passive time reversal—PPC-DFE. Following the focusing, only one channel DFE is required to remove residual ISI [8], when one DPLL is implemented for carrier-phase tracking. The focusing mitigates ISI, the number of taps for the one channel DFE is much reduced, and thus the complexity of PPC-DFE is much lower than that of McDFE. Note that the focusing degrades with time in time-varying channels.

Figure 6. Block diagram of passive time reversal receiver structure PPC-DFE. $\left(\hat{H}_k^{-n}\right)^*$ denotes complex conjugation of the time reversed channel estimate $\hat{H}_k^n$. $\hat{\bar{\theta}}_k^n$ denotes the estimate of the phase offset $\bar{\theta}_k^n$ after focusing.

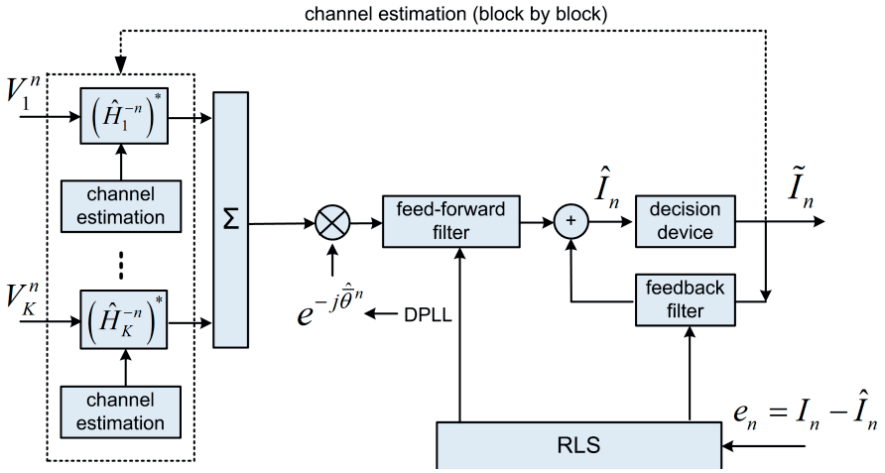

As suggested by Song [15], a block-based approach extends PPC-DFE to be implemented in time-varying channels. The idea is that channel estimations $\left\{\hat{H}_k^n\right\}$ are updated on a block-by-block basis, when the channel is assumed time-invariant within each block of a short time interval. The channel estimations $\left\{\hat{H}_k^n\right\}$ are subsequently updated using detected symbols in the previous block. This block-based approach does not change the basic principle of TR focusing, which obtains spatial diversity by to mitigate ISI. Zhang *et al*. [13] has discussed the impact of the time variant interchannel correlations on the performance of PPC-DFE.

The receiver structure PPC-McDFE is shown of Figure 7. Here, pulse compression is achieved by PPC processing in each individual channel, and then a subsequent McDFE is implemented to remove residual ISI by adaptive multichannel combining. The RLS algorithm updates the tap coefficients to minimize output mean square error (MSE). Pulse compression is achieved in the same way for single receiver [20,21]. Thus it is used by PPC-McDFE to reduce the complexity of the subsequent McDFE which obtains spatial gain. As discussed by Yang [7], the peak-to-sidelobe ratio of pulse compression is determined by the channel response, while the pulse compression acts as a rake receiver recombining time delayed arrivals. In time-varying channels, PPC-McDFE can be extended using the block-based approach [15].

Figure 7. Block diagram of PPC-McDFE.

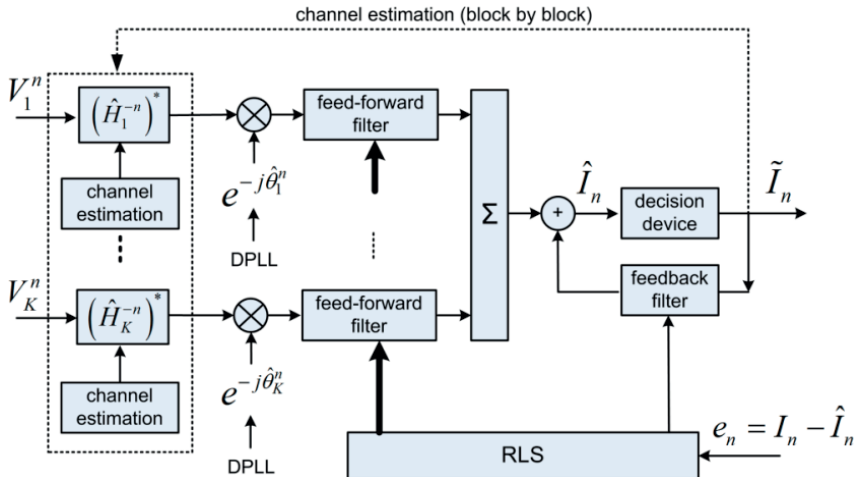

4. Channel Estimations

This section briefly introduces two channel estimation methods. Using training symbols, the channel estimations for PPC processing can be obtained using both the LS method [22] and the MP algorithm [16].

By combining M observed symbols, Equation (1) is rewritten as:

$$\begin{bmatrix} V_k^{n-M+1} \\ V_k^{n-M} \\ \vdots \\ V_k^{n} \end{bmatrix} = \begin{bmatrix} I_{n-M+1} & \cdots & I_{n-L+2} \\ \vdots & & \vdots \\ I_n & \cdots & I_{n-L+1} \end{bmatrix} \begin{bmatrix} H_k^0 \\ H_k^1 \\ \vdots \\ H_k^{L-1} \end{bmatrix} + \begin{bmatrix} W_k^{n-M+1} \\ W_k^{n-M} \\ \vdots \\ W_k^{n} \end{bmatrix} \tag{2}$$

which is simplified to:

$$V_k = IH_k + W_k \tag{3}$$

In the channel estimation problem, the information matrix I is known as training symbols. An estimation of $\hat{H}_k$ can be obtained by solving LS problem:

$$\hat{H}_k = \arg\min_{\tilde{H}_k} \left\{ \left\| V_k - I\tilde{H}_k \right\|^2 \right\} \tag{4}$$

which gives the solution:

$$\hat{H}_k = \left[I^H I \right]^{-1} I^H V_k \tag{5}$$

In practice, the LS method is sensitive to noise. When a channel is sparse, the CIR consists of a large number of zeros among several dominant taps, and the LS method will suffer from the noise between dominant taps. Besides, the LS method involves matrix inversion, and it sometimes suffers ill-conditioned problem of a matrix of large eigenvalue spread.

To exploit the sparse property of channels, the channel estimation problem can be reconsidered as an approximation problem. It is assumed that the received signal vector is approximated by:

$$\left(\hat{V}_k\right)_M = \sum_{i=0}^{M-1} \hat{H}_k^{p_i} \left(I\right)_{p_i} \tag{6}$$

where $\left(I\right)_{p_i}$ is the p_i th column of information matrix I . Finding the approximation of $\left(\hat{V}_k\right)_M$ that minimizes $\left\|\left(\hat{V}_k\right)_M - V_k\right\|$ is an non-deterministic polynomial-time hard problem [23,24], which means there is unknown polynomial time algorithm that can solve this problem. MP [16] is a greedy algorithm that achieves non-optimal yet computational efficient approximation of V_k.

The MP algorithm selects one column in matrix I which is best aligned with residual signal r_{p-1}, where $r_0 = V_k$ at initial step. In practice at the pth step, the selected l_p th column of I is determined by:

$$l_p = \arg\max_l \left\{\left\|\left(I\right)_l^H r_{p-1}\right\| / \left\|\left(I\right)_l\right\|\right\} \tag{7}$$

Correspondingly, the tap value $\hat{H}_k^{l_p}$ is estimated by:

$$\hat{H}_k^{l_p} = \frac{\left(I\right)_{l_p}^H r_{p-1}}{\left\|\left(I\right)_{l_p}\right\|^2} \tag{8}$$

and r_p is updated by:

$$r_p = r_{p-1} - \frac{\left(I\right)_{l_p}^H r_{p-1}}{\left\|\left(I\right)_{l_p}\right\|^2} \left(I\right)_{l_p} \tag{9}$$

This iteration is terminated until the preset P taps have been estimated. In practice, one column in I is probably selected more than once. To deal with this problem, we can either exclude previously selected columns in the search press shown in Equation (7), or the tap value calculated in Equation (8) can be added to the value found in previous steps [25]. In this paper, we use the former method.

5. Results and Analysis

Recorded signals of 15 periods are processed with parameters given in Table 1, in which some are chosen in an *ad hoc* manner. For instance, the number of taps N^1_{ff}, and N^1_{fb}. As suggested by Stojanovic [26], the integral tracking constant K_2 is chosen as 10 time smaller than the proportional tracking constant K_1. In subsections of 5.2 and 5.3, the performance of McDFE is selected as a benchmark.

Table 1. Parameters used in the signal processing of the three receiver structures.

Parameters	Description	Value
F_s	Sampling frequency at the receiver	96 kHz
f_c	Carrier frequency	12 kHz
R	Symbol rate	1, 2 kilo-symbol/s
P	Number of taps in the MP processing	4
N	Over sampling factor	2
N^1_{ff}	Number of the feed-forward filter taps (McDFE)	20
N^1_{fb}	Number of the feedback filter taps (McDFE)	5
N^2_{ff}	Number of the feed-forward filter taps (PPC-DFE)	8
N^2_{fb}	Number of the feedback filter taps (PPC-DFE)	2
N^3_{ff}	Number of the feed-forward filter taps (PPC-McDFE)	8
N^3_{fb}	Number of the feedback filter taps (PPC-McDFE)	2
T_{block}	Time duration of each block	1 s
λ	RLS forgetting factor	0.999
K	Number of receiving channels	12
K_1	Proportional tracking constant in DPLL	0.01
K_2	Integral tracking constant in DPLL	0.001

5.1. Performance Using Different Shaping Pulses

As mentioned in Section 2.1, both LFM and RRC were used as shaping pulses. In the scenario of using LFM as a shaping pulse, the peak-to-average power ratio (PAPR) is large [9], and it could result in lower power efficiency for a linear amplifier. With a constant transmission power, the source level is reduced. However, the advantage is that the received channel probe signal is immediately used for PPC processing. Using RRC as a shaping pulse, PAPR is reduced, and then the channel response is estimated using different methods.

In terms of output signal-to-noise ratio (SNR), Figure 8 shows the performance of PPC-DFE using different shaping pulses, where the symbol rate is 1 kilo-symbol/s. Due to low input SNRs in the 10th period of Figure 8(a) and the 9th–11th periods of Figure 8(b), the receiver structures fail to recover distorted information. For RRC shaping pulse, the LS method is used to estimate the CIR within 40 ms. The observed time variant performance of PPC-DFE may be caused by the channel variations which resulted in sometimes a low input SNR, as for example at the 10th period. Generally the performance difference between LFM and RRC is small for BPSK, as shown in Figure 8(a). In Figure 8(b), there are small differences over the 9 periods, and large differences in other periods, in particular for 7th and 13th periods. Channel estimations obtained by the LS method are impacted by the noise in the scenarios of low input SNRs, and thus using a LFM as a shaping pulse has shown its advantage. There is also a spreading gain by using the LFM as the shaping pulse, since the bandwidth of the LFM of 2.2 kHz is larger than the signals bandwidth of 1 kHz.

Figure 8. Performance of PPC-DFE using different shaping pulses. (**a**) BPSK; (**b**) QPSK. LFM is used (□), and RRC is used (○).

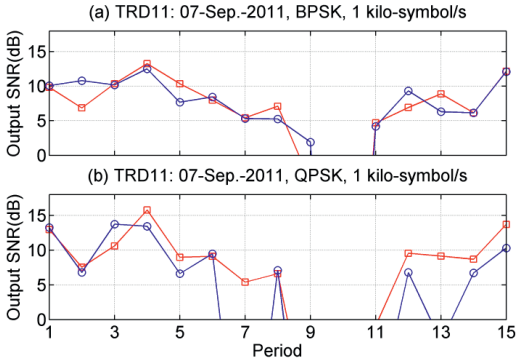

5.2. The One-Block Approach

In this subsection, the channel is estimated only once for PPC processing in each data packet. The channel is estimated using training symbols, which are specified symbols in the beginning of communications. Following PPC processing, ISI is removed by the adaptive channel equalizers.

Figure 9 shows scatter plots of soft output estimates $\{\hat{I}_n\}$ of different receiver structures, where the LS method is used to estimate the channel for PPC processing. The output SNR given by (1-MSE)/MSE, and the bit error rate (BERs) are given in the legends. Obviously, McDFE achieves the best performance with an output SNR of 9.2 dB, PPC-McDFE approximates the performance of McDFE with an output SNR of 8.5 dB, and PPC-DFE achieves the worst performance with an output SNR of 3.8 dB and a BER of 2.0e–3. As shown in Section 3, the difference between PPC-McDFE and PPC-DFE is the multichannel combining scheme.

Figure 9. Scatter plot of estimated 8-QAM symbols using different receiver structures. (**a**) McDFE; (**b**) PPC-McDFE; (**c**) PPC-DFE.

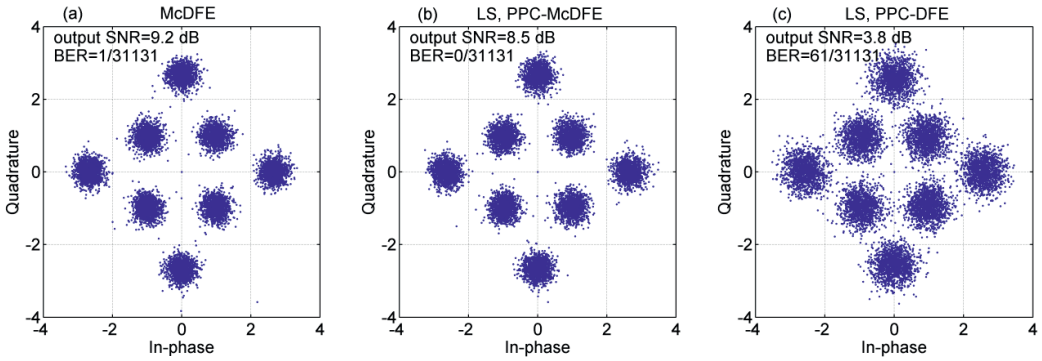

The results of 15 periods are shown in Figure 10, where the symbol rate is 2 kilo-symbol/s. PPC-DFE achieves the worst performance for both BPSK and QPSK, and obviously it fails in several periods for QPSK. It is apparent that the performance of PPC-McDFE consistently follows that of

McDFE. For BPSK shown in Figure 10(a), PPC-McDFE overtakes PPC-DFE with a maximum 6.6 dB output SNR (the 3rd period) and a minimum 2.7 dB output SNR (the 11th period).

Figure 10. Performance in terms of output SNR for different modulations. (**a**) BPSK; (**b**) QPSK. McDFE (□), PPC-McDFE (○), and PPC-DFE (◊).

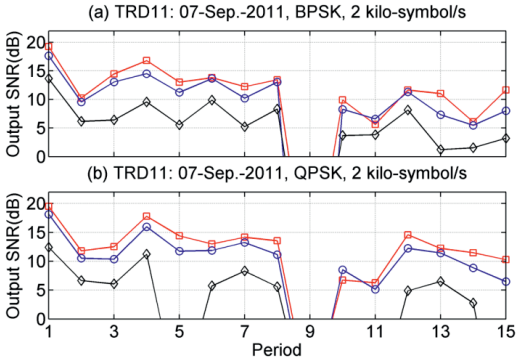

Figure 11 shows the spatial coherence measured in the 3rd and 11th periods, respectively. The spatial coherence between the *k*th and *m*th channel is calculated by:

$$\psi(k,m)=\frac{\left|r_k(-t)\otimes r_m(t)\right|_{\max}}{\sqrt{\left|r_k(-t)\otimes r_k(t)\right|_{\max}\left|r_m(-t)\otimes r_m(t)\right|_{\max}}} \tag{10}$$

where $\left|r_k(-t)\otimes r_m(t)\right|_{\max}$ denotes the maximum absolute value of the correlation between $r_k(t)$ and $r_m(t)$, and $r_k(t)$ is the received signal of the *k*th hydrophone. Interchannel correlations shown in Figure 11(a) are stronger than those shown in Figure 11(b), where the time elapse between these two periods is 1,760 s. For instance, the correlation coefficient between Ch #3 and Ch #4 is 0.84 in Figure 11(a), and it is 0.23 in Figure 11(b). Furthermore, in Figure 11(a), it is interesting that there are stronger correlations among the signals received by the vertical array (Ch #1–8) than those among the signals received by the horizontal array (Ch #9–12).

Figure 11. Spatial coherence in different periods. (**a**) The 3rd period; (**b**) The 11th period.

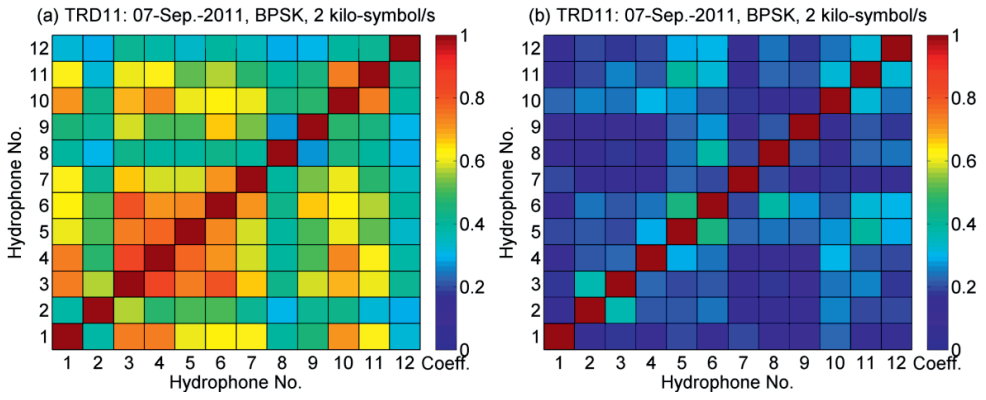

The strength of interchannel correlations correlates with the performance difference between PPC-McDFE and PPC-DFE, which is shown in Figure 10(a). Since it is difficult to predict the time variant spatial coherence in a real oceanic environment [10], it is advantageous to obtain spatial gain using the adaptive multichannel combining, especially in the scenario of a small number of receivers. Thus it is preferable to use McDFE in a channel of short time spread, while PPC-McDFE is suggested in a channel of long time spread.

As shown in Figure 4, the channel impulse response is sparse. This property can be exploited by the MP algorithm. The conventional LS method obtains values for the taps that should be zero in sparse channels, and the MP algorithm only estimates dominant arrivals. For both methods, it is required that the time window is long enough to include all time-spanned arrivals that cause ISI. For the LS method, the time window should not be too long, since a long window may introduce unnecessary noise in the estimate.

Figure 12 shows the CIR obtained by both LS and MP methods. The number of taps for the MP algorithm was preset to $P = 4$ and finds two main peaks at 12–15 ms, and another main peak at 48 ms. This observation supports the earlier findings there are two main groups of arrivals separated by approximately 35–40 ms. The MP algorithm estimates the same dominant arrivals, but the LS algorithm introduces noise-like values for the taps that should be zeros.

Figure 12. CIR estimated by the LS method and the MP algorithm.

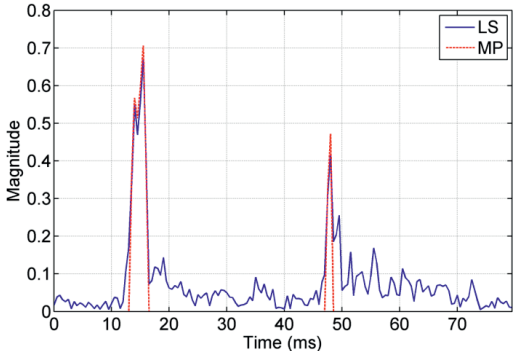

Using both the MP and LS algorithms, performances of PPC-McDFE and PPC-DFE are compared. Figure 13 show the performance comparison at a symbol rate of 2 kilo-symbol/s. The performance of the three structures changes with time, as measured in period. Using the MP algorithm, the performance of both PPC-McDFE and PPC-DFE is improved in most periods. Even though the performance of PPC-DFE is improved by the MP algorithm, e.g., 2.1 dB in maximum (the 15th period), it is still far less than the performance of PPC-McDFE, which overtakes that of PPC-DFE from 3.1 dB (the 11th period) to 7.0 dB (the 3rd period). In average, McDFE leads the performance. In this performance evaluation, it is important to consider the computational time. Based on the same personal computer, McDFE consumed about 20 times computational time than PPC-McDFE (MP) to achieve the approximate performance.

Figure 13. Performance in terms of output SNR at a symbol rate of 2 kilo-symbol/s.

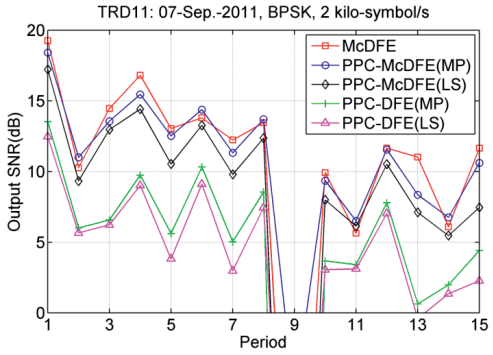

5.3. The Multi-Block Approach

It is well known that pulse compression degrades with time evolution, as the channel is time variant in practice. In the Section 5.2, the degradation is neglected, where the subsequent adaptive channel equalizers manage to track the channel variations. In the current subsection, the multi-block approach is used to counter for the variations within each data packet. It is understood that the channel can be assumed constant within a short time interval, correspondingly a data block.

Figure 14 shows an example of performance comparison between one-block and multi-block approaches. For the multi-block approach, the received data packet of 8.128 s was split into eight blocks of 1 s each and one block of 0.128 s. The right panel of Figure 14(a) shows that the single channel DFE encounters difficulties in tracking the channel variations, as the output MSE increases with time. As shown in the left panels of Figure 14, BER is reduced from 4.9% to 2.2%, when the multi-block approach is implemented. As follows for the multi-block approach, each block has time duration of 1 s.

Figure 15 shows the performance assessment, in which the multi-block approach is used for PPC processing. Performance of PPC-McDFE still consistently approximates that of McDFE, and PPC-DFE achieves the worst performance. McDFE fails in the 14th period, which may be due to the impropriate parameters for McDFE, while both PPC-McDFE and PPC-DFE succeed in recovering the distorted information. In observation, the MP algorithm shows advantages over the LS method for the multi-block approach. For instance, using the MP algorithm, 4.1 dB improvement (the 11th period) is obtained by PPC-DFE, and 3.3 dB improvement (the 9th period) is obtained by PPC-McDFE.

The multi-block approach operates on the decision directed mode, and hence there is the issue of error-propagation. In the scenario of low input SNR, the LS method is sensitive to errors of detected symbols of the previous block, while the MP algorithm estimates only dominant arrivals with less impact from the errors. Temporal focusing is more enhanced by the MP algorithm, which leads to better performance. Therefore, the MP algorithm is suggested for the multi-block approach.

Figure 14. Performance of PPC-DFE with different approaches. (**a**) One block; (**b**) 9 blocks. The MP algorithm is used, and the symbol rate is 2 kilo-symbol/s.

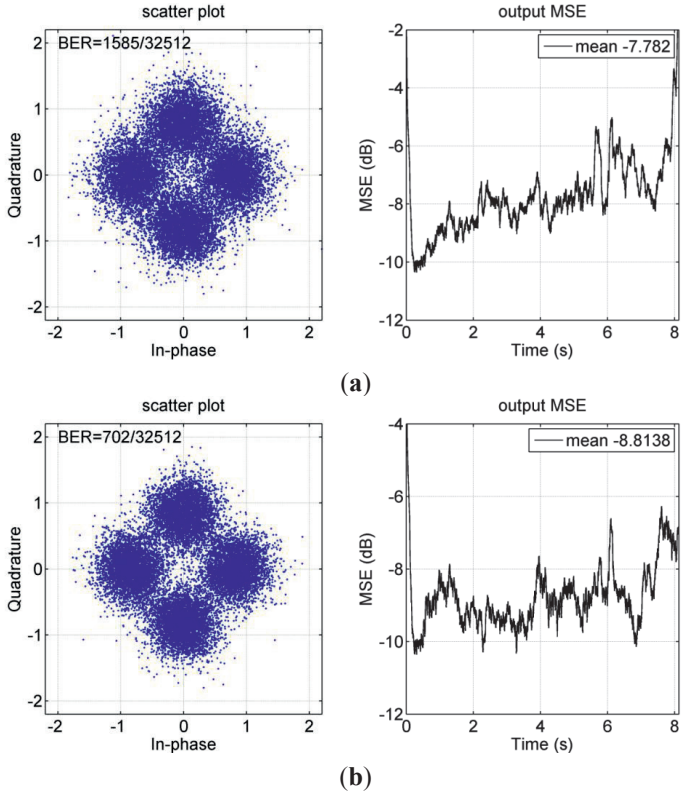

Figure 15. Performance of three receiver structures. There are 16 blocks for PPC processing.

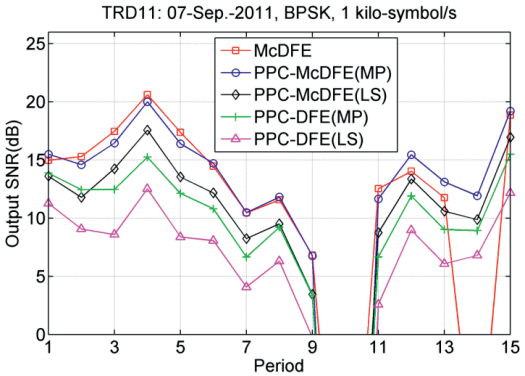

The multi-block approach may be better than the one block approach, but it depends on the rate of channel variation. Figure 16 shows the comparison between using the one block and multi-block approaches. For PPC-McDFE, there is trivial improvement with a maximum improvement of 0.5 dB (the 12nd period). For PPC-DFE, there is improvement in 11th periods, with mean improvement of 0.6 dB, and the maximum improvement is 1.4 dB (the 2nd period). In the current case, only modest

improvement has been obtained when using the multi-block approach, and this can be understood that the collected data were moderately time variant. The multi-block approach cannot avoid the issue of error-propagation, and hence caution should be paid when using this approach, especially in the scenario with low input SNRs.

Figure 16. Performance comparison between the one block approach and the multi-block approach.

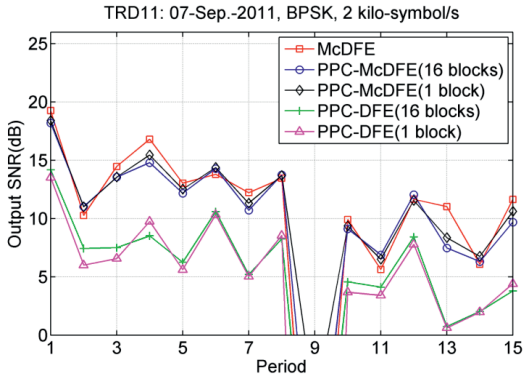

6. Summary and Conclusions

Three receiver structures have been assessed by processing data collected in a recent experiment conducted over a range of 7.4 km. In this high frequency (10–14 kHz) experiment, coherent underwater communications of different symbol rates were achieved, e.g., 1 to 2 kilo-symbol/s. In a large time scale, in terms of period of 202.044 s, the time-variant characteristics of underwater channel are observed by the communication results in terms of output SNR.

As shaping pulses, it is shown that the difference between LFM and RRC is minimal. The LFM shaping pulse provides a simple method for PPC processing, where the received channel probe signal of LFM is immediately used. Using a RRC shaping pulse, it is flexible to select a channel estimation method for PPC processing, e.g., the MP algorithm. In addition, the block-based approach can be implemented in time-varying channels.

As evident, PPC-DFE achieves the worst performance in the assessment, and the performance of PPC-McDFE approximates that of McDFE. Time-variant reverberations result in unpredictable spatial coherence, which may impact on the performance of PPC-DFE. Therefore, it is preferable that the adaptive multichannel combining obtains much spatial gain, especially in the scenarios of a small number of receivers. For instance, it is preferable to use PPC-McDFE instead of PPC-DFE in a channel of long time spread.

In the sparse channel, the MP algorithm has been assessed in two modes. One is the conventional single block approach, and the other is the multi-block approach. The multi-block approach assumes that the channel is constant within each block of a short time interval, and then PPC processing is extended to time-varying channels. Comparing with PPC-DFE, PPC-McDFE is less sensitive to the channel variations. It has been demonstrated that the MP algorithm improves the performance of communications using PPC processing, and thus the MP algorithm is suggested in sparse channels.

Acknowledgments

The authors would like to thank NTNU Ph.D. candidate Bo Peng for his comments, and Ph.D. candidates Yan Jiang and Qin Liu, all the participants, technical engineer Tim Cato Netland and crew of R/V Gunnerus at NTNU for their help during the sea trial on 7 September 2011.

References

1. Kilfoyle, D.B.; Baggeroer, A.B. The state of the art in underwater acoustic telemetry. *IEEE J. Ocean. Eng.* **2000**, *25*, 4–27.
2. Stojanovic, M.; Catipovic, J.; Proakis, J.G. Adaptive multichannel combining and equalization for underwater acoustic communications. *J. Acoust. Soc. Am.* **1993**, *94*, 1621–1631.
3. Fink, M. Time reversal of ultrasonic fields. I. Basic principles. *IEEE Trans. Ultrason. Ferroelectr. Freq. Control* **1992**, *39*, 555–566.
4. Edelmann, G.F.; Akal, T.; Hodgkiss, W.S.; Seongil, K.; Kuperman, W.A.; Song, H.C. An initial demonstration of underwater acoustic communication using time reversal. *IEEE J. Ocean. Eng.* **2002**, *27*, 602–609.
5. Edelmann, G.F.; Song, H.C.; Kim, S.; Hodgkiss, W.S.; Kuperman, W.A.; Akal, T. Underwater acoustic communications using time reversal. *IEEE J. Ocean. Eng.* **2005**, *30*, 852–864.
6. Rouseff, D.; Jackson, D.R.; Fox, W.L.J.; Jones, C.D.; Ritcey, J.A.; Dowling, D.R. Underwater acoustic communication by passive-phase conjugation: Theory and experimental results. *IEEE J. Ocean. Eng.* **2001**, *26*, 821–831.
7. Yang, T.C. Correlation-based decision-feedback equalizer for underwater acoustic communications. *IEEE J. Ocean. Eng.* **2005**, *30*, 865–880.
8. Song, H.C.; Hodgkiss, W.S.; Kuperman, W.A.; Stevenson, M.; Akal, T. Improvement of time-reversal communications using adaptive channel equalizers. *IEEE J. Ocean. Eng.* **2006**, *31*, 487–496.
9. Song, H.C.; Kim, J.S.; Hodgkiss, W.S.; Kuperman, W.A.; Stevenson, M. High-rate multiuser communications in shallow water. *J. Acoust. Soc. Am.* **2010**, *128*, 2920–2925.
10. Yang, T.C. A study of spatial processing gain in underwater acoustic communications. *IEEE J. Ocean. Eng.* **2007**, *32*, 689–709.
11. Stojanovic, M. Retrofocusing techniques for high rate acoustic communications. *J. Acoust. Soc. Am.* **2005**, *117*, 1173–1185.
12. Yang, T.C. Differences between passive-phase conjugation and decision-feedback equalizer for underwater acoustic communications. *IEEE J. Ocean. Eng*. **2004**, *29*, 472–487.
13. Zhang, G.; Dong, H. Spatial diversity in multichannel processing for underwater acoustic communications. *Ocean Eng.* **2011**, *38*, 1611–1623.
14. Dowling, D.R. Acoustic pulse compression using passive phase-conjugate processing. *J. Acoust. Soc. Am.* **1994**, *95*, 1450–1458.
15. Song, A.; Badieym, M.; Songm, H.C.; Hodgkiss, W.S.; Porter, M.B.; The KauaiEx, Group. Impact of ocean variability on coherent underwater acoustic communications during the Kauai experiment (KauaiEx). *J. Acoust. Soc. Am.* **2008**, *123*, 856–865.

16. Cotter, S.F.; Rao, B.D. Sparse channel estimation via matching pursuit with application to equalization. *IEEE Trans. Commun.* **2002**, *50*, 374–377.
17. Song, H.C. Time reversal communication in a time-varying sparse channel. *J. Acoust. Soc. Am.* **2011**, *130*, EL161–EL166.
18. Hovem, J.M.; Yan, S.; Bao, X.; Dong, H. Modeling Underwater Communication Links. In *Proceedings of Second International Conference on Sensor Technologies and Applications, 2008 (SENSORCOMM 2008)*, Cap Esterel, France, 25–31 August 2008; pp. 679–686.
19. Haykin, S. *Adaptive Filter Theory*; Prentice Hall: Upper Saddle River, NJ, USA, 2001.
20. Hursky, P.; Porter, M.B.; Siderius, M.; McDonald, V.K. Point-to-point underwater acoustic communications using spread-spectrum passive phase conjugation. *J. Acoust. Soc. Am.* **2006**, *120*, 247–257.
21. Yang, T.C.; Yang, W. Low probability of detection underwater acoustic communications using direct-sequence spread spectrum. *J. Acoust. Soc. Am*. **2008**, *124*, 3632–3647.
22. Flynn, J.A.; Ritcey, J.A.; Rouseff, D.; Fox, W.L.J. Multichannel equalization by decision-directed passive phase conjugation: Experimental results. *IEEE J. Ocean. Eng*. **2004**, *29*, 824–836.
23. Stephane, M.A. *Wavelet Tour of Signal Processing*, 2nd ed.; Academic Press: Waltham, MA, USA, 1999.
24. Davis, G.; Mallat, S.; Avellaneda, M. Adaptive greedy approximations. *Constr. Approx.* **1997**, *13*, 57–98.
25. Taehyuk, K.; Litis, R.A. Matching Pursuits Channel Estimation for an Underwater Acoustic OFDM Modem. In *Proceedings of IEEE International Conference on Acoustics, Speech and Signal Processing, 2008 (ICASSP 2008)*, Las Vegas, NV, USA, 31 March–4 April 2008; pp. 5296–5299.
26. Stojanovic, M. Efficient processing of acoustic signals for high-rate information transmission over sparse underwater channels. *Phys. Commun.* **2008**, *1*, 146–161.